ANALYSIS OF BOW CRUSHING IN SHIP COLLISION

by

JI YOUNG KIM

B.S. Naval Architecture & Ocean Engineering
Pusan National University , Pusan, Korea, 1996

Submitted to the Department of Ocean Engineering
in Partial Fulfillment of the Requirements for the Degree of

MASTER OF SCIENCE IN OCEAN ENGINEERING

at the

MASSACHUSETTS INSTITUTE OF TECHNOLOGY

February 2000

Signature of Author..
Department of Ocean Engineering
January 15, 2000

Certified by..
Professor Tomasz Wierzbicki
Thesis Supervisor

Accepted by...
Professor Nicholas M. Patrikalakis
Chairman, Departmental Graduate Committee
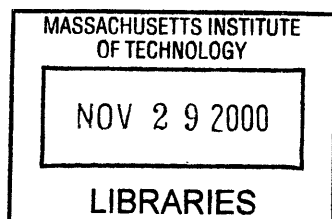
ANALYSIS OF BOW CRUSHING IN SHIP COLLISION

by

JI YOUNG KIM

Abstract

Collision of ships with oil tankers poses, next to grounding, one of the most serious environmental threats at sea. In many previous analyses of the collision problem, the bow of the impacting ship was considered rigid. The objective of the present research is to include the finite strength of the bow in the overall collision simulation. The emphasis will be placed on typical raked shapes because some work already has been reported in the past on bulbous bows. The main structural members will include side shell and the deck. Transverse and longitudinal stiffeners will be taken into account by means of a smearing technique. A structural model is developed by identifying localized zones of plastic deformations from photographs of damaged ships. Then, the contributions of the membrane and bending resistance is assessed and a simple computational model is developed. The solution includes determination of the force-indentation relationship, a number of folds and a total amount of damage for a given speed of a ship. Five scale model tests were run and the force-deflection characteristics were recorded. A good correlation was obtained between the analytical solution and experimental results.

Acknowledgments

Contents

6

List of Figure

8

Nomenclature

σ	Stress
σ_0	Flow stress
σ_u	Ultimate stress
σ_y	Yielding stress
σ_{ij}	Stress tensor
$\sigma_1, \sigma_2, \sigma_3$	Principal stresses
$\sigma_{\alpha\beta}$	Stress tensor
ε	Strain
$\varepsilon_{\eta\xi}$	Strain tensor (Plane stress)
ε_{ij}	Strain tensor
ε^p_{ij}	Plastic strain tensor
ε^e_{ij}	Elastic strain tensor
$\theta_1, \theta_2, \theta_3, \theta_4$	Hinge rotation angle
θ	Deck angle
β	Deformation angle
φ	Bow angle
l	Bow length
l_m	Side length $\cong$ Bow length
lu	Upper deck length = l_1
R_1	Contact point rotation radius
R_2	Hinge rotation radius (Model A), Bow tip rotation radius (B)
R_3	Bow tip rotation radius (A)
δ	Indentation depth
t	Plate thickness

u	Displacement function
$U_1, U_2, U_3\ldots$	Displacement function
Δ	Maximum side stretching length
μ	Maximum bow stretching length
H	Folding wave length
$S_1, S_2, S_3\ldots$	Stretched areas
S	Surface area
L	Ship over all length
B	Midship breath
d	Moulded depth
D	Depth
$\forall$	Volume of a body
T	External surface force
P	Instantaneous crush force
E_{ext}	External work
P_m	Mean crushing force
U_m	Membrane energy
U_b	Bending energy
E_m	Membrane energy
$E_{m1}, E_{m2}\ldots$	Membrane energy of area $S_1, S_2,\ldots$
E_b	Bending energy
$E_{b1}, E_{b2}\ldots$	Bending energy of hinge folding element 1, 2,...
E_{mbo}	Membrane energy of bow
E_{ms}	Membrane energy of side
E_{mst}	Total membrane energy of side
E_{sf}	Bending energy of sides
E_{db}	Deck bending energy

M	Bending moment
M_0	Fully plastic bending moment per unit length
$M_{\alpha\beta}$	Bending moment tensor
N	Membrane force
N_0	Fully plastic tension load per unit length
$N_{\alpha\beta}$	Membrane force tensor

List of Table

Chapter 1

INTRODUCTION

1.1 Background

A ship undergoes wave loads as well as extreme accidental loads in its lifetime. Among many types of ship accident, collision is directly related to the ship structural strength. Especially, collisions of the hazardous substance carriers such as oil tankers, LNG/LPG...can cause serious environment threats when occurring near the coastal areas or narrow channels.

The accident of the Exxon Valdez off the Alaska coast in 1989, and the accident of the Sea Empress in the channel near the Wales in England in 1996, and several other tanker accidents have created serious need for the sea environmental protection and initiated prompt discussions on the methods, which will prevent perilous substance spills such as oil. As a result, the U.S. Oil Pollution Act was introduced in 1990 (OPA 90) that requires double hull tankers in U.S. waters by the year 2015. The International Maritime Organization (IMO) has also established compatible regulation which contains design rules against accidental or extreme loads such as MARPOL 73/78 Annex 13F, 13G.

In preventing environmental disaster the reduction of the human error and the improvement of the traffic system must be first considered. However, it is very difficult to avoid human errors totally. Therefore, it is important to establish rational ship structural design guidelines that minimize the perilous substance outflow of ships. To establish new design guidelines many researchers analyzed mainly two accident scenarios. One is ship grounding and the other is ship collision. Furthermore, the ship collision also can be classified into two groups, side collision and head-on collision. The side collision generally represents a ship-to-ship collision situation. In other words, a striking ship collides with the side structure of the struck ship. A typical head–on collision represents a situation when a bow of a ship collides into a fixed embankment such as pier or bridge crossing international shipping route or gravity-supported offshore installations.

Even though the head-on collision might be treated as a less serious case as compared with grounding case and side collision, there must be no priority in preventing disaster. Moreover, for more than four decades the value of contributions of many design guidelines in this field is questionable. When we evaluate of the progress of the science and technology in late 20th, better methods must be developed in this field.

1.2   Current Methodologies

In the history of the ship collision research there have been many methodologies since Minorsky (1959) proposed an energy method for predicting collision damage to protect nuclear power plants. These methods can generally be classified into three categories that are numerical based, empirical based, analytical method.

The numerical method is mainly based on the commercial finite element computer programs such as DYNA3D, PAM-CRASH, ABAQUS, ADINA, MSC/DYTEAN. This method is becoming popular as computer programs are being sophisticated, and is being widely used especially for a parametric study. However, it needs enormous computing time and efforts in modeling.

The empirical based method was first introduced by Minorsky[2]. He proposed a linear relationship between the resistance and penetration based on statistics of 26 ship-to-ship collision. This method has been widely used by industry, and has been confirmed and modified by many researchers such as Woisin[37], Akita[5], Kitamura[38],Vaughan[39], Hysing,[40], Choi[41],and others.

The analytical method is mainly based on the application of the theory of large plastic deformation of shells. It is appears that Wierzbicki[14] first applied this theory to ship collision analysis with his insightful modeling skill. The paper on the "Intersecting plates method" was published in 1982. Later this theory has been extended and modified by Amdahl[16], Abramowicz[20], Yang,&Caldwell[24], Kierkegaard[29], Paik[33], Pedersen[28].etc. Since this method is deeply rooted in principles of classical mechanics, it is gains increasing popularity and also enjoying high accuracy.

1.3   Previous Research

It is difficult to predict the mean crushing force of the complex bow structure of a ship in a frontal collision. Thus, it was necessary to study simplified bow structure, and many researchers approached the problem through the study of axial crushing of circular cylinders or square tubes. In fact, the mechanism of axial crumpling of thin-walled structures is a common phenomenon in damage of ships' bow during a collision, and it is a crucial element to understand the energy absorption characteristic of structural elements that constitute the bow structure and control its crushing performance.

An extensive literature surveys by Jones[10] ,van Mater & Giannotti[9] had set up the foundation of the ship collision research.

Nagasawa et al [7] performed structural model tests, simulating the collision of ship side with the buffer placed on the corner part of a bridge pear. They used two kinds of buffer models, referred to as grid-type and composite-type. Through this experiment they compared force-deformation curves of both types of the buffer models and estimated the amount of energy absorbed by the composite-type of buffer in both side and bow collision cases.

Ohnishi et al [15] performed a theoretical calculation by the F.E.M. on an ideal mathematical frame model of bow construction, and compared it with 1/10 scale bow model test results. Through this process they estimated the collapse loads of bow construction of actual ships and obtained the load-deformation curves.

Wierzbicki[14] developed a new method and introduced the term "Crashworthiness". He assumed that a typical ship's hull section consists of an assemblage of plastic plates with "L", "T", "X" shaped "super-folding elements", and calculated mean crushing force of the each elements through equating the rate of the external work and the linear superposition of the bending energy dissipation rate and membrane energy dissipation rate.

Meng et al [17] calculated the mean crushing force of axially loaded square tube using the concept of the moving plastic hinge, and found that the linear relation holds between the folding modes and the ratio of plate thickness per plate width.

Amdahl derived a formula for the mean crushing force of the bow collision with the same assumption as Wierzbicki's and verified it through various types of bow model tests.

Abramowicz and Jones [20] develop analytical method to determine the effective crushing distance in axially compressed thin-walled metal columns, and derived an expression for the mean crushing force of the stiffened and unstiffened tube.

Abramowicz & Jones[23] performed dynamic axial crushing tests on the square tubes which have two different ratios of the plate width to thickness . Through this experiment they checked validity of some assumptions such as asymmetric folding mode, and observed the Euler collapse of the longer columns. They used the effective crushing distance ratio for the calculation of the static mean crushing force, and included dynamic effects by considering the material strain rate sensitivity.

Kawai et al [22] developed the numerical method for estimating the energy absorption of the structural impact in which they modeled structure as a mass spring system based on the Finite Element Method and the axial crushing theory of square tubes due to Wierzbicki, and Abramowicz. In the tests they ignored the inertial force and took the 73% of the initial length as an effective crushing distance, and found good correspondence between the theoretical solution and test results.

Yang & Caldwell [24] proposed a formula based on Wierzbicki's collapse mechanism to predict the mean crushing strength of complex structures and applied to the ship's bow structure collision into a concrete pier. Their formulation included the increment of the crushing strength due to material strain-rate effects and longitudinal stiffeners in the analysis of the energy absorption behavior of panels.

Toi et al [25] performed numerical and experimental study on axially loaded square tube. The experimental data on the buckling load, deformation mode, and mean crushing force were compared the conventional analytical based method, numerical based method, and empirical based method.

Jones & Birch [27] performed experimental study on the axially stiffened square tube. In the experiments the ratio of the column length to plate width was held constant. Studied were effects of the stiffener height, number, inside stiffened case and outside stiffened. They tested both stiffened and unstiffened square tubes under static or dynamic load. In their calculation of the mean crushing force the effective crushing distance were not considered but the dynamic effects were included.

Kierkegaard[29] used an orthotropic theory of plated to take into consideration the effect of stiffeners.

Pederden et al [28] presented a basis for the estimation of the collision forces between conventional vessels and large volume offshore structures. They derived an expression for the crushing loads as a function of penetrations for different bow structures, and crushing forces as functions of vessels size, vessel speed and bow profile. They also integrated analysis results into the probabilistic procedure for the design of the fixed marine structures against ship collision, based on an accepted maximum annual frequency of severe collision accidents.

Ohtsube and Suzuki [30] improved Yang & Caldwell's technique of deriving simplified equation of mean collapse force, and applied to the ship bow structure. The finite element analysis using MSC/DYTRAN was applied to verify the validity of the approach. The comparisons are made with experiment result of Nagasawa et al [11].

In 1995, Wang Susuki [32] proposed a simple one-term formula for predicting the crushing strength of ship bow structures, through introducing energy absorption ability of structures and energy absorption reduction effect which is caused by inclination load.

1.4 Motivation

Large ship such as crude oil carrier or container carrier can be considered to be composed of three parts that are bow, mid-parallel, and stern part. In frontal collision usually the damage is confined within the bow part. This is because of a smaller cross-section horizontally and vertically. Furthermore, the bow can also be conceptually divided into two parts that are tetrahedral part Fig. (1) and the remainder. Since the bottom plate does not support the tetrahedral part, it can be considered the most vulnerable part of the ship. In fact, the crushing force and deformation curve of this part of the formulas of the previous researches [16], [24], [28], [32] and tests results show the steep angle increase of the crushing force to indentation depth. Thus, this thesis will focus on the analysis of this tetrahedral part.
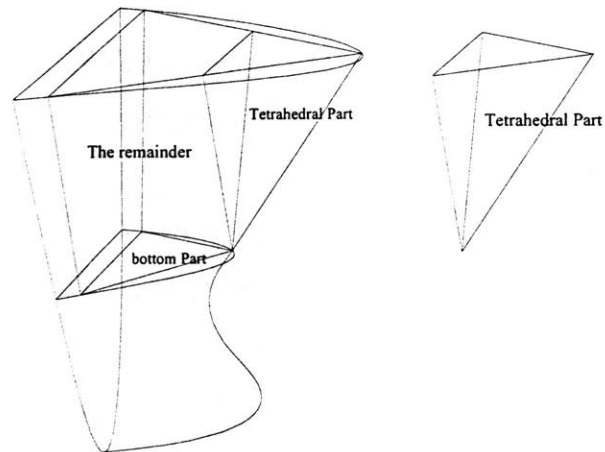
Figure 1: Conceptual Division

As far as previous methods for the bow crushing analysis were concerned, they all were derived through a microscopic approach based on Wierzbicki's intersecting plates method using super-folding elements ("L", "T", "X") whether those were improved or expended. Recently, Wang and Suzuki [32] considered the inclination of plate intersection to collision load. However, it is obvious that the reasonable method in mathematics and mechanics to represent an approximate 3-dimensional bow crushing force requires the macroscopic 3- dimensional approach at least for the shell part of the bow.

Moreover, to develop design guidelines for the ship building industry, solutions must be able to provide an optimum spacing for the stiffeners of the bow structure. Therefore, the author will develop a simple formula that is reasonable both mathematically and mechanically. Through the combination of the kinematic approach due to Wierzbicki's [14] and the formula obtained for the unstiffened shell part, a one term formula for the mean crushing force is derived, and application to the bow models and the comparison with the theoretical solution is made.

1.5 Problem Formulation

A ship with an orthogonal stiffened bow structure is considered. The ship is moving forward with the initial velocity V and hits the embankment. It is assumed that the contact point of the ship is above the bulbous bow and below the upper deck sideline. The encounting impact angle is 90 degree vertically and ϕ (bow angle) horizontally. The bow elevation and the trim effect are neglected, thus no friction force between the bow and embankment is considered.

The embankment is assumed to be rigid right angle-edged. The collision is assumed to be perfectly inelastic, thus the external kinetic energy is fully converted to the structural damage of the striking ship.
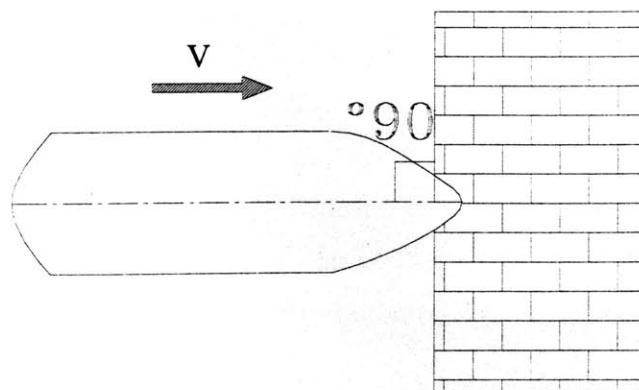
Figure 2: Collision Over view
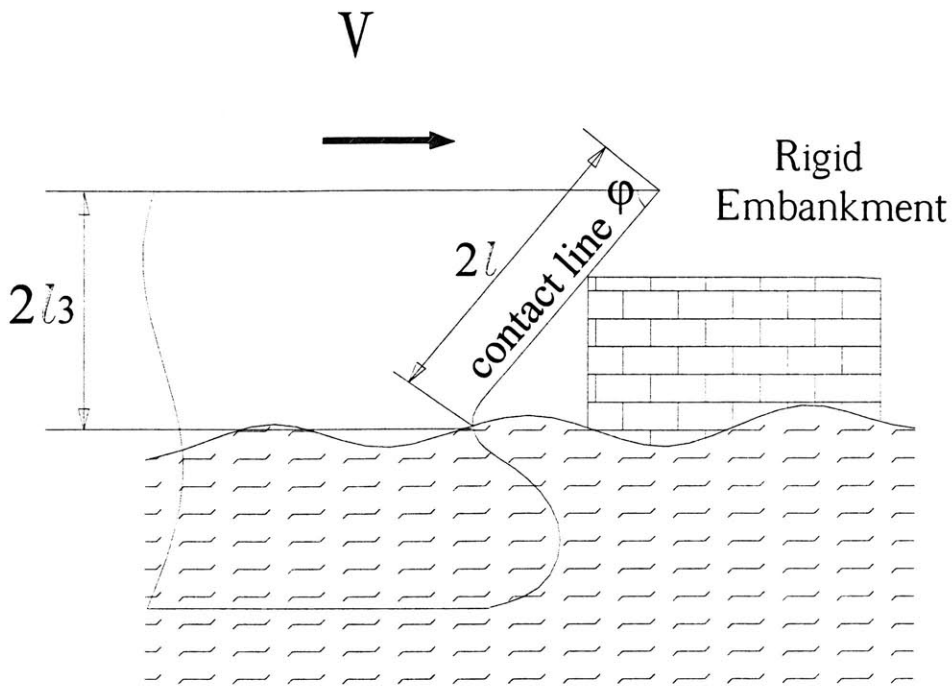
Figure 3: Collision Side View

The above assumptions simplify the external dynamics of the ship motion. However, the result of the internal mechanics of the collision process to be developed in this report can be used for an overall collision analysis with small modifications.

Chapter 2

THEORETICAL BACKGROUND

2.1 General

The deformation mode during the collapse of ship's bow structures naturally involves very large strains, and strain rates well into the plastic range. The material behavior after yielding is nonlinear and elastic effects are negligible. Therefore the behavior of structures can be treated as rigid-plastic. The Following three sections provide review of the elementary theory of plasticity.

2.2 Yield Criteria

For a one-dimensional body under a one-dimensional stress state, it is relatively simple to define and find experimentally the yielding point. Plasticity occurs when the stresses attain a certain material-dependant value termed the yielding stress. However for more than one-dimensional bodies under combination of stresses, the situation is not so straightforward and several theories were advanced to define yielding criteria that help us to find a direct comparison with simple uniaxial yield stress of the tension test. The most important three yielding criteria are the criterion of Rankin, the criterion of Coulomb-Tresca, and, von Misses yielding criterion.

A. Criterion of Maximum Principal Stresses of Rankin and the Deviator Tensor

This criterion, for which good agreement with experiments on brittle material was found, assumes that yielding limit of the material is defined by the simple uniaxial test. For a two-dimensional stress state, this can be represented by the quadratic yielding boundary sketched in Fig.4. This simple yielding criterion encounter difficulties related to experimental observation such as hydrostatic pressure that has no effect on yielding. The experimental fact implies mathematically that yielding is not affected by the first invariant of the stress tensor, $I= \sigma_x + \sigma_y + \sigma_z = \sigma_1 + \sigma_2 + \sigma_3$, as shown in the following analysis.

Thus
$$\sigma_{ij} = \begin{bmatrix} \sigma_x & \sigma_{yx} & \sigma_{zx} \\ \sigma_{xy} & \sigma_y & \sigma_{zy} \\ \sigma_{xz} & \sigma_{yz} & \sigma_z \end{bmatrix} \tag{1}$$

can be regarded as the result of the superposition of two stress

$$\sigma_{ij} = \begin{bmatrix} \sigma_x - P & \sigma_{yx} & \sigma_{zx} \\ \sigma_{xy} & \sigma_y - P & \sigma_{zy} \\ \sigma_{xz} & \sigma_{yz} & \sigma_z - P \end{bmatrix} + \begin{bmatrix} P & & \\ & P & \\ & & P \end{bmatrix} \tag{2}$$

where P is the hydrostatic pressure

$$p = \frac{1}{3}(\sigma_x + \sigma_y + \sigma_z) = \frac{1}{3}(\sigma_1 + \sigma_2 + \sigma_3) = \frac{1}{3}I_1 \tag{3}$$
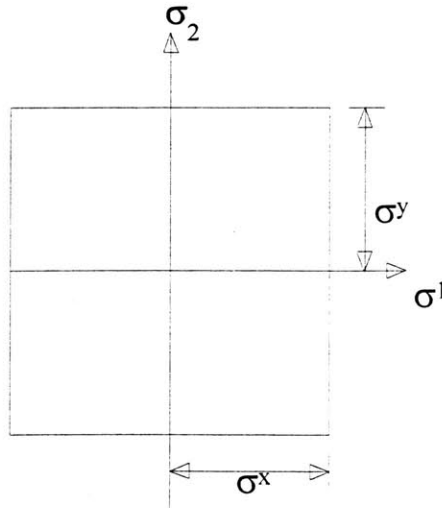
Figure 3: Rankin Field Criterion

The tensor notation is:

$$\sigma_{ij} = \sigma'_{ij} + pI \qquad (4)$$

where, I is the unit spherical tensor and σ_{ij} is the stress deviator tensor simply referred to as the deviator, and yielding depends of the deviator only.

B. Coulom-Tresca Criterion of Maximum Shearing Stresses

There is also an experimental observation which may agree with the intuitive expectation that yielding in the case of a two-dimensional tension-compression stress state will occur earlier than for tension-tension or compression-compression. In this way, another criterion due to Coulomb and Tresca can be viewed. Mathematically, Coulomb-Tresca yielding can be stated as follows:

$$[(\sigma_1 - \sigma_2)^2 - \sigma_y^2)][(\sigma_2 - \sigma_3)^2 - \sigma_y^2)][(\sigma_3 - \sigma_1)^2 - \sigma_y^2)] = 0 \qquad (5)$$

The plasticity boundaries given by this criterion are shown in Fig 5. for the two-dimensional stress state.
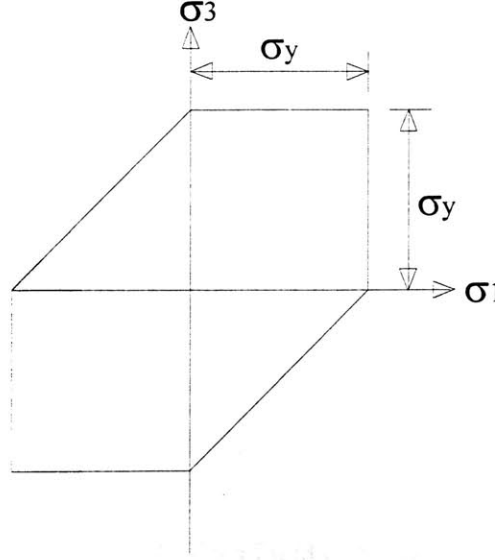
Figure 5: Tresca Field Criterion

When (σ_1, $\sigma_2 = \sigma_3 = 0$), one obtains $\sigma_1 = \sigma_y$. As expected, it is reduced to the known one-dimensional stress state yielding. When $\sigma_1 = -\sigma_3$, $\sigma_2 = 0$, one obtains $\sigma_1 = \pm 1/2 \sigma_y$. As the smallest yielding stress, it is only the half the value of the unaxial test.

C. von Mises Criterion

A yielding criterion developed by Beltrami, Huber, von Mises and Hencky, and which stood better with experimental results, especially for ductile material, is that of maximum distortion energy which is frequently referred to as the von Mises yielding criterion. Mathematically, this leads to the condition.

$$(\sigma_1 - \sigma_2)^2 + (\sigma_2 - \sigma_3)^2 + (\sigma_3 - \sigma_1)^2 = 2\sigma_y^2 \qquad (6)$$

In two-dimensional stress space, this condition forms an ellipse such as that shown in Fig.6. When $\sigma_2 = \sigma_3 = 0$, one obtains $\sigma_1 = \sigma_y$ while in the case of $\sigma_1 = \pm\dfrac{1}{\sqrt{3}}\sigma_y$ as compared to $\sigma_1 = \pm\dfrac{1}{2}\sigma_y$ in the previous case of the Coulomb-Tresca yielding condition. In Fig. 7 all these conditions are compared together and it be seen that they are identical for four points only and that the difference between the condition of Tresca and von Mises is minor.
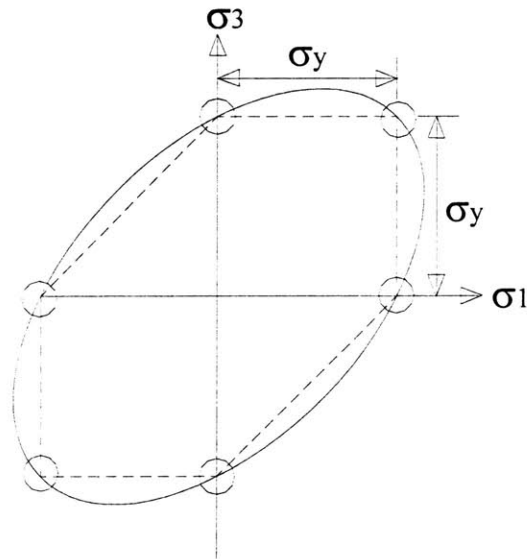
Figure 6: von Mises Field Criterion

The Tresca criterion is often applied to derive analytical solution of elastic-plastic problems, due to its simple linear form. The von Mises criterion has a nonlinear form in terms of stress components, and is therefore more complicated to use. Various plasticity theories exist. For strain hardening materials, the most common are the deformation

theory and the incremental theory. The deformation theory totally neglects the loading history dependency, and is therefore the simplest and the one most extensively used in engineering practice. The incremental theory does consider loading path dependency, and is thus somewhat more complex.

When the material is idealized as perfectly plastic the analysis is greatly simplified. For such materials, the limit theorems of plasticity may be established. These theorems can be used to develop methods for estimation of load-carrying capacity of structures. Perfectly plastic materials may be described by the flow theory, which is presented in next section.
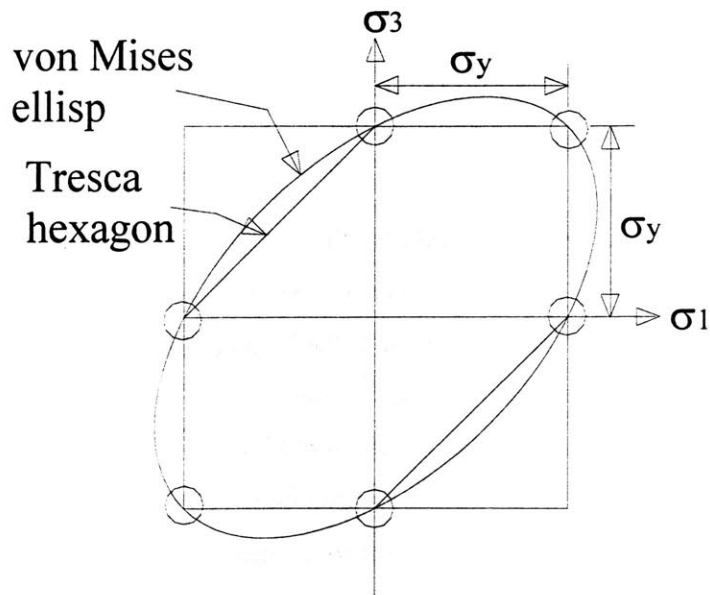
Figure 7: Comparison of the Critera

14

2.3 The Flow Theory of Plasticity

The yielding function is considered to remain constant as plastic deformation progress for a perfectly plastic material. Thus the yielding condition can be expressed as:

$$f(\sigma_{ij}) = 0 \qquad (7)$$

The total strain increment tensor can be assumed as the combination of the elastic and plastic parts:

$$d\varepsilon_{ij} = d\varepsilon_{ij}^e + d\varepsilon_{ij}^p \qquad (8)$$

The ratio of the components of the plastic increment tensor $d\varepsilon_{ij}^p$ that defines the direction of the plastic strain increment vector $d\varepsilon_{ij}^p$ in the space, and is called flow rule can be expressed as:

$$d\varepsilon_{ij}^p = d\lambda \frac{\partial f}{\partial \sigma_{ij}} \qquad (9)$$

where $d\lambda$ is a positive scalar factor of proportionality that is nonzero only when plastic deformation occurs.

The combination of the flow rule and yielding criteria will give us the components of the plastic strain increment. The very general properties of the yielding material are the Druckers' stability postulate, which considers that a material body subjected to certain surface and body forces, including certain displacements, strain, and stresses. He postulated that stable system that satisfies equilibrium and compatibility conditions is one that satisfies the following conditions

A. When an additional set of forces are applied, the work done by the additional forces and the associated changes in displacement are positive.

$$\dot{\sigma}_{ij}\, \dot{\varepsilon}_{ij} > 0 \qquad (10)$$

B. Over a cycle of adding and removing an additional set of forces, the work done by the additional forces and the associated changes in displacements are non-negative

$$\oint \dot{\sigma}_{ij}\, \dot{\varepsilon}_{ij} \geq 0 \qquad (11)$$

Both conditions imply that the yield surface must be convex, and the plastic increment vector must be normal.

2.4 Limit Analysis

Development of an estimation method for the collapse load of a structure requires an idealized body. Two basic assumptions are made for such a body.

A. Perfectly plastic material: The material shows perfect plasticity character with the associate flow rule without strain hardening or softening

B. Small structural deformations: Changes in geometry of the body or structure that occur at the limit load are negligible hence, the geometric description of the body or structure remains unchanged during the deformation at the limit load.

The second assumption allow for the use of the virtual work principle:

$$\int_S T_i \delta u_i \, dS + \int_\forall F_i \delta u_i \, d\forall = \int_\forall \sigma_{ij} \delta \varepsilon_{ij} d\forall \tag{12}$$

where T_i are surface forces and F_i are body forces, and σ_{ij} is a set of stress state in equilibrium with T_i and F_i while $\delta \varepsilon_{ij}$ is a set of strain increments compatible with the displacement increments δu_i. The left hand side represents external work increment δE_{ext} on the body, and the right hand side represents internal work increment δE_{int} dissipated in the body.

For the above equation, any equilibrium set may be substituted into. For example, the rate of change of displacements and strains($\dot{u}_i, \dot{\varepsilon}_{ij}$) can be used, and expressed as follows:

$$\int_S T_i \dot{u}_i \, dS + \int_\forall F_i \dot{u}_i \, d\forall = \int_\forall \sigma_{ij} \dot{\varepsilon}_{ij} \, d\forall \tag{13}$$

Generally, there are three basic relations that must be satisfied for a solution of a problem in solid mechanics. These are the equilibrium equations, the constitutive relations, and the compatibility equations. In the limit analysis, a lower-bound solution is found by only considering the equilibrium equations and constitutive relations, and an upper-bound solution is found by only considering the compatibility equations and the constitutive relations. This approach leads to formulation of the limit theorems of plasticity.

16

C. Lower Bound Theorem: If an equilibrium distribution of stress σ_{ij}^S can be found which balances the body force F_i in the volume $\forall$ and the applied load T_i on the stress boundary S_T and is everywhere below yield $f(\sigma_{ij}^S) < 0$ then the body at the loads T_i, F_i will not collapse.

D. Upper-Bound Theorem: If a compatible mechanism of plastic deformation $\dot{\varepsilon}_{ij}^P, \dot{u}_{ij}^P$ is assumed which satisfies the condition $\dot{u}_i^P = 0$ on the displacement boundary S_u then the load T_i, F_i determined by equation energy dissipation will be either higher than or equal to the actual limit load.

When applying the upper-bound theorem, a kinematically admissible displacement field is used to equate the rate of work done by external forces of the internal energy or rate of energy dissipation. In practice application, the collapse mode can often be predicted from geometrical consideration. Kinematically admissible displacement fields can then be found, and the upper bound theorem is therefore particular useful.

Chapter 3

REVIEW OF THE THEORY

3.1 Crushing Strength of Plate Intersection

A typical cut through a ship's hull consists of an assemblage of plates with various shapes of stiffeners. However, one can distinguish three structural configurations, that is Angle elements "L" (Two intersecting plates), "T" elements (Three intersecting plates), "X" elements (Four intersecting plate). The crushing strength of plate intersection can be represented by the mean crushing strength of these elements that can be calculated through the energy absorption of the super folding elements. As a simple example of the method, the calculation of the mean crushing force of the thin square tube is considered.

A. Mean Crushing Strength of a Square Tube

The analysis of the crushing mechanism of the thin plate structure provides a solution for the relation between the load and displacement. But it is very difficult to find the instantaneous force, and it is more convenient to calculate the mean crushing force as shown in Fig.8, which means that if we know the mean crushing force, we can find the corresponding amount of the absorbed energy for a given crushing distance.
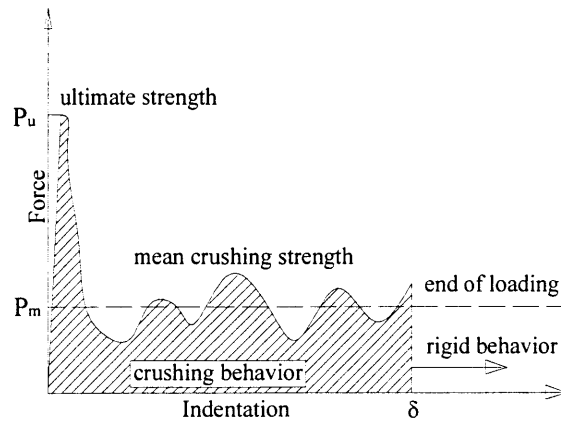
Figure 8: A Typical Plot of Load vs. Axial displacement for Square Box Column

B. Simplified Deformation Mode

There can be many deformation modes, and if the ratio b/t is very large, typically over 100 often collapses in asymmetric, irregular deformation modes, and the incompatibility of folding modes is of frequent occurrence. Shown in the figure below are two typical symmetric A and B, and the calculation is based on mode A.
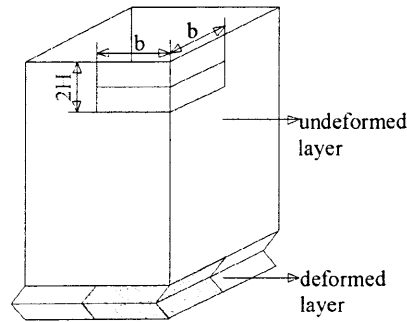
Figure 9:Deformation Mode
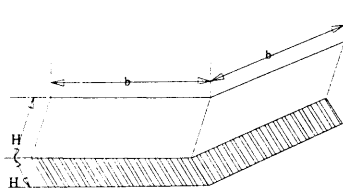
Folding Mode A
Figure 10
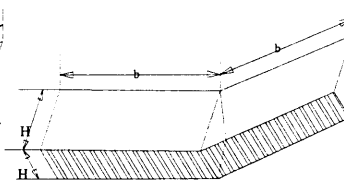
Folding Mode B
Figure 11

The known parameters are width b, thickness t, flow stress σ_0, and the unknown parameters are crushing strength P, half folding wave H.

C. Principle of Virtual Velocity

The crushing strength can be found through the Principle of Virtual Velocity.

$$P \cdot \dot{\delta} = \dot{U}_b + \dot{U}_m \tag{14}$$

The left hand side represent rate of external work, and the left hand side represents a sum of the rate of the bending energy dissipation and membrane energy dissipation.
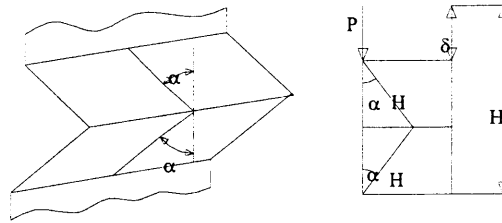
Figure12: One Folding Element

From the geometry of a single fold:

$$\delta = 2H(1 - \cos\alpha) \qquad \dot{U}_b : rate\, of\, bending\; energy$$

$$\dot{\delta} = 2H\sin\alpha\, \dot{\alpha} \qquad \dot{U}_m : rate\; of\; membrane\; energy \tag{15}$$

$$\delta_{max} = 2H$$

The integral form of the principle of virtual work is.

$$\int_0^{t_1} P \cdot \dot{\delta}\, dt = \int_0^{t_1} \dot{U}_b dt + \int_0^{t_i} \dot{U}_m\, dt$$

$$\int_0^{t_1} P \cdot \dot{\delta}\, dt = \int_0^{\delta_{max}} P(\delta)\, d\delta = \frac{1}{\delta_{max}} \{ \int_0^{\delta_{max}} P(\delta)\, d\delta \} \delta_{max} = P_m \cdot 2H \tag{16}$$

20

Mean Crushing Force is defined as:

$$P_m = \frac{1}{\delta_{max}} \{ \int_0^{\delta_{max}} P(\delta) \, d\delta \}$$

And

$$U_b = \int_0^{t_1} \dot{U}_b \, dt \tag{17}$$

$$U_m = \int_0^{t_1} \dot{U}_m \, dt$$

3.2 Membrane Resistance

The rate of membrane energy dissipation can be expressed as follows:

$$\dot{U}_m = \int_S N_{\alpha\beta} \, \dot{\varepsilon}_{\alpha\beta} \, dS \tag{18}$$

The assumption for the strain tensor, and the fully plastic membrane force tensor are:

$$\dot{\varepsilon}_{\alpha\beta} = \begin{vmatrix} \dot{\varepsilon} & 0 \\ 0 & 0 \end{vmatrix} \qquad \dot{N}_{\alpha\beta} = \begin{vmatrix} \dot{N}_0 & 0 \\ 0 & 0 \end{vmatrix} \tag{19}$$

An approximation of the total membrane stretching energy can be obtained by considering only final stage of deformation. The velocity rate of the strain follows:

$$\dot{\varepsilon} = \frac{d\dot{u}}{dx} \tag{20}$$

From the deformed model A, the displacement field can be found as linear function of y:

$$u(y) = \frac{y}{H} H = y \tag{21}$$
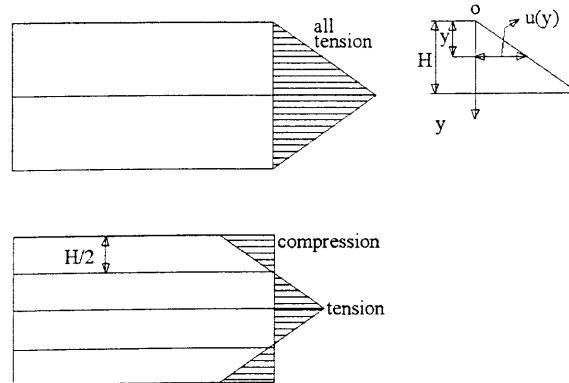
Figure13: Tension Field for Mode A, B

21

Substituting equations (19), (20) into (17), the equation becomes

$$U = 2\int_0^H\int_0^b N_0 \frac{du}{dx}\,dxdy = 2\int_0^H N_0 u(y)dy \tag{22}$$

where $u(y) = u(x = b, y) - u(y = 0, y)$

Therefore, the membrane energy for the model A becomes:

$$U_m = 2N_0\int_0^H u(y)dy = N_0 H^2 \tag{23}$$

For the alternative model B, the membrane energy becomes:

$$U_m = N_0 \frac{H^2}{2} \quad \text{where H becomes } \frac{H}{2} \tag{24}$$

Normalization with respect to $M_0 = \frac{\sigma_0 t^2}{4}$ gives the final expression for the membrane energy of one plate intersection:

$$U_m = M_0 \frac{H^2}{t} \tag{25}$$

3.3 Bending Resistance

The rate of bending energy dissipation can be expressed as follows:

$$\dot{U}_b = \sum_{i=0}^n M_0 \dot{\theta}_i b_i = 4M_0 \dot{\theta} b \tag{26}$$

Therefore, the bending energy for the model B becomes:

$$U_b = \int_0^{t_1} \dot{U}_b\, dt = 4M_0 b\int_0^{\frac{\pi}{2}} d\theta = [M_0 b\theta] = 2\pi M_0 b \tag{27}$$

22

3.4 Global Equilibrium

Energy balance equation for the one complete folding that does not involve the current indentation depth, δ :

$$P_m \cdot 2H = U_m + U_b$$

$$P_m \cdot 2H = 2M_0 \frac{H^2}{t} + 2\pi M_0 b \qquad (28)$$

$$\frac{P_m}{M_0} = \frac{H}{t} + \pi \frac{b}{H}$$

It is postulated that H adjust itself so as to minimize the mean indentation force. Which means that the length of the folding wave H_{opt} is still to be determined, and it can be found by minimization of P_m with respect the H.
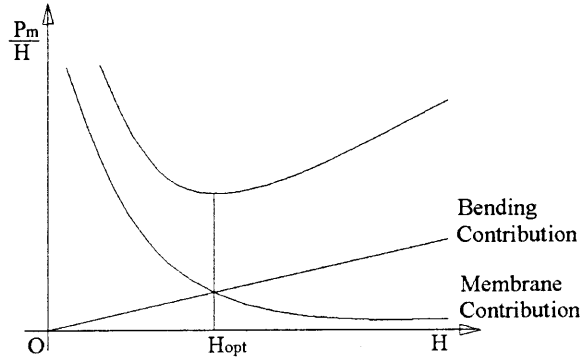
Figure 14: Minimum Plastic Energy

$$\frac{dP_m}{dH} = 0$$

$$\Rightarrow \frac{1}{t} - \frac{\pi b}{H^2} = 0 \qquad (29)$$

$$\Rightarrow H_{opt} = \sqrt{\pi bt}$$

Eliminating the wavelength H from the equation (27), the final expression for the mean crushing force per one contributing flange becomes.

$$\frac{P_m}{M_0} = 2\sqrt{\pi \frac{b}{t}}$$

$$P_m = \frac{\sqrt{\pi}}{2} \sigma_0 t^{1.5} b^{0.5} \qquad (30)$$

23

Chapter 4

SIMPLIFIED MODEL

4.1 Simplified Geometry

Since the bow has a complex three-dimensional shape, it is necessary to simplify the bow geometry. As already mentioned in Chapter 1, this thesis deals with the tetrahedral part that is most vulnerable part of the bow structure. In this thesis the tetrahedral part will be called just "bow" for convenience.

A. Boundary of the Deforming Part

The first step is to specify the contact point between the ship and the rigid obstacle, and defining the tetrahedral part on the bow structure. From the observation of the actual accidents and model tests it was determined that the contact point divides the bow length in two parts with same length, and the vertical extension of the line from the end of the bow length to the deck plate defines the extent of the deforming part of the tetrahedral part of bow structure Fig1, Fig 15.

B. Bow Parameters

The second step is to define the bow model with simple geometric variables keeping the number of variables as few as possible. In this thesis the simplified

model involving three input parameters, which are the bow length (l), bow angle (φ), deck angle (θ). The bow length is twice of the length between the apex and the contact point. The bow angle, as shown in Figure 15, is the angle between the upper deck and contact line. The deck angle shown in Figure 16 is the approximate angle taken in the upper deck horizontally and between the forefront and l_5 vertically.

C. Defining the lines

The third step is to define all the edge lines in terms of the given parameters (l, φ, θ). By this step the approximate computation procedure of the internal energy dissipation including all the edge lines will be simple and the final formula for the mean crushing force will be compact. Fig 15.
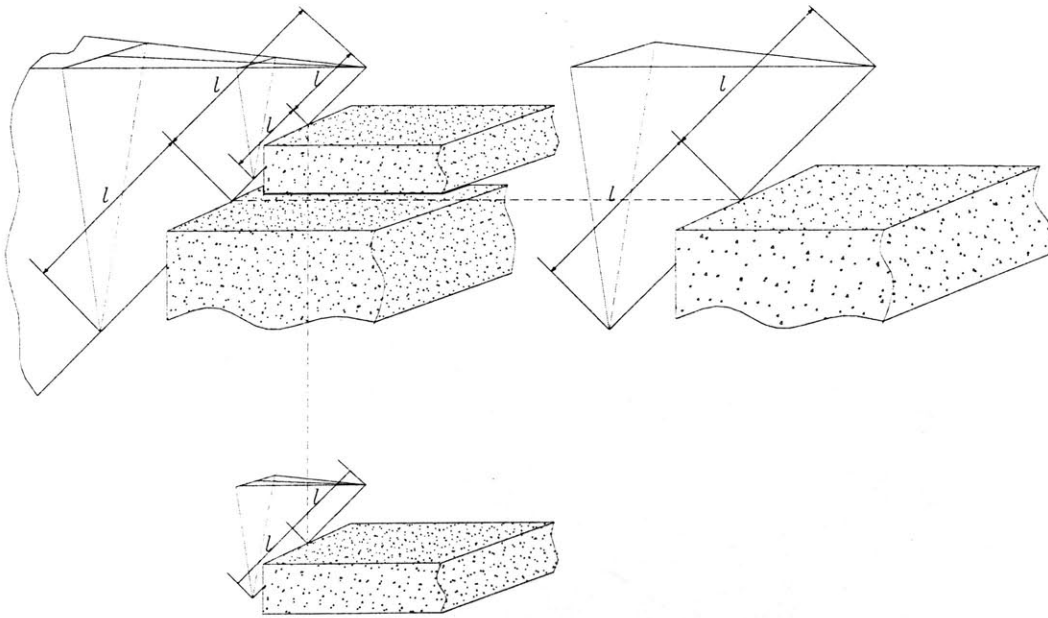
Figure 15: Boundary of the deforming Part of the Bow
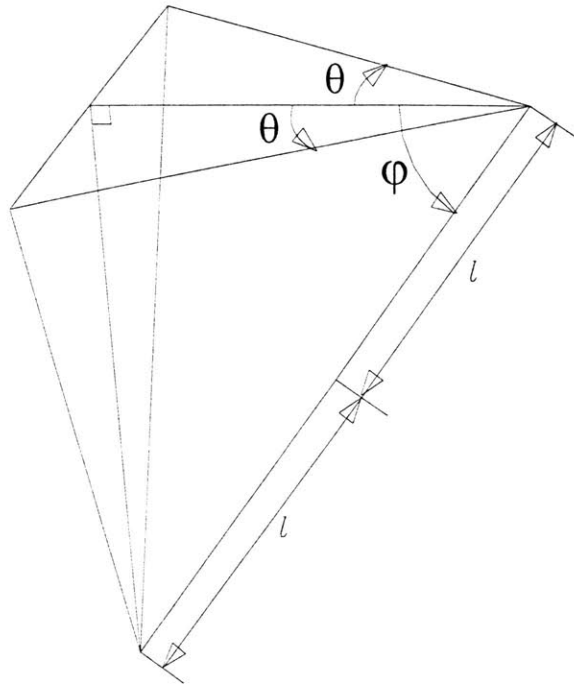
Figure 16:Geometric Parameters
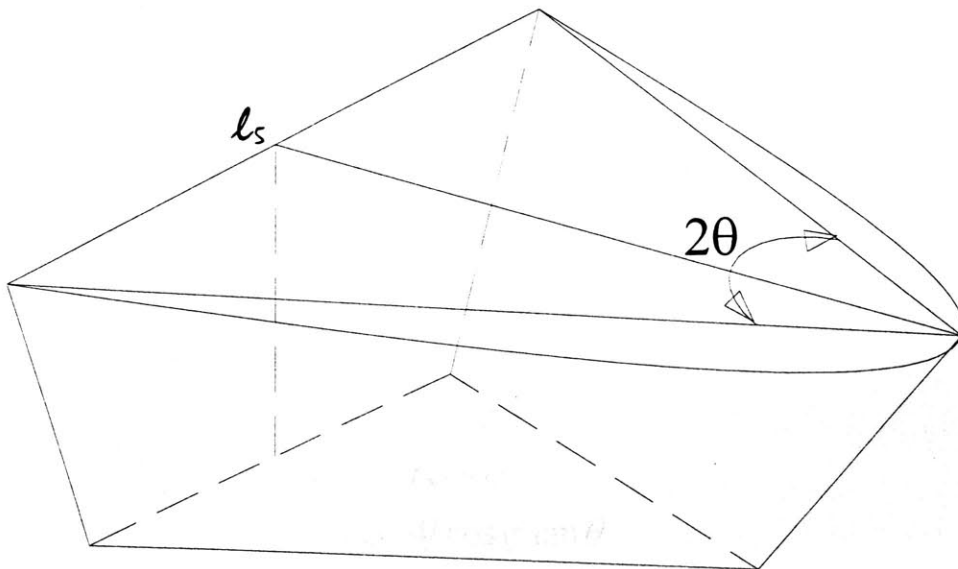
Figure 17: Deck Angle
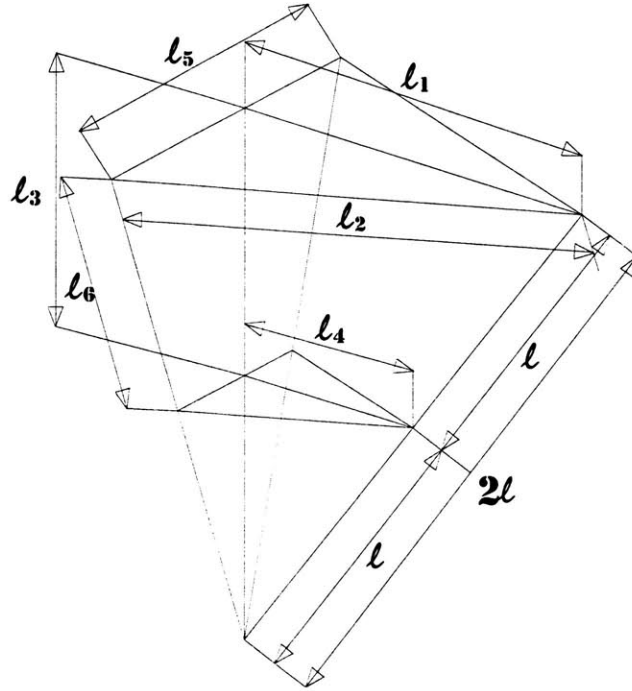
Figure 18: Defining Edge Lines

The length of the edge lines in Figure 3.4 can be expressed as:

$$l_1 = 2l\cos\varphi$$

$$l_2 = 2l\frac{\cos\varphi}{\cos\theta}$$

$$l_3 = l\sin\varphi$$

$$l_4 = l\cos\varphi \qquad (31)$$

$$l_5 = 4l\cos\varphi\tan\theta$$

$$l_6 = l\sqrt{\cos^2\varphi\tan^2\theta + \sin^2\varphi} \approx l_3$$

Chapter 5

SIMPLIFIED DEFORMATION MODEL

5.1 General Considerations

In constructing a deformation model it is important to keep the folding mode simple, and still reproducing the real deformation shape. In search for the kinematically admissible displacement fields, photos and various paper models were used. In this crushing scenario it is assumed that the velocity of the ship is constant for the entire crushing process. Alternatively, it can be also assumed that the bow part is fixed with suitable boundary conditions and the embankment crushes the bow with a constant velocity V. Since the indentation displacement changes from zero to δ_1 the mean crushing force P_m over the range $(0 \leq \delta \leq \delta_1)$ can be defined as:

$$P_m = \frac{1}{\delta_1} \int_0^{\delta_1} P(\delta)d\delta \tag{32}$$

where $P(\delta)$ is the instantaneous crushing force

So, the total work of the external forces becomes:

$$E_{ext} = \int_0^{\delta} P(\delta)d\delta = P_m \cdot \delta \tag{33}$$

Three bow models were developed. Historically, the model with outward folding (Model A) was developed first. However, the crushing force predicted by the corresponding solution was approximately ten times higher then the measured force. Subsequently, new

models (Model A and Model B) were created with inward folds that gave satisfactory results. The 'outward' model calculation is performed in section 6.1, 6.2 and the inward folding models for the first folding were calculated in section 6.3, 6.4. Since the inward first folding model gave us a satisfactory result, this model B was used for the calculation of the second folding case and transversely stiffened case in section 6.5, 6. 6.

5.2 Real Ship Collision

Photographs of the real accident observed show quite a complex deformation mode, Fig.18. However, by careful inspection, it is observed that there are four major internal energy dissipation areas, which are side shell folding, deck tilting, frontal bow stretching, and side shell stretching. It is also noticed that one fold of the side shell of the bow matches one bent on the deck and the large stretching area from the contact point and small stretching area on the sides.
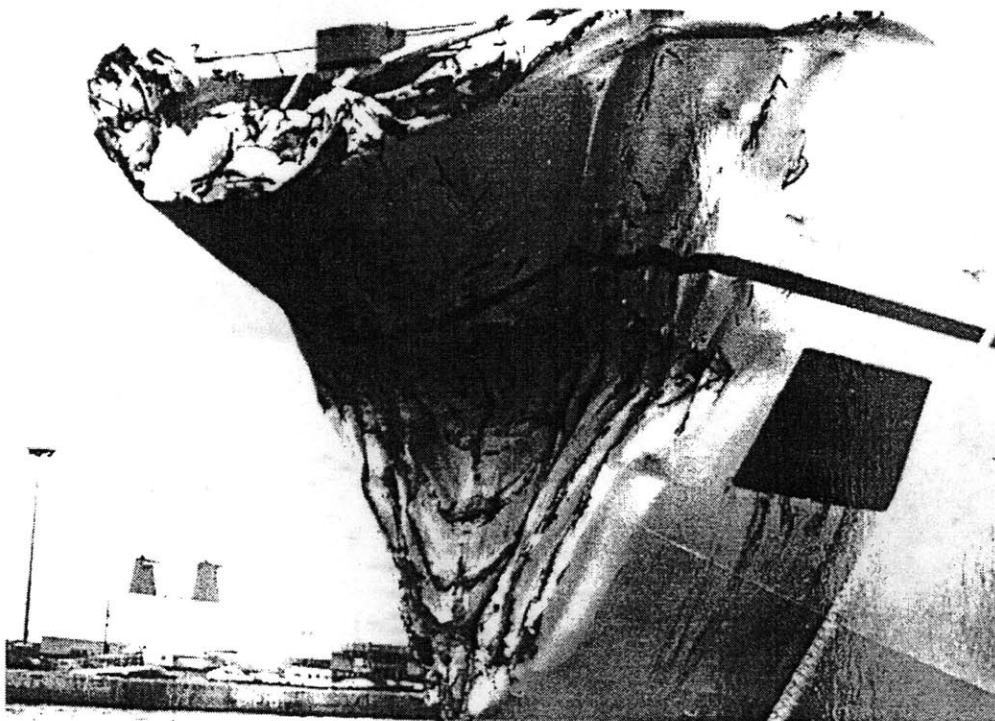
Figure 19: Diagonal View of damaged DALEDDA
(Courtesy of M..Maestro and A. Marino)

29
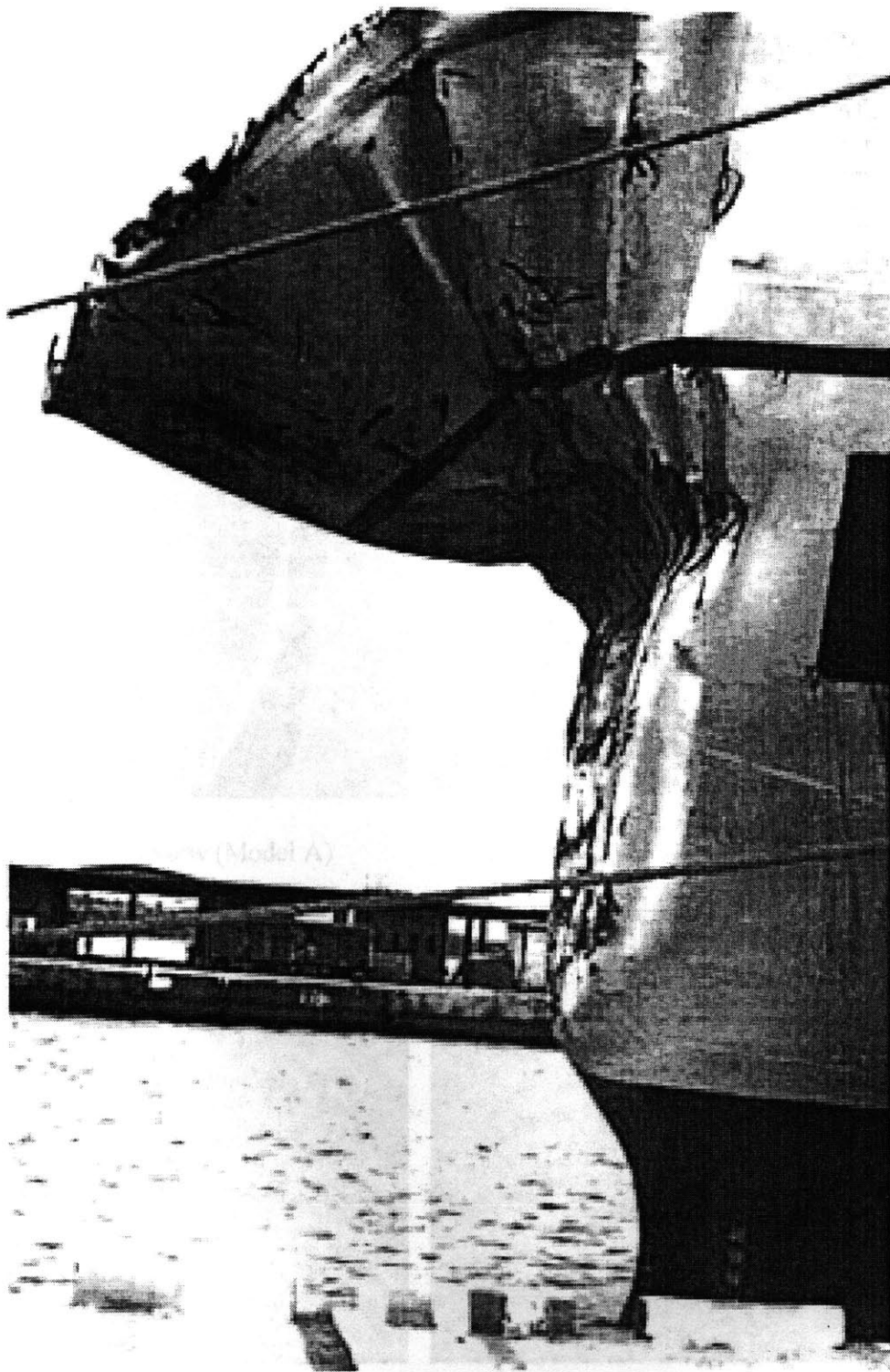
Figure 20: Side View

5.3 Three Dimensional Paper Model

Figures (20~26) show the paper models used in computation. Shown in these photos are simplified membrane and bending zones. The displacement field was defined in terms of the simple geometric parameters defined in the previous section.

Model A
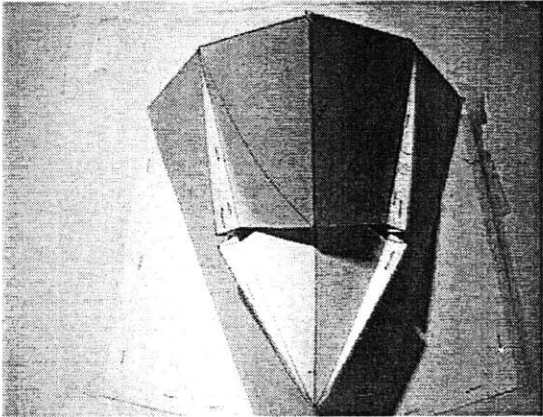
Figure 21: Front view (Model A)
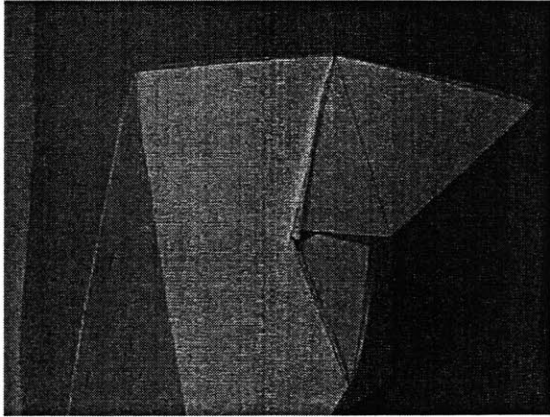
Figure 22: Side view (Model A)
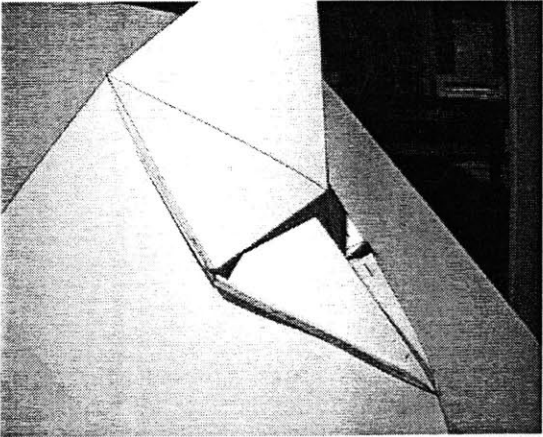
Figure 23: Diagonal view (Model A)
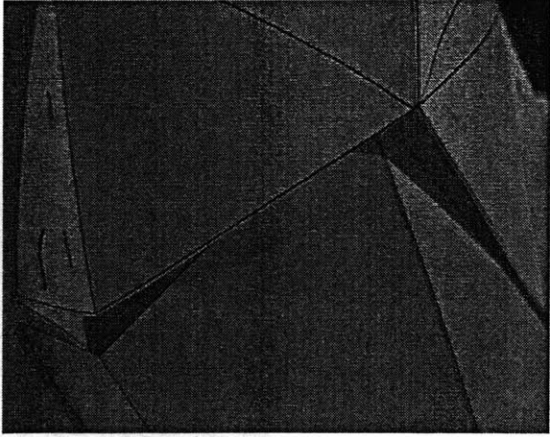
Figure 24: Close look (Model A)

Model B
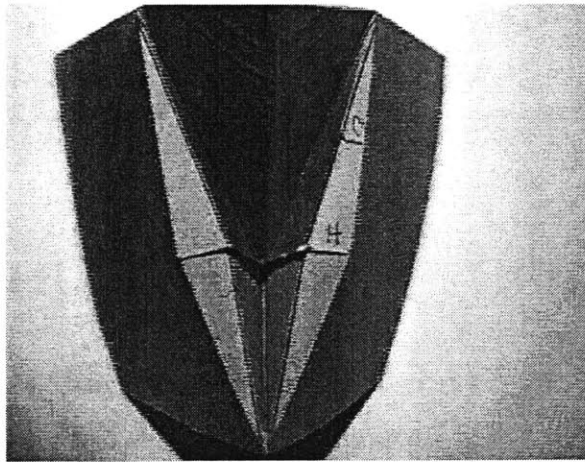
Figure 25: Front view (Model B)
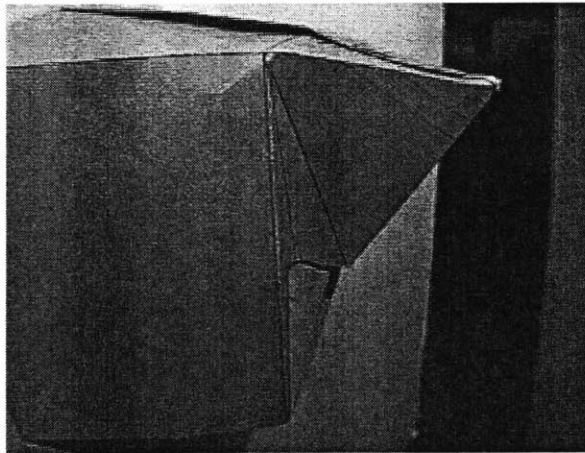
Figure 26: Side view (Model B)
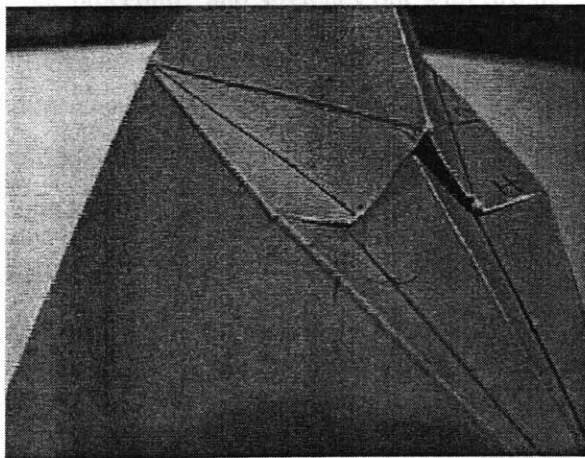
Figure 27: Diagonal view (Model B)

Chapter 6

STRENGTH OF THE BOW STRUCTURE

6.1 Mean Crushing Strength (Model A)

The calculation of the mean crushing strength of the deformation model A that folds outwardly is constructed, and two computational methods are tried in the subsection 1 and 2. The first method is based on the final deformation shape and the second is based on the deformation paths.

1. Method-1

A. Kinematics of Deformation Mode A

While the embankment moves horizontally along the l_6 the initial contact point is divided in two part, as shown in Figure (28, 29), and moves along the R1 and R₂ with radii l and l_3. When the indentation depth becomes δ, the vertically overlapped distance of the initial contact point is denoted as μ, the other point Q follows similar procedure, and stretches out with distance Δ. Consequently, the stretched zones S₁, S₂, S₃, S₄, S₅, and S₆ are formed and the side shell is folded. This procedure can be restated that the upper bow part and lower bow part divided by middle horizontal cross section rotate by the angle β, and the side shell is folded with wavelength 2H. For simplicity, the above lengths are expressed in terms of l. β, φ as follows:

$$\mu = 2l\{\sin(\varphi + \beta) - \sin\varphi\}$$
$$\Delta = 2l\sin\varphi(1 - \cos\beta) \tag{34}$$
$$H = \frac{1}{2}l\beta\sin\varphi$$

Thus, the angle β and the length of the folding wave 2H uniquely define the geometry of the fold.
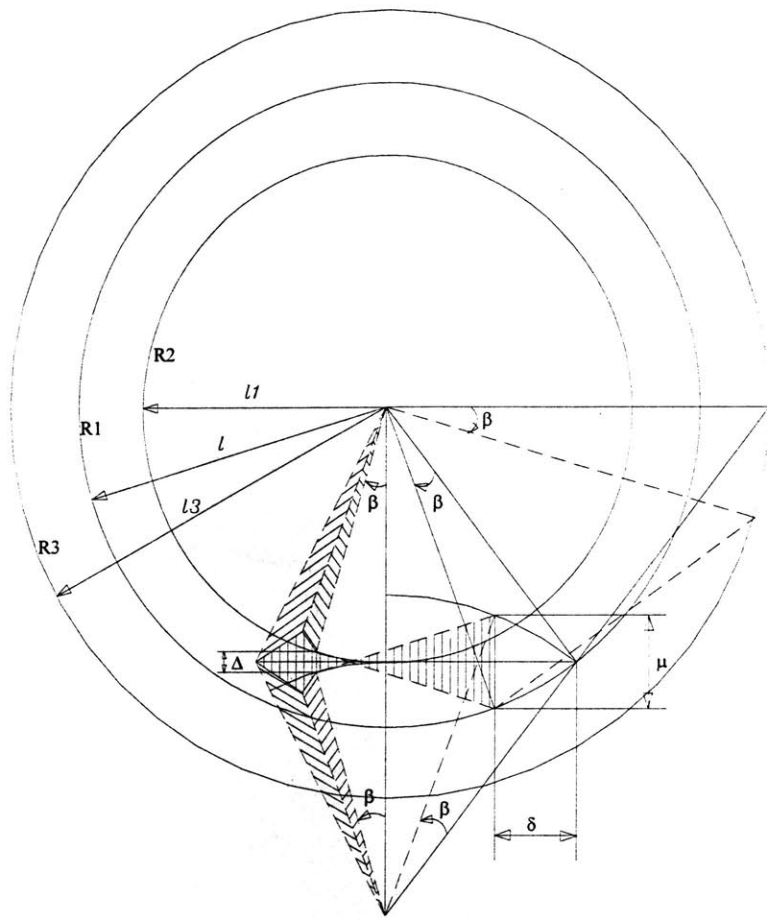
Figure 28: Kinematics of deformation mode (Model A Side View)

Figure 29: Kinematics of deformation mode (Model A Over View)

B. Frontal Bow Stretching

The areas S_1, S_2, S_3, and S_4 that are made up of two triangular shaped cross-sections visualizing deformation zones of frontal bow stretching. Those stretching areas are developed from the contact point where the contact line and the rigid-embankment meet. As the embankment penetrates deeper, the angle 2β in between two horizontal cross sections will be increased. However, the areas will grow only to a certain angle of β. When the initial contact points rotate up to β, the indentation depth δ becomes 2H.

Figure 30: Simplified stretched areas (Bow part)

Assumption is made that for the strain is uniaxial in the local coordinate system (η, ξ):

$$\varepsilon_{\xi\eta} = \begin{vmatrix} 0 & 0 \\ 0 & \varepsilon_{\eta\eta} \end{vmatrix}. \tag{35}$$

Rigid perfectly plastic isotropic material is assumed:

$$N_{\alpha\beta} = \begin{vmatrix} 0 & 0 \\ 0 & N_0 \end{vmatrix} \tag{36}$$

where $N_0 = \sigma_0 t$ is the fully plastic membrane force per unit length and σ_0 is the average flow stress of the material, see Figure 31.
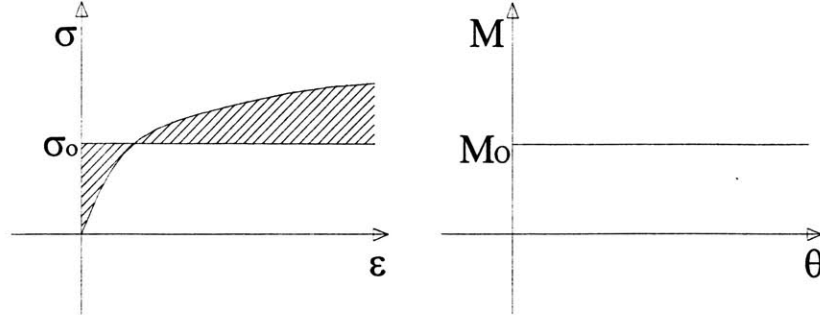
Figure 31: Flow Stress

With the above assumptions the membrane energy dissipation becomes:

$$E_m = \int_S N_{\alpha\beta} \, \varepsilon_{\alpha\beta} dS = \int_S N_0 \, \varepsilon_{\eta\eta} \, dS \qquad (37)$$

As shown in Figure 32, in this deformation zones the strain rate is uniform in x direction and varies in y direction, thus the displacement function U_1 and U_2 for the stretching zones $(0 \leq \xi \leq l_8)$ and $(0 \leq \xi \leq l_7)$ are found as:

$$U_1 = \frac{\Delta}{2 l_8} \xi$$

$$U_2 = -\frac{\mu}{2 l_7} \xi \qquad (38)$$

In performing integration over the deformation zones S_1, S_2, S_3, and S_4, a local coordinate system (η, ξ) is introduced. Therefore, the strain $\varepsilon_{\eta\eta}$ over the deforming zones is a function of η and ξ:

$$\varepsilon_{\eta\eta} = \frac{dU_1}{d\eta} , \frac{dU_2}{d\eta} \qquad (39)$$
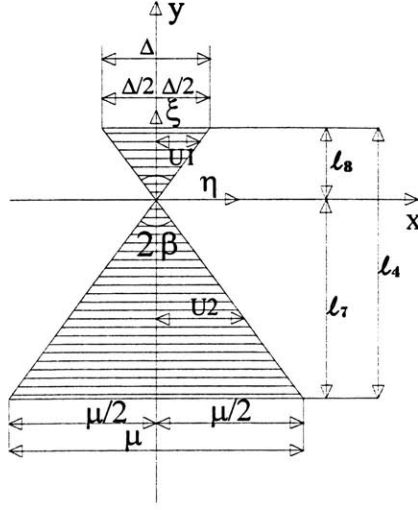
Figure 32:Membrane Stretching Zone (Bow)

The membrane energy dissipation for total deformation zones by the above expression can be expressed as:

$$E_{m1} = 2\int_0^{l_8}\int_0^{\eta} N_0 \frac{dU_1}{d\eta}\,d\eta d\xi = N_0 S_1 = \frac{\Delta^2}{4}\cot\beta$$

$$E_{m2} = 2\int_0^{l_8}\int_0^{\eta} N_0 \frac{dU_2}{d\eta}\,d\eta d\xi = N_0 S_2 = \frac{\mu^2}{4}\cot\beta \qquad (40)$$

As shown in Figure 32 the deformation zones S_1, S_2, and S_3, S_4 are identical, therefore the total membrane energy of the frontal bow stretching becomes:

$$\begin{aligned} E_{mbo} &= E_{m1} + E_{m2} + E_{m3} + E_{m4} = 2E_{m1} + 2E_{m2} \\ &= 2N_0 l^2 \cot\beta\{\sin(\varphi+\beta) - \sin\beta\}^2 \\ &\quad + 2N_0 l^2 \cot\beta\sin^2\varphi(1-\cos\beta)^2 \end{aligned} \qquad (41)$$

Since the angle β is assumed small, the above expression can be written as:

$$E_{mbo} = 2N_0 l^2 \beta\cos^2\varphi \qquad (42)$$

where
$$\sin\beta = \beta, \cos\beta = 1$$

38

C. Side Shell Stretching

The areas S_5 and S_6 that are the areas found between two folding elements simplify the deformation zone of the side shell stretching. In this deformation model the side shell folding is idealized in the triangular and rectangular shapes and fold is formed as the l_3 rotates in clockwise. Since the length l_3 rotates, there must be a stretched area to meet the difference of the length. As shown in Figure 32 the stretched length U can be expressed as:

$$U_X = \Delta - \frac{\Delta}{2H}\xi$$

$$U_0 = \frac{\Delta}{2}$$

(43)

The membrane energy dissipation of the one side can be expressed as follow:

$$E_{ms} = E_{m5} + E_{m6}$$
$$= N_0(S_5 + S_6)$$
$$= N_0(\frac{3}{2}\Delta H)$$

(44)

where E_5 and E_6 are:

$$E_{m5} = \int_S N_0 \varepsilon_{\eta\eta} dS = 2\int_0^H \int_0^\eta N_0 \varepsilon_{\eta\eta} d\eta\, d\xi$$

$$2\int_0^H N_0 U_0 d\xi = N_0 S_5$$

$$E_{m6} = \int_S N_0 \varepsilon_{\eta\eta} dS = 2\int_H^{2H} \int_0^\eta N_0 \varepsilon_{\eta\eta} d\eta\, d\xi$$

$$2\int_H^{2H} N_0 U_0 d\xi = N_0 S_6$$

(45)

Therefore, the side stretching in both sides becomes as:

$$E_{mst} = 2E_{ms}$$
$$= 3N_0 \Delta H$$
$$= 3N_0 l^2 \beta \sin^2 \varphi (1 - \cos\beta)$$

(46)

39
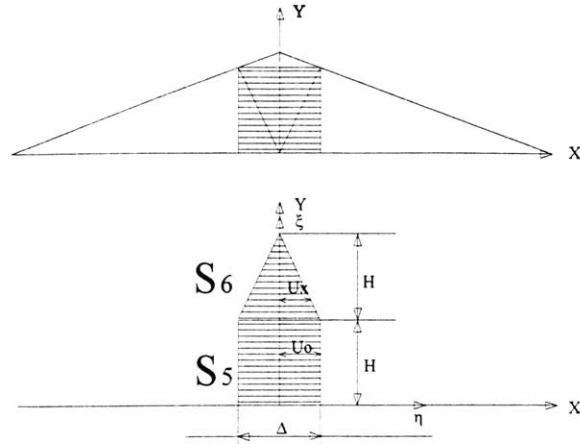
Figure 33:Membrane Stretching Zone (Side)

D. Side Shell Folding

The rate of the bending energy of the side shell folding is calculated from the folding element. In this model (Model A) four identical folding elements are deformed at the same time by the external load. A folding element has four stationary hinge lines, and the bending energy dissipation is calculated from the rotation of these hinge lines. As soon as the as external force is applied the side shell is being folded with wavelength H until another folding is formed. The rate of bending energy of the one folding can be calculated as a sum of the contribution from the four straight hinge lines:

$$\dot{E}_{b1} = \sum_{i=1}^{4} M_0 \dot{\theta}_i l_{3i} \qquad (47)$$

In the above expression it is also assumed that the fully plastic bending moment develops is defined by:

$$M_0 = \frac{\sigma_0 t^2}{4} \qquad (48)$$

40
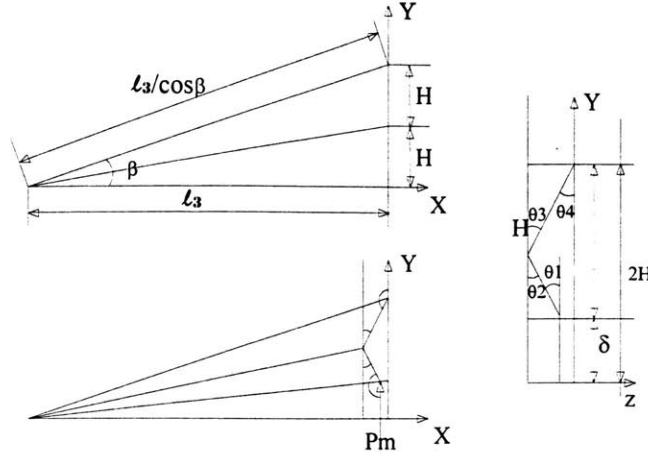
Figure 34: Folding element

As shown in Figure 34 the length of the each hinge line is different. However, if the angle β is assumed small, all hinge lines can be treated as having the same length l. With the above assumption the expression for the bending energy can be written as:

$$E_{b1} = \int_0^{t_1} \dot{E}_{bi}\, dt = 4M_0 l_3 \sum_{i=1}^{4} \int_0^{t_1} \dot{\theta}_i dt \qquad (49)$$

where $\dot{\theta}$ is the rotation rate of the plastic hinge, and the $\dot{\theta}_1 \dot{\theta}_2 \dot{\theta}_3$, and $\dot{\theta}_4$ are assumed same. The t_1 is the total time for the whole deformation process when the θ reaches θ_{max}. Therefore, the above expression can be expressed as:

$$\begin{aligned}
E_{b1} &= 4M_0 l_3 \int_0^{\delta_{max}} \frac{d\delta}{\sqrt{4\delta H - \delta^2}}\, dt \\
&= 4M_0 l_3 \left[\cos^{-1}(1 - \frac{\delta}{2H}) \right]_0^{2H} \\
&= 2\pi M_0 l_3 \sin\varphi
\end{aligned} \qquad (50)$$

Since the four folding elements are deforming at the same time, the total energy dissipation of the side shell folding is:

$$E_{sf} = 8\pi M_0 l \sin\varphi \qquad (51)$$

41

E. Deck Bending

As shown in Figure 35 the rigid body motion of the upper frontal part of the bow is supposed to bend the deck plate. If the thickness of the deck plating is the same as the thickness of the side shell, the expression of the deck bending energy dissipation can be written as:

$$\dot{E}_{db} = M_0 \dot{\beta} l_s \tag{52}$$

$$
\begin{aligned}
E_{db} &= \int_0^{t_1} \dot{E}_{bb} dt = M_0 l_s \int_0^{t_1} \dot{\beta}\, dt \\
&= 4 M_0 l \beta \cos\varphi \tan\theta \\
&= 4 M_0 \delta \cos\varphi \tan\theta
\end{aligned}
$$

When the indentation depth δ reaches 2H, the above expression becomes:

$$E_{db} = 8 M_0 H \cos\varphi \tan\theta \tag{53}$$
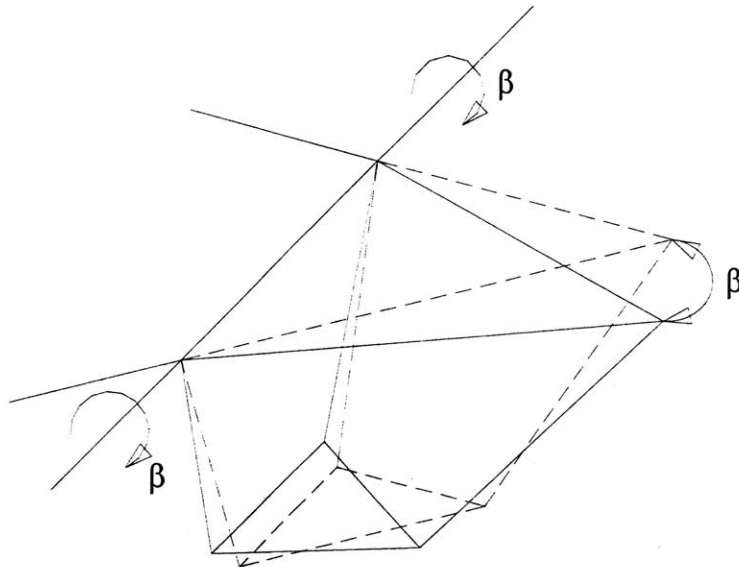
Figure 35: Deck bending

F. Global Equilibrium

With the calculated membrane energy and bending dissipation the crushing force can be found from the global equilibrium. The total external work is:

$$E_{ext} = P_m \cdot 2H \qquad (54)$$

where Pm is the mean crushing force. The integrated form of the principle of the virtual work is:

$$P_m \cdot 2H = (E_m + E_b)\cos\theta \qquad (55)$$

Using equations (41), (51), (53) and (55), the mean crushing force becomes:

$$P_m \cdot l\beta \sin\varphi = (E_{mbo} + E_{mst} + E_{sf} + E_{db})\cos\theta$$
$$= (2N_0 l^2 \beta \cos^2\varphi + 8\pi M_0 l \sin\varphi + 4M_0 l\beta \cos\varphi \tan\theta)\cos\theta \qquad (56)$$

$$P_m = (2N_0 l \cot\varphi\cos\varphi + 8M_0\pi\frac{1}{\beta} + 4M_0 \cot\varphi\tan\theta)\cos\theta \qquad (57)$$

It is postulated that the wavelength H adjusts itself to minimize the mean crushing force. In order to find the unknown H, the mean crushing force is minimized with respect to H (l, β)

$$\frac{dP_m}{dH} = \frac{\partial P_m}{\partial l}\frac{\partial l}{\partial H} + \frac{\partial P_m}{\partial \beta}\frac{\partial \beta}{\partial H} = 0 \qquad (58)$$

We can find optimum H:

$$H_{opt} = \frac{1}{2}t\pi\tan^2\varphi \qquad (59)$$

Substituting the equation (59) into (57), we can obtain the expression for the mean crushing force:

$$P_m = \sigma_0 t \cot\varphi\{8l\cos\varphi + t\tan\theta\}\cos\theta \qquad (60)$$

43

Following table shows the optimum H and Mean Crushing Force (P_m) predicted by the equation (59), (60)

Table 1: Predicted Mean Crushing Strength and Optimum Wave Length

	φ	θ	l(mm)	t(mm)	σ_0(Mpa)	H_{opt}(mm)	P_m(N)
Bow1	60^0	30^0	130	0.7	312	3.297	56828
Bow2	60^0	30^0	65	0.7	312	3.297	28436
Bow3	60^0	30^0	87	0.7	312	3.297	38045
Bow4	60^0	30^0	130	1.2	312	5.652	97473

2. Method-2

The first method gave too high value of the mean crushing force. Therefore, in this section alternative method is tried by considering the path of the membrane deformation area for the same model A.

A. Kinematics of Deformation Mode A

All the assumptions and deformation model are same as 6.1, thus the maximum stretched distances are:

$$\mu = 2l(\sin(\varphi + \beta) - \sin\varphi)$$
$$\Delta = 2l\sin\varphi(1 - \cos\beta) \tag{60-1}$$
$$H = \frac{1}{2}l\beta\sin\varphi$$

B. Frontal Bow Stretching

As shown in Figure 36, in this deformation zones the strain rate is uniform in x direction and varies in y direction, thus the displacement function μ for the stretching zone ($0 \le x \le l_4$) is found as:

$$\mu(\eta) = 2\{l\sin(\varphi + \beta) - l_3\}$$
$$= 2l\{\sin(\varphi + \beta) - \sin\varphi\} \tag{61}$$

The strain in the deforming region is then found as a function of β:

$$\varepsilon_{xx} = \frac{du}{dx} = \frac{\mu}{l} = 2\{\sin(\varphi + \beta) - \sin\varphi \tag{62}$$

If the rotation angle β is assumed small, the above expression can be written as:

$$\varepsilon_{xx} = \sin\varphi(\frac{\delta}{l})^2 + \cos\varphi\frac{\delta}{l} \tag{63}$$

where $\delta = 2H(1-\cos\alpha)$, $\delta_{max} = 2H$ at $\alpha = 90^0$

$$l\beta = \delta_{max} = 2H$$

45
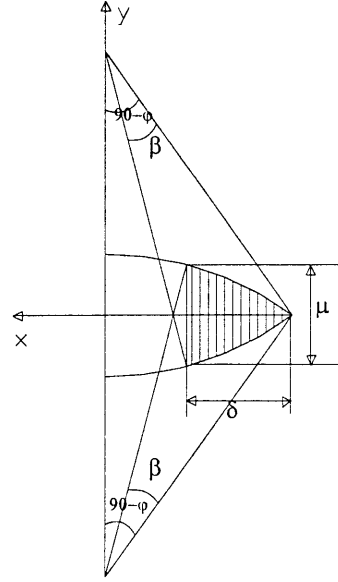
Figure 36: Membrane stretching zone (bow)

The membrane energy dissipation for total deformation zones through the above expression can be expressed as:

$$E_{mbo} = \int_S N_0 \left\{ -\sin\varphi(\frac{\delta}{l})^2 + 2\cos\varphi\frac{\delta}{l} \right\} dS$$

$$= 2(N_0 l\delta^2 \sin^2\varphi \, \cos\varphi + N_0 l\delta \sin\varphi\cos^2\varphi) \qquad (64)$$

where the area of deforming zone $S = H \times 2l_3 = 2l^2 \sin\varphi\cos\varphi$

when δ becomes 2H, above expression is:

$$E_{mbo} = 8(N_0 H^2 \sin^2\varphi \, \cos\varphi + N_0 lH \sin\varphi\cos^2\varphi) \qquad (65)$$

Therefore, the membrane energy dissipation of the both sides becomes:

$$E_{mbo} = 16(N_0 H^2 \sin^2\varphi \, \cos\varphi + N_0 lH \sin\varphi\cos^2\varphi) \qquad (66)$$

46

C. Side Shell Stretching

The deformation field of the side shell can be represented by the function U, see Figure 37.

$$U = l_3 (\frac{1}{\cos \beta} - 1) \tag{67}$$

As assumed in subsection A, the displacement and strain measured in y direction can be written as:

$$\frac{\Delta}{2} = U \cos \beta = l_3 (1 - \cos \beta)$$

$$\varepsilon_{xx} = \frac{d\Delta(y)}{dx} = \frac{2l_3 (1 - \cos \beta)}{l_3} = 2(1 - \cos \beta) \tag{68}$$

Since the β is assumed small, the strain can be written as:

$$\varepsilon_{xx} = \frac{\Delta(y)}{l_3} = 2(1 - \cos \beta) = (\beta^2)$$

$$= (\frac{\delta}{l_3})^2 \tag{69}$$
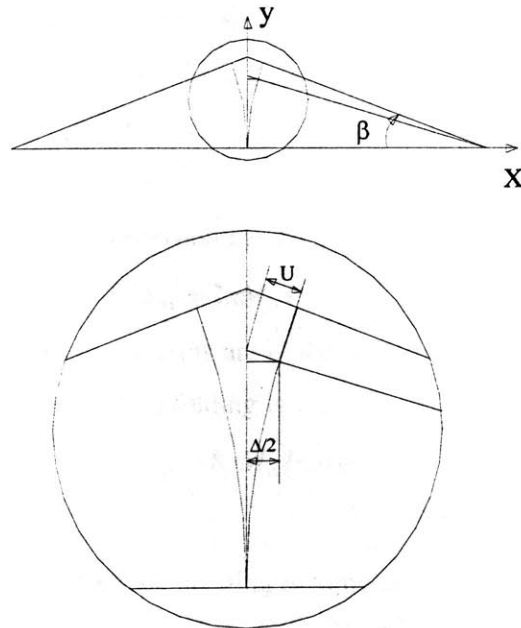
Figure 37: Displacement function Δ(y)

47

The membrane energy dissipation of the side shell stretching is:

$$E_{ms} = \int_S N_0 \varepsilon_{xx} dS$$

$$= \int_S N_0 (\frac{\delta}{l_3})^2 dS \tag{70}$$

$$= 2N_0 \frac{\delta^2}{l_3} H$$

where the area of the stretching zone, S = $l_3 \times 2H$, for both sides:

$$E_{ms} = 8N_0 \frac{\delta^2}{l_3} H \tag{71}$$

when δ becomes $2H$, the above can be written as:

$$E_{ms} = 32 N_0 \frac{H^3}{l \sin \varphi} \tag{72}$$

D. Side Shell Folding

There are no differences between method 1 and 2 in the side shell folding calculation. Thus, the rate of bending energy of the one folding can be calculated as a sum of the contribution from the four straight hinge lines:

$$\dot{E}_{b1} = \sum_{i=1}^{4} M_0 \dot{\theta}_i l_{3i} \tag{73}$$

The bending energy for one folding element is:

$$E_{b1} = \int_0^{t_1} \dot{E}_{bi} dt = 4M_0 l_3 \sum_{i=1}^{4} \int_0^{t_1} \dot{\theta}_i dt \tag{74}$$

Therefore, the above expression can be expressed as:

$$E_{b1} = 2\pi M_0 l_3 \sin \varphi \tag{75}$$

Since the four folding elements are deforming at the same time, the total energy dissipation of the side shell folding is:

$$E_{sf} = 8\pi M_0 l \sin \varphi \tag{76}$$

E. Deck Bending

The expression for the deck bending is same as method 1

$$E_{db} = 8M_0 H \cos \varphi \tan \theta \tag{77}$$

48

F. Global Equilibrium

With the calculated membrane energy and bending dissipation the mean crushing force can be found from the global equilibrium: The total external work is:

$$E_{ext} = P_m \cdot 2H \tag{78}$$

Here, Pm is the mean crushing force. The integrated form of the principle of the virtual work is:

$$P_m \cdot 2H = (E_m + E_b)\cos\theta \tag{79}$$

Using equations (66), (72), (76), and (77), above can be written as:

$$P_m \cdot 2H = (E_{mbo} + E_{ms} + E_{sf} + E_{db})\cos\theta$$

$$= 32N_0 \frac{H^3}{l\sin\varphi}\cos\theta + 16(N_0 H^2 \sin^2\varphi\cos\varphi + N_0 lH \sin\varphi\cos^2\varphi)\cos\theta \tag{80}$$

$$+ (8\pi M_0 l\sin\varphi + 8M_0 H\cos\varphi\tan\theta)\cos\theta$$

or

$$P_m = 18N_0 \frac{H^2}{l\sin\varphi}\cos\theta + 8(N_0 H \sin^2\varphi\cos\varphi + N_0 l\sin\varphi\cos^2\varphi)\cos\theta$$

$$+ (4\pi M_0 \sin\varphi\frac{l}{H} + 4M_0 \cos\varphi\tan\theta)\cos\theta \tag{81}$$

The mean crushing force is minimized with respect to H:

$$\frac{dP_m}{dH} = 0 \tag{82}$$

$$H^3 + \frac{1}{4}H^2 l\sin^2\varphi\cos\varphi - \frac{1}{32}\pi l^2 t\sin\varphi = 0$$

or

$$\left(\frac{H}{l}\right)^3 + \frac{1}{4}\left(\frac{H}{l}\right)^2 \sin^2\varphi\cos\varphi - \frac{\pi}{32}\left(\frac{t}{l}\right) = 0 \tag{83}$$

There is a positive real root of the above cubic equation that minimizes P_m. Table 1, shows H values for each case:

49

Table 2: Optimum H

	φ	θ	l(mm)	t(mm)	EQUATION	H_{opt}(mm)
Bow1	60^0	30^0	130	0.7	$H^3+10.6H^2-1005=0$	7.4
Bow2	60^0	30^0	65	0.7	$H^3+5.3H^2-251=0$	4.95
Bow3	60^0	30^0	87	0.7	$H^3+6.98H^2-440=0$	5.86
Bow4	60^0	30^0	130	1.2	$H^3+10.6H^2-1724=0$	9.4

Substituting the above values into equation (81) gives the final mean crushing force:

Table 3 :Predicted mean crushing forces (Model A)

Bow1	Bow2	Bow3	Bow4
45949 N	30804 N	37048 N	87540 N

Assuming $\varphi=60°$, the inverted form of the solution of the equation (81) is:

$$\left(\frac{t}{l}\right)=\frac{32}{\pi}\left[\left(\frac{H}{l}\right)^3+\frac{1}{32}\left(\frac{H}{l}\right)^2\right] \tag{84}$$

Figure 38

Nondimensional Wavelength to Thickness
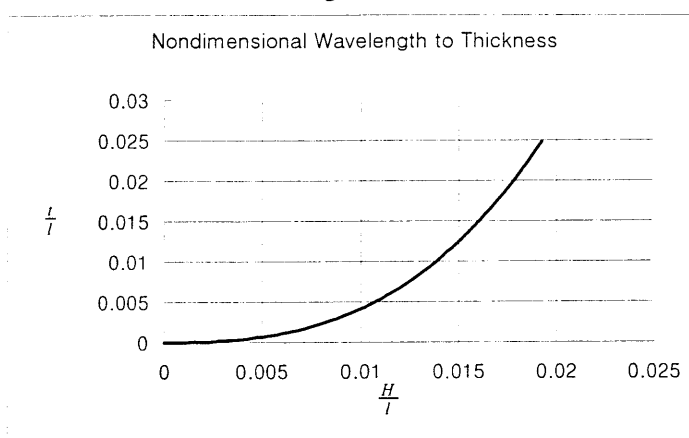
A plot of the function (84) is shown in Fig. 38. For each length to thickness ratio t/l, the corresponding optimum wavelength can be found.

6.2 Mean Crushing Strength (Model B)

The calculation of the mean crushing strength of the deformation model A method 1 and method 2 gave higher value than the actual model test results. Therefore, the improved computation model is made, which folds inwardly. For this model two computational methods are tried in the subsection 1 and 2.

1. Method -1

A. Kinematics of the Deformation Mode

It is assumed that folds in the side shell are formed inward rather than outward, as shown in Fig.25, 26, 27. This assumption dramatically reduces the amount of bending and membrane energies, suggesting that in reality inward folds must be formed. Indeed, the photograph of the damaged picture shows a multiple inward folds, resembling much the present simplified model (Model B). In order to give quick estimates on the mean crushing load, only one fold is considered. The present computational model captures another important feature that is a drop of the tip section of the bow. This section rotates almost as a rigid body about a line on the deck formed by the intersection with the vertical plane. As shown in Fig 39 and 40, the line l_P rotates along the radius R_2 and the line l_M rotates along the radius R_1. Unlike the model A, there is no side shell stretching for model B thus, the side shell folding mode should be different from model A. As we can notice from the Figure 39, 40 the active hinge line l_6 and l_7 allow only the rotation in the clockwise direction. As the rotation angle β starts to form the initial contact point is divided into two parts like the model A case. Since we assumed no side shell stretching and inward folding, the initial length of the H keep constant by the geometric compatibility while the overlapped frontal stretching are being developed to the δ reaches δ_{max} which is 2H, the stretched zones S_1 and S_2 are formed and the side shells are folded inwardly to the angle of $\frac{\pi}{2}$.
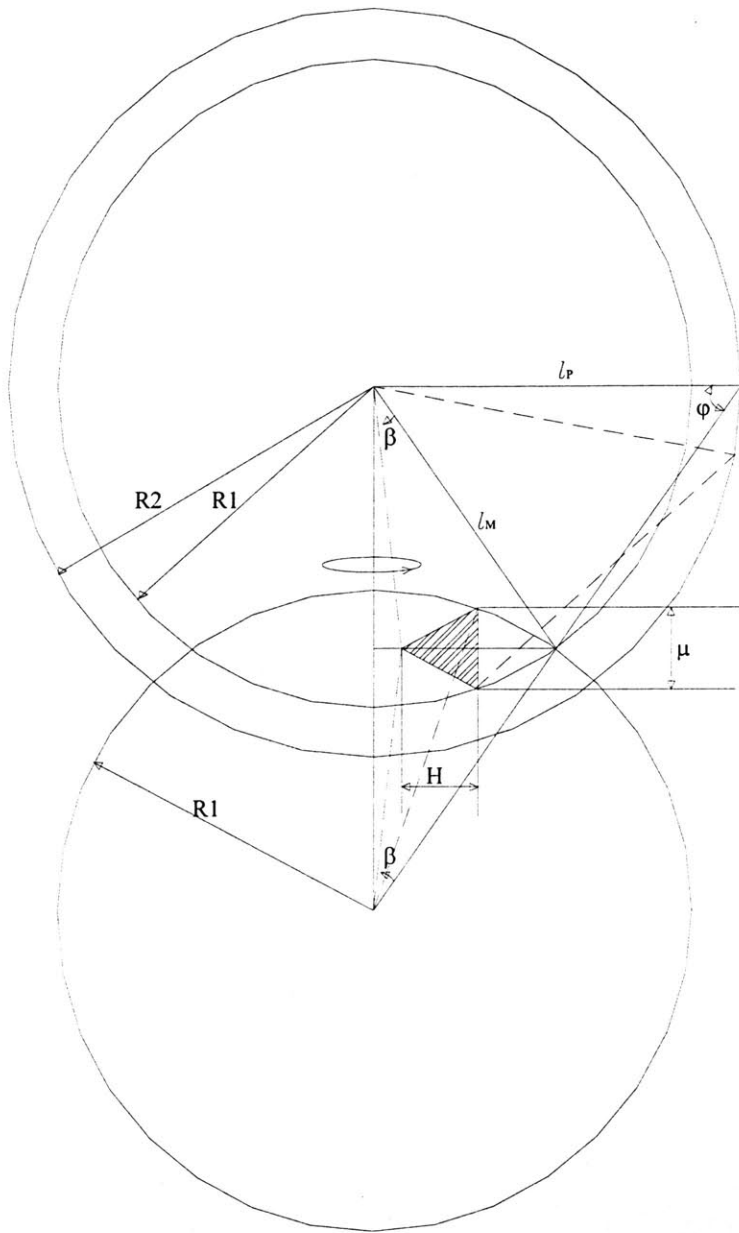
Figure 39:Kinematics of Deformation Mode (Model B-Side View)
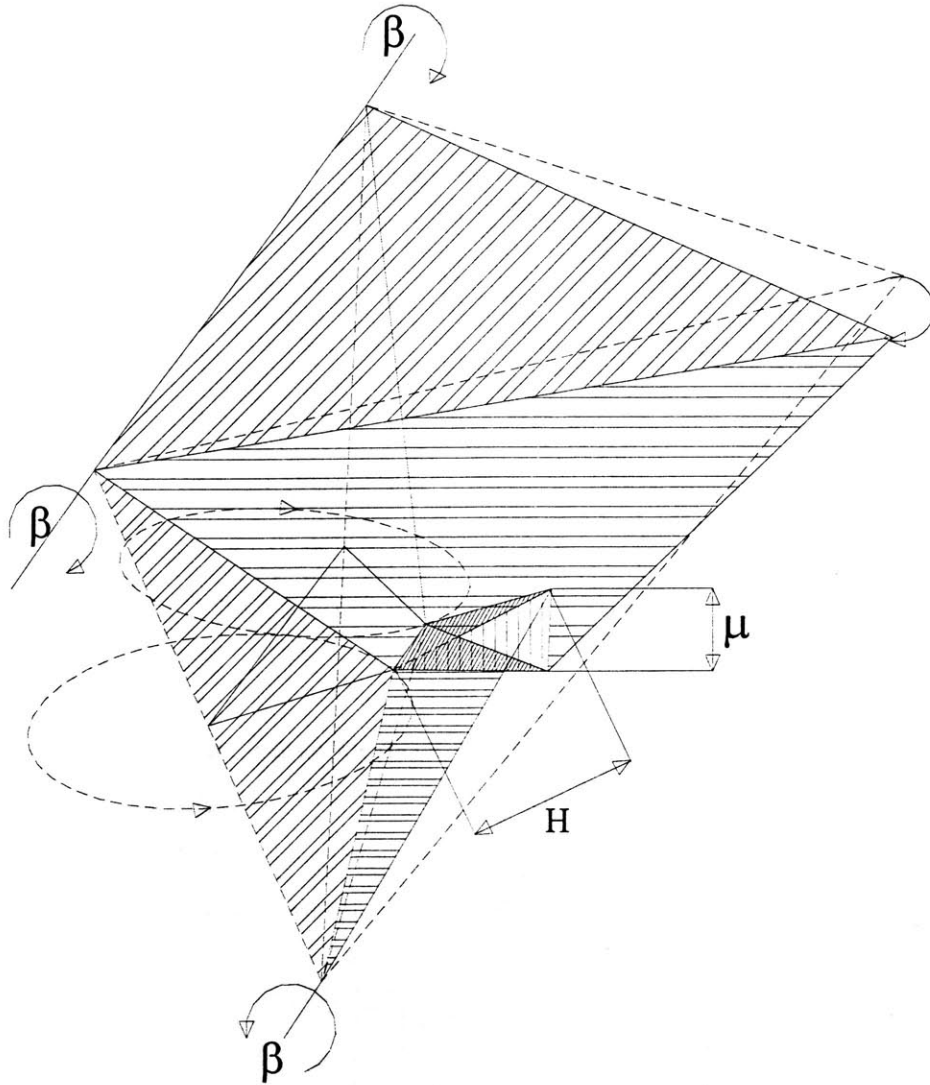
Figure 40:Kinematics Deformation Mode (Model B-Overview)

B. Frontal Bow Stretching

Two triangular shaped cross section S_1 and S_2 represent the frontal bow stretching. As already mentioned in subsection A, once the initial β is formed, the H of the S_1 and S_2 stay constant to the end. Thus, the identical two area S_1 and S_2 becomes just proportional to H and μ, and for the value of H, and μ, in terms of l, β, φ as follow:

$$\mu = 2l(\sin(\varphi + \beta) - \sin\varphi) \approx 2l\beta\cos\varphi$$
$$H \approx \frac{1}{2}l\beta$$

(85)
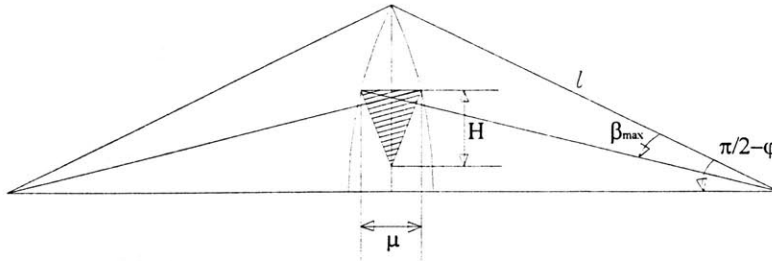
Figure 41: Membrane Stretching Zone (Side).

Another important feature for the bow stretching of the model B is that the base line l_8 is reduced to l_9 by the effect of the side shell folding. However, the reduction of the base line has no effect on the total membrane energy dissipation because we only consider the area S_1 and S_2.
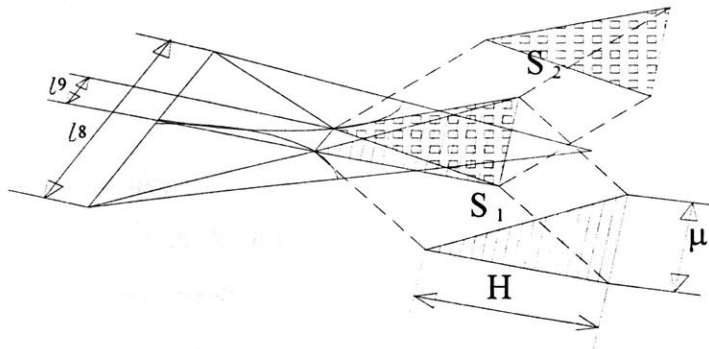
Figure 42: Membrane Stretching Zone (Side S_1, S_2- Over View)

With the same material assumptions for the model A the total membrane energy dissipation can be obtained by the following formula:

$$E_m = \int_s N_{\alpha\beta}\varepsilon_{\alpha\beta}ds$$
$$= \int_s N_0\varepsilon_{\eta\eta}ds$$

(86)

As shown in the figure 42 the sum of the deformed zones S_1 and S_2 become:

$$S_1 + S_2 = 2(\frac{1}{2}\mu H) = 4H^2\cos\varphi$$

(87)

Thus, the total membrane work is equal to:

$$E_m = 4N_0 H^2\cos\varphi$$

(88)

C. Side Shell Folding

The side shell bending energy dissipation for the model B is calculated from the four folding elements. As we already seen for the model A, model B has also four active stationary hinge lines. The only difference is the direction of the folding which does not affect the amount of the total bending energy dissipation. As shown in the Fig.42, the rate of the bending energy dissipation for one folding element becomes:

$$E_{b1} = \sum_{i=1}^{4} M_0 \dot{\theta} l_i$$

(89)

With the same material assumption for the model A the total bending energy dissipation becomes:

$$E_{sb} = 8\pi M_0 l$$

(90)

D. Deck Bending

As we can see from the Figure 38 and 39 the deck bending energy dissipation is exactly same as the model A case. Thus the total deck bending energy becomes:

$$E_{db} = 8M_0 H\cos\varphi\tan\theta$$

(91)

55

E. Mean Crushing Force

The expression for the total external force for model B is given by:

$$E_{ext} = P_m 2H \tag{92}$$

where, P_m is the mean crushing force over the distance H.

Thus, by the principle of the virtual work the global equilibrium can be expressed as:

$$P_m 2H = (E_b + E_m)\cos\theta \tag{93}$$

Substituting the expressions (88), (90), (91) and into equation (93), we can get the expression for the mean crushing force.

$$P_m 2H = (4N_0 H^2 \cos\varphi + 8\pi M_0 l + 8M_0 H \cos\varphi \tan\theta)\cos\theta$$

$$P_m = (2N_0 H^2 \cos\varphi + \frac{4}{H}\pi M_0 l + 4M_0 \cos\varphi \tan\theta)\cos\theta \tag{94}$$

By the minimization of the mean crushing force we can obtain the minimum length of H:

$$\frac{dP_m}{dH} = 0$$

$$H_{opt} = \sqrt{\frac{\pi}{2\cos\varphi}} \, tl \tag{95}$$

Substituting the minimized length H into equation (95), the final mean crushing force can be obtained as:

$$P_m = \sigma_0 (2\sqrt{2\pi \cos\varphi}\ t^{\frac{3}{2}} l^{\frac{1}{2}} + t^2 \cos\varphi \tan\theta)\cos\theta \tag{96}$$

Note that the length l is a distance from the tip to the point of the application of the load. The solution depends on three input parameters σ_0, l, and l.

Following tables show the Optimum H and Mean Crushing Force predicted by the equation (96).

Table 4: Optimum Spacing Length of the Transverse Stiffeners

	φ	θ	σ_0(Mpa)	l(mm)	t (mm)	P_m(N)
Bow1	60	30	312	130	0.71	6394
Bow2	60	30	312	65	0.71	4521
Bow3	60	30	312	86	0.71	5200
Bow4	60	30	312	130	1.2	14352

Taking φ=60° and θ=30°, the above equation becomes

$$P_m = \sigma_0(2\sqrt{2\pi}\,t^{\frac{3}{2}}l^{\frac{1}{2}} + 0.28t^2)\cos\theta = \sigma_0(3.07t^{\frac{3}{2}}l^{\frac{1}{2}} + 0.25t^2) \qquad (97)$$

2. Method -2

A. Kinematics of the Deformation Mode

All the Kinematic assumptions are the same as the Method-1 but the meaning of β. In the previous section β represents an angle within /2- but in this section β= /2- . This assumption makes mathematical calculation simple and neat.

B. Frontal Bow Stretching

As we assumed that the maximum angle β is fixed by initial contact to an embankment, all the hinge lines are stationary hinge lines, and the stretched two triangular shaped cross section S_1 and S_2 can be calculated as following procedure:

$$\mu = 2l(1-\cos\beta) \ = 2l(1-\sqrt{1-\sin^2\beta}) = \frac{4H^2}{l} \tag{98}$$

where
$$H = \frac{1}{2}l\beta$$
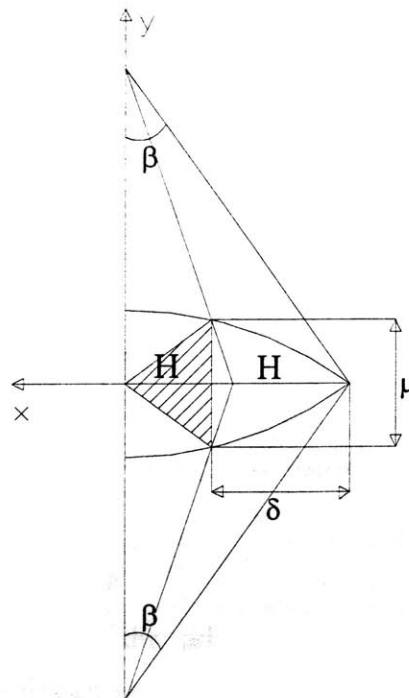
Figure 43: Membrane Stretching Zone (Side).

With the same material assumptions for the model A the total membrane energy dissipation can be obtained by the following formula:

$$E_m = \int_S N_{\alpha\beta}\varepsilon_{\alpha\beta}ds$$
$$= \int_S N_0\varepsilon_{\eta\eta}ds$$

(99)

The deformed areas in the figure 43 is on the both sides of the bow, thus the sum of the total stretched areas becomes:

$$2S = 2(\frac{1}{2}\mu H) = \frac{4H^3}{l}$$

(100)

Thus, the total membrane energy is equal to:

$$E_m = \frac{4H^3}{l}N_0$$

(101)

C. Side Shell Folding

With the same material assumption and kinematic model as the method-1 the total bending energy dissipation becomes:

$$E_{sb} = 8\pi M_0 l$$

(102)

D. Deck Bending

As we can see from the Figure 38 the deck bending energy dissipation is exactly same as the method-1 case. Thus the total deck bending energy becomes:

$$E_{db} = 8M_0 H \cos\varphi \tan\theta$$

(103)

E. Mean Crushing Force

Considering bow angle , the principle of the virtual work the global equilibrium can be expressed as:

$$P_m\, 2H = (E_b + E_m)\cos\theta$$

(104)

59

Substituting the expressions (101), (102), (103) and into equation (104), we can get the expression for the mean crushing force:

$$P_m 2H = (\frac{4H^3}{l}N_0 + 8\pi M_0 l + 8M_0 H \cos\varphi \tan\theta)\cos\theta$$

$$P_m = (\frac{4H^2}{l}N_0 + \frac{8\pi}{H}M_0 l + 8M_0 \cos\varphi \tan\theta)\cos\theta$$

(105)

By the minimization of the mean crushing force we can obtain the minimum length of H:

$$\frac{dP_m}{dH} = 0$$

$$H_{opt} = \left(\frac{t}{4}l^2\pi\right)^{\frac{1}{3}}$$

(106)

Substituting the minimized length H into equation (105), the final mean crushing force can be obtained as:

$$P_m = \sigma_0 t^2 (5.10\left(\frac{l}{t}\right)^{\frac{1}{3}} + \cos\varphi \tan\theta)\cos\theta$$

(107)

Following tables show the Optimum H and Mean Crushing Force predicted by the equation (106) and (107).

Table 5: Optimum Spacing Length of the Transverse Stiffeners

	φ	θ	σ_0(Mpa)	l(mm)	t (mm)	H_{opt}(mm)
Bow1	60	30	312	130	0.71	21.01
Bow2	60	30	312	65	0.71	13.24
Bow3	60	30	312	86	0.71	15.95
Bow4	60	30	312	130	1.2	25.15

Taking φ=60° and θ=30°, the above equation becomes

$$P_m = \sigma_0 t^2 (5.10\left(\frac{l}{t}\right)^{\frac{1}{3}} + 0.288)\cos\theta$$

(108)

60

3. Method-3 (Quick Estimation)

A. Analysis of the Kinematics

The present computational model is the same as the method 1 and 2. In order to give a quick estimate on the mean crushing load, only one fold is considered. Unlike the method 1 and 2 for which an exact geometry was worked out, the degree of overlapping plates and the amount of rotation about stationary hinge lines were determined from measurement taken on the paper model of the bow.

B. Simplified Kinematics

1. There is no overlapping between the triangles ADE and BDE meaning that the membrane energy is zero over these areas.

2. There is a triangular overlap in the triangle AEF and BEF with the maximum value $\frac{\Delta}{2}$ on each side.

3. The relative rotation along active hinge lines ADB and AEB is approximately equal to $\alpha_f = \pi/2$.

4. The energy of deck rotation is small compared to the other contribution and, this is neglected.

C. Calculation

From the geometry one can find that:

$$\Delta = 2l(1 - \frac{2}{\sqrt{3}}) = 0.27l \tag{109}$$

Now, the membrane work is equal to:

$$E_m = 2N_0(\frac{\Delta}{2} \cdot \frac{l}{4}) = 0.066N_0 l^2 \tag{110}$$

where the coefficient 2 stands for two sides of the bow.

There are eight hinge lines, each of the length l . The bending energy is thus:

$$E_b = 8M_0 l \alpha_f = 4\pi M_0 l \tag{111}$$

61

The external work is given by:

$$E_{ext} = P_m \frac{l}{2} \tag{112}$$

where, P_m is the mean crushing force over the distance $l/2$.

Substituting the expression (109), (110) and (111) into equation (112) one gets the final expression for the mean crushing force.

$$P_m = \sigma_0 (0.134l\, t + 6.28t^2)\cos\theta \tag{113}$$

Note that l is a distance from the bow tip to the point of the application of the load. The solution depends on three input parameters σ_0, l, and t.
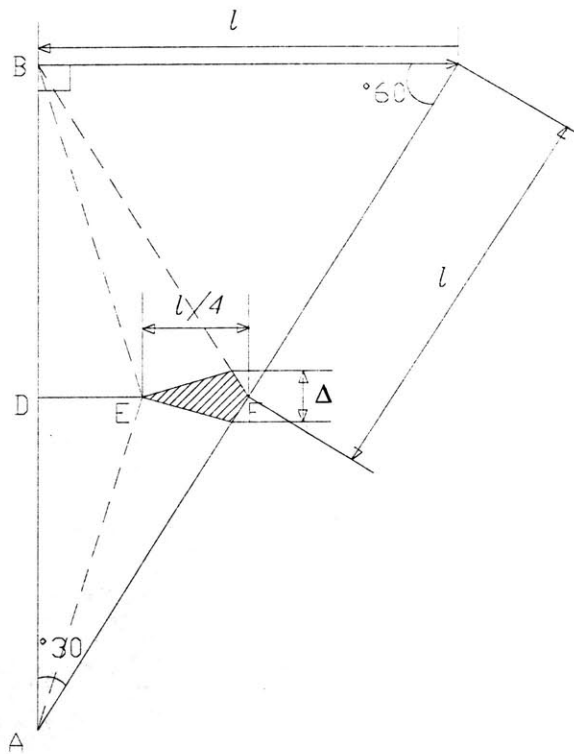

Figure 44: Kinematics of deformation mode (Model B-Method 3)

6.3 Mean Crushing Strength (Two Folding Model)

1. Unstiffened Two Folding Model

A close investigation of the model test results reveals that the tetrahedral part generally has natural two folding wave when the ratio $\frac{l}{t}$ is about $100 < \frac{l}{t} < 250$, which is also observed in the Force-Indentation graph of model test (Fig.61, 71, 76, 81, 86) except bow model 2 that has ratio of 92. Therefore, this section will treat two folding cases that are natural two-fold case and stiffened two-fold case. The mathematical calculation procedure is based on model B-method 2.

A. Kinematics of the Deformation Mode

It is assumed that the first fold is divided by 2:1 ratio as observed in model test (see figure 45.46). The second fold is divided by 1: 1 ratio as usual. As one can see from figure 47, the dimension of the l_{10}, wavelength, and maximum side stretching of the first folds are calculated as follow:
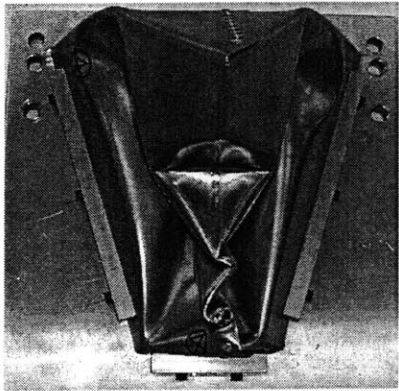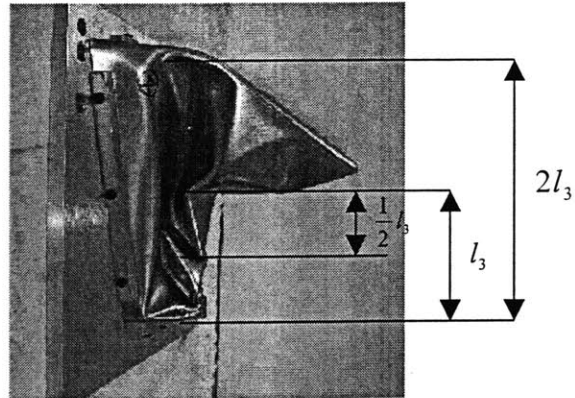

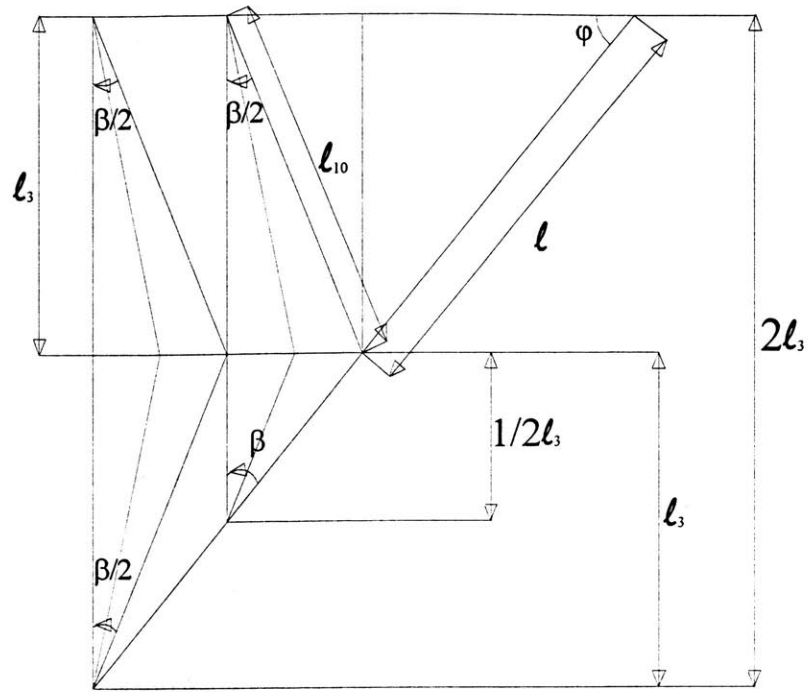Figure 45: Two Folding Model   Figure 46: Folding Measurement

Figure 47: Kinematics of two folding case

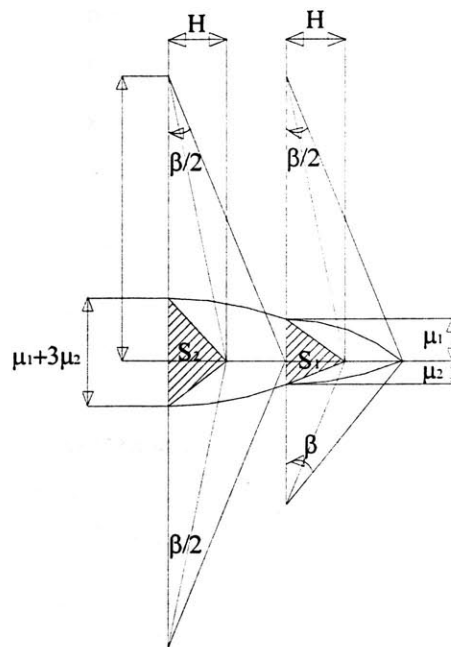
Figure 48: Membrane stretching zones

$$H \approx \frac{1}{4}l\beta$$

$$l_{10} \approx l$$

$$u_1 = \frac{l}{2}\{1 - \cos\beta\} \approx \frac{4H^2}{l} \qquad (114)$$

$$u_2 \approx l(1 - \cos\frac{\beta}{2}) \approx \frac{2H^2}{l}$$

where
$$\sqrt{1 - (\sin\frac{\beta}{2})^2} \approx 1 - \frac{1}{2}\left(\frac{2H}{l}\right)^2$$

Once the wavelength H is formed in the first fold, it keeps the H in the second fold. Therefore, the angle and the length of folding wave uniquely define the geometry of each fold (see figure 47).

B. Mean Crushing Force for the First Folding

(1) Membrane Energy

The calculation of the membrane energy of the bow part can be calculated by the superposition of the first fold case and second fold case, and calculation procedure of the first fold as follows:

The stretched area of the first fold (one side of bow) is:

$$S_1 = \frac{1}{2}H(u_1 + u_2)$$

$$= \frac{3H^3}{l} \qquad (115)$$

Therefore, the total membrane energy dissipation of both side of bow become:

$$E_{bm1} \approx 2S_1 N_0 = \frac{6H^3}{l}N_0 \qquad (116)$$

(2) Bending Energy

Since the lower part of the first fold has the hinge length $\frac{l}{2}$, the bending energy for the first folding become:

$$E_{yf1} \approx 6M_0 l\pi \qquad (117)$$

65

(3) Deck Bending Energy

The first deck bending energy dissipation occurs at the $\frac{3}{4}l_s$ and $l_s = 4lcon\varphi \tan\theta$

thus, the first deck bending energy dissipation becomes:

$$E_{db1} = 12M_0 H \cos\varphi \tan\theta \qquad (118)$$

(4) Global Equilibrium

The mean crushing force for the first fold can be obtained as:

$$P_{m1}2H = (\frac{6H^3}{l}N_0 + 6M_0 l\pi + 12M_0 H \cos\varphi \tan\theta)\cos\theta$$

$$P_{m1} = (\frac{3H^2}{l}N_0 + \frac{3}{H}M_0 l\pi + 6M_0 \cos\varphi \tan\theta)\cos\theta \qquad (119)$$

To find an optimum wavelength, and the mean crushing force, the above equation is minimized with respect to H:

$$\frac{\partial P_{m1}}{\partial H} = 0$$

$$H_{opt1} = \frac{1}{2}\left(tl^2\pi\right)^{\frac{1}{3}} \qquad (120)$$

Substituting the expression (120) into equation (119), we can obtain the expression for the mean crushing force for the first folding:

$$P_{m1} = \sigma_0 t^2 \{4.82\left(\frac{l}{t}\right)^{\frac{1}{3}} + 1.5\cos\varphi \tan\theta\}\cos\theta \qquad (121)$$

To compare the obtained mean crushing force with the model test result, the dimension of the bow model 5 (θ=30°, φ=60°, l=150mm, t=0.71mm.) were plugged into equation (110):

$$P_{m1} = \sigma_0 t^2 \{4.82\left(\frac{l}{t}\right)^{\frac{1}{3}} + 0.433)\cos\theta$$

$$P_{m1} \approx 3876N$$

$$H_{opt1} \approx 18.35mm \qquad (122)$$

66

C. Mean Crushing Force for the Second Folding

(1) Membrane Energy

As we can see from the figure 48, the second fold has the increased stretched areas by $2\mu_2$. Thus, the total membrane energy for the second fold becomes:

$$E_{bm2} \approx 2S_2 N_0 = H(u_1 + 3u_2) = \frac{10H^2}{l} N_0 \qquad (123)$$

(2) Bending Energy

For the second folding all hinge lines are assumed to have the length l therefore, the side shell bending energy for both side of bow becomes:

$$E_{sf2} \approx 8M_0 l\pi \qquad (124)$$

(3) Deck Bending Energy

The second deck bending energy dissipation becomes:

$$E_{db2} = 16M_0 H \cos\varphi \tan\theta \qquad (125)$$

(4) Global Equilibrium

The mean crushing force for the second fold can be obtained as:

$$P_{m2} 2H = (\frac{10H^3}{l} N_0 + 8M_0 l\pi + 16M_0 H \cos\varphi \tan\theta)\cos\theta$$

$$P_{m2} = (\frac{5H^2}{l} N_0 + \frac{4}{H} M_0 l\pi + 8M_0 \cos\varphi \tan\theta)\cos\theta \qquad (126)$$

To find optimum wavelength, and the mean crushing force, the above equation is minimized with respect to H:

$$\frac{\partial P_{m2}}{\partial H} = 0$$

$$H_{opt2} = \left(\frac{1}{10} t l^2 \pi\right)^{\frac{1}{3}} \qquad (127)$$

Substituting the expression (127) into equation (126), we can obtain the expression for the mean crushing force for the first fold:

$$P_{m2} = \sigma_0 t^2 \{6.92 \left(\frac{l}{t}\right)^{\frac{1}{3}} + 2\cos\varphi \tan\theta\} \cos\theta \tag{128}$$

To compare the obtained mean crushing force to the model test result, the dimension of the bow model 5 (θ=30°, φ=60°, l=150mm, t=0.71mm.) were plugged into equation (128):

$$P_{m2} = \sigma_0 t^2 \{6.92 \left(\frac{l}{t}\right)^{\frac{1}{3}} + 0.577) \cos\theta$$

$$P_{m2} \approx 5533N$$

$$H_{opt2} \approx 17.03mm \tag{129}$$

The visual comparison is made in the chapter 7

2. Analysis on the Stiffened Bow Structure (Two Folds)

As we can see from the figure 44 the transversely stiffened structure is supposed to be folded two times because the stiffeners played as the bending guide are located at the wavelength 2*H*. Therefore, the general deformation mode of the stiffened model (model 6) can be treated similarly as the natural two folding case (bow 4). The material character and the thickness of the stiffeners are the same as the shell part. Therefore, if the bending occurs at the stiffened zones, one can calculate mean crushing force simply by smearing the stiffeners' thickness to the shell plate. However, the important feature in the stiffened bow crash observed is the side shell bending occurs by escaping the stiffened areas, which is very difficult case to predict mean crushing force analytically. But it is not impossible to predict boundary of the mean crushing forces and also validate the effectiveness of the optimum space of the stiffeners through the comparison of the mean crushing forces of the stiffened and unstiffened bow.
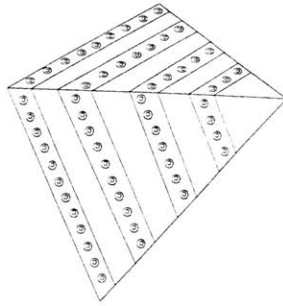
68

Figure 49: Stiffened bow structure
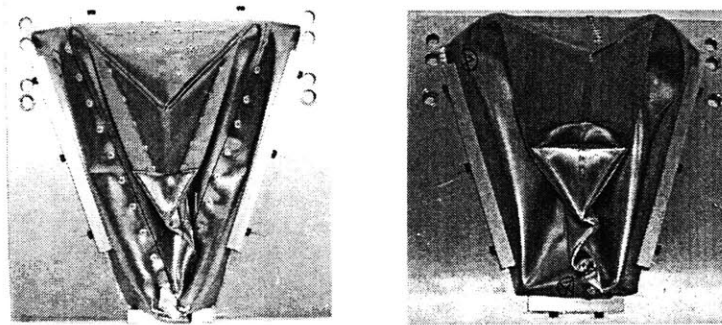
Figure 50: Comparison of stiffened and unstiffened two folds

A. Membrane Energy Calculation with Equivalent Thickness

The ratio of the width of the stiffeners and the space between the stiffeners is 3 (see figure 51), and the thickness of the shell and stiffener is same, therefore the fully plastic tension load per unit length can be as follows:

$$N_0 = \sigma_0 (1 + \frac{1}{3})t = \frac{4}{3}\sigma_0 t \approx 1.33\sigma_0 t \qquad (130)$$

Figure 51: Equivalent Thickness

B. Mean Crushing Force (Bow 6)

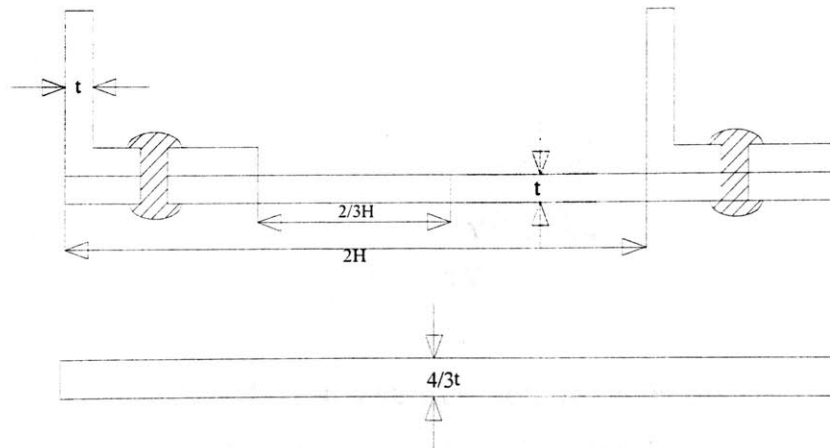As already mentioned, the stiffeners only contribute to confine the pattern of the side shell folding, and the shell folding occurs by escaping the stiffened areas. The mean crushing force of the stiffened bow structure should be calculated by considering the equivalent thickness for membrane energy calculation and reduced wavelength $2/3H$ (unstiffened areas) where the actual bending occurs. (Figure 51):

$$
\begin{aligned}
P_{m1} &= \{\frac{3H^2}{l} N_0 + \frac{3}{H} M_0 l\pi + 6M_0 \cos\varphi \tan\theta\} \cos\theta \\
&= \{\frac{3(\frac{2}{3}H)^2}{l} \sigma_0(\frac{4}{3}t) + \frac{3}{\frac{2}{3}H} \cdot \frac{1}{4}\sigma_0 t^2 l\pi + 6\frac{1}{4}\sigma_0 t^2 \cos\varphi\tan\theta\}\cos\theta \\
&= \{\frac{16}{9l} H^2\sigma_0 t + \frac{9}{8H}\sigma_0 t^2 l\pi + \frac{3}{2}\sigma_0 t^2 \cos\varphi\tan\theta\}\cos\theta
\end{aligned}
\tag{131}
$$

$$
\begin{aligned}
P_{m2} &= (\frac{5H^2}{l} N_0 + \frac{4}{H} M_0 l\pi + 8M_0 \cos\varphi\tan\theta)\cos\theta \\
&= \{\frac{80}{27l} H^2\sigma_0 t + \frac{3}{2H}\sigma_0 t^2 l\pi + 2\sigma_0 t^2 \cos\varphi\tan\theta\}\cos\theta
\end{aligned}
\tag{132}
$$

C. Application

To compare the obtained mean crushing force with the model test results, the dimensions of the bow model 6 (H=18.75mm, θ=30°, φ=60°, l=150mm, t=0.71mm.) were substituted into the equation (131), (132), and the mean crushing forces were obtained as follows:

$$
\begin{aligned}
P_{m1} &\approx 4586N \\
P_{m2} &\approx 6378N
\end{aligned}
\tag{133}
$$

If we assume that the side shell folds were occurred at the stiffened area, we can obtain the mean crushing force by substituting the 1.33 t into the equation

(122) and (128) however, these values can be used as the upper limits of the mean crushing forces of the transversely stiffened bow structure:

$$P_{m1} \approx 6243N$$
$$P_{m2} \approx 8992\,N \tag{134}$$

Furthermore, if we assume that the values of the mean crushing forces (133) represent the true value of mean crushing forces, in fact those show good match with test result (see figure 85), the mean crushing forces increased by stiffeners is about 18% for P_{m1} and is about 15% for P_{m2} by the comparison with the natural two folds calculation (Eq.122, 128). These prove that the application of the transverse stiffeners is less effective to increase bow structural strength than the use of equivalent thickness because the mean crushing forces P_{m1} and P_{m2} were increased about 62% by the use of $1.33t$ to (Eq.134). Although the use of the transverse stiffeners turned out less effective than the use of equivalent thickness for above case, transverse stiffeners could increase the bow strength more effectively by using narrow and thin stiffeners that are barely enough to create side shell folds. In the next subsection 3 a comparison is made for three-fold case and smeared natural two-fold case to see the effectiveness in increasing structural strength.

3. Analysis on the Stiffened Bow Structure (Multi Folds)

If we assume that the bow structure has more transverse stiffeners as shown in figure 52, the general deformation mode will be like figure 53.
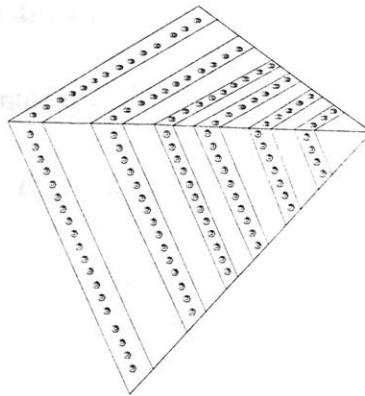

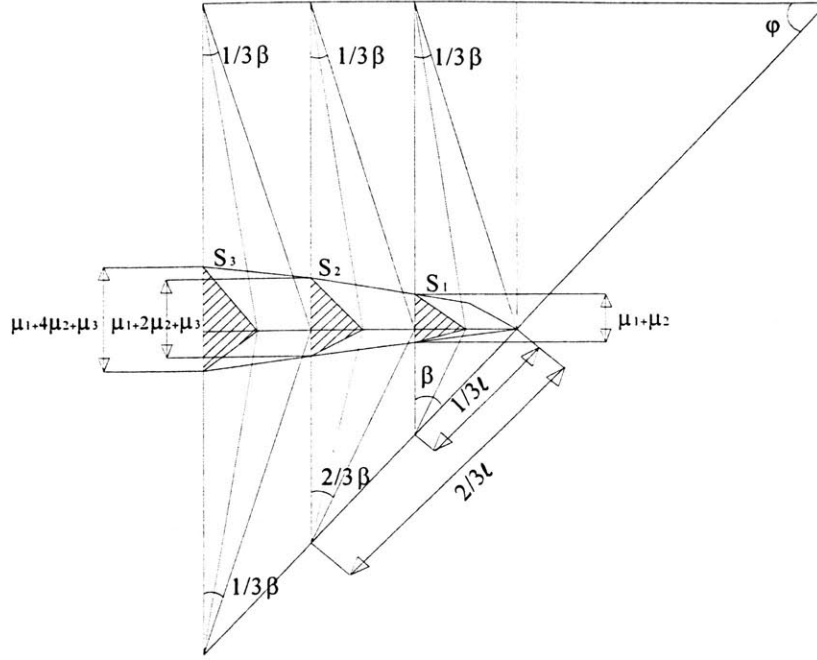Figure 52: Three folds induce stiffened bow structure

Figure 53: Kinematics of the three folding bow

A. Membrane Energy

The calculation of the membrane energy can be calculated by the superposition of the first fold, second fold, and third fold.

The stretched areas for each folding case are:

$$
\begin{aligned}
S_1 &= \frac{1}{2} H(u_1 + u_2) = \frac{1}{2}\left(\frac{6H^3}{l} + \frac{2H^3}{l}\right) = \frac{4H^3}{l} \\
S_2 &= \frac{1}{2} H(u_1 + 2u_2 + u_3) = \frac{1}{2}\left(\frac{6H^3}{l} + 2\frac{2H^3}{l} + \frac{3H^3}{l}\right) = \frac{13H^3}{2l} \\
S_3 &= \frac{1}{2} H(u_1 + 4u_2 + u_3) = \frac{1}{2}\left(\frac{6H^3}{l} + 4\frac{2H^3}{l} + \frac{3H^3}{l}\right) = \frac{17H^3}{2l}
\end{aligned}
\tag{135}
$$

Therefore, the membrane energies for each fold on both sides of the bow are:

$$
E_{bm1} \approx 2S_1 N_0 = \frac{8H^3}{l} N_0
$$

$$
E_{bm2} = 2S_2 N_0 = \frac{13H^3}{l} N_0
\tag{136}
$$

$$
E_{bm3} = 2S_3 N_0 = \frac{17H^3}{l} N_0
$$

B. Bending Energy

Since the lower part of the first fold and second fold have the hinge length $\frac{l}{3}, \frac{2l}{3}, l$, the bending energies for the first fold, second fold, and third fold become:

$$E_{sf1} = 4M_0 l\pi + \frac{4}{3}M_0 l\pi = \frac{16}{3}M_0 l\pi$$

$$E_{sf2} = 4M_0 l\pi + \frac{8}{3}M_0 l\pi = \frac{20}{3}M_0 l\pi \tag{137}$$

$$E_{sf3} = 4M_0 l\pi + 4M_0 l\pi = 8M_0 l\pi$$

C. Deck Bending Energy

The first deck bending energy dissipation occurs at $\frac{2}{3}l_s$, the second at $\frac{5}{6}l_s$, and the third at $l_s = 4lcon\varphi \tan\theta$ thus, each deck bending energy dissipation becomes:

$$E_{db1} = 8M_0 H \cos\varphi \tan\theta$$

$$E_{db2} = 10M_0 H \cos\varphi \tan\theta \tag{138}$$

$$E_{db3} = 12M_0 H \cos\varphi \tan\theta$$

D. Global Equilibrium

The mean crushing forces for each fold are:

$$P_{m1}2H = (\frac{8H^3}{l}N_0 + \frac{16}{3}M_0 l\pi + 8M_0 H \cos\varphi \tan\theta)\cos\theta$$

$$= (\frac{4H^2}{l}N_0 + \frac{8}{3H}M_0 l\pi + 4M_0 \cos\varphi \tan\theta)\cos\theta$$

$$P_{m2}2H = (\frac{13H^3}{l}N_0 + \frac{20}{3}M_0 l\pi + 10M_0 H \cos\varphi \tan\theta)\cos\theta$$

$$= (\frac{13H^2}{2l}N_0 + \frac{10}{3H}M_0 l\pi + 5M_0 \cos\varphi \tan\theta)\cos\theta \tag{139}$$

$$P_{m3}2H = (\frac{17H^3}{l}N_0 + 8M_0 l\pi + 12M_0 H \cos\varphi \tan\theta)\cos\theta$$

$$= (\frac{17H^2}{2l}N_0 + \frac{4}{H}M_0 l\pi + 6M_0 \cos\varphi \tan\theta)\cos\theta$$

73

E. Strength Comparison

By adding two more stiffeners to the bow 6, one more stiffener is in the undeformable bow tip part, three folds are induced, and equivalent thickness becomes 1.5t, and the reduced wavelength becomes 1/2H for this time. The calculation of the mean crushing forces is similar as the calculation of the equation (131). By considering the increased plate thickness 1.5t for membrane energy calculation and decreased wavelength 1/2H, the calculation becomes:

$$P_{m1} = (\frac{4(\frac{1}{2}H)^2}{l}\sigma_0(1.5t) + \frac{8}{3(\frac{1}{2}H)}\frac{\sigma_0 t^2}{4}l\pi + 4\frac{\sigma_0 t^2}{4}\cos\varphi\tan\theta)\cos\theta$$

$$= (\frac{3H^2}{2l}\sigma_0 t + \frac{4}{3H}\sigma_0 t^2 l\pi + \sigma_0 t^2 \cos\varphi\tan\theta)\cos\theta$$

$$P_{m2} = (\frac{13(\frac{1}{2}H)^2}{2l}\sigma_0(1.5t) + \frac{10}{3(\frac{1}{2}H)}\frac{\sigma_0 t^2}{4}l\pi + 5\frac{\sigma_0 t^2}{4}\cos\varphi\tan\theta)\cos\theta$$

$$= (\frac{39H^2}{16l}\sigma_0 t + \frac{5}{3H}\sigma_0 t^2 l\pi + \frac{5}{4}\sigma_0 t^2 \cos\varphi\tan\theta)\cos\theta$$

$$P_{m3} = (\frac{17(\frac{1}{2}H)^2}{2l}\sigma_0(1.5t) + \frac{4}{(\frac{1}{2}H)}\frac{\sigma_0 t^2}{4}l\pi + 6\frac{\sigma_0 t^2}{4}\cos\varphi\tan\theta)\cos\theta$$

$$= (\frac{51H^2}{16l}\sigma_0 t + \frac{2}{H}\sigma_0 t^2 l\pi + 1.5\sigma_0 t^2 \cos\varphi\tan\theta)\cos\theta$$

(140)

Subsisting the dimensions of the bow 5 (H=18.75mm, l=150mm, t=0.7mm, φ=60°, θ=30°), mean crushing forces above are found as:

$$P_{m1} \approx 5137N$$
$$P_{m2} \approx 6671N$$
$$P_{m3} \approx 7373N$$

(141)

To compare the effectiveness of the stiffeners, the equivalent thickness 1.5t=1.05mm is substituted to the minimized mean crushing forces of natural two folding case (equation 121, 128):

$$P_{m1} \approx 7635N$$
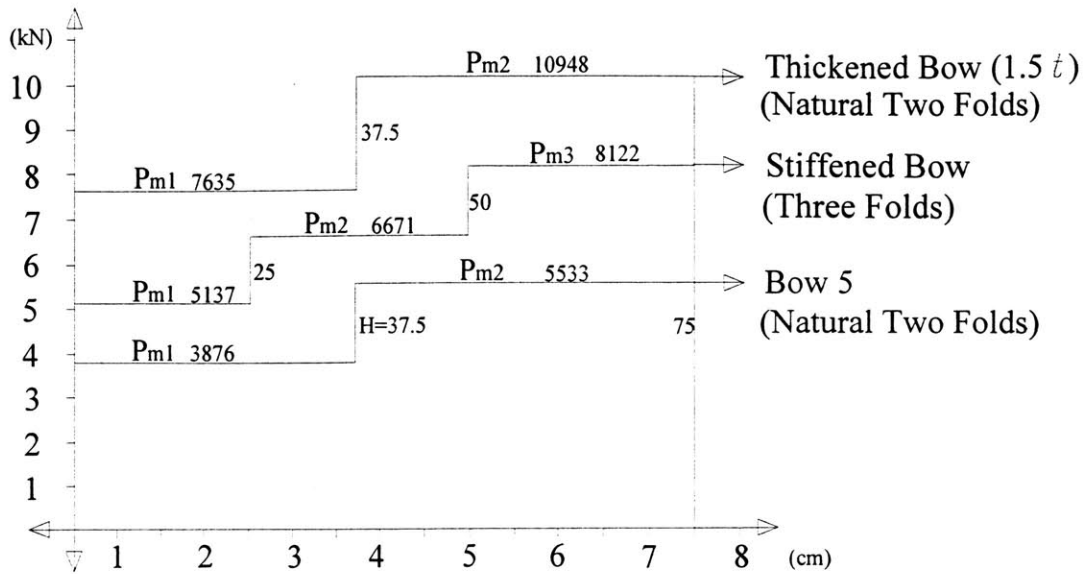$$P_{m2} \approx 10948N$$

(142)

Figure 54: Strength comparison

As we can see from above graph, the comparison is made with unstiffened two folds case of bow 5. The simple smearing (1.5t) of the transverse stiffeners increases the P_{m1} 96% and P_{m2} 97 %, while the three folds induced bow structure increases overall mean crushing force by 38%. This results show that the importance of the using the stiffeners wisely.

F. Crashworthiness Analysis of Multi-Folding Case

In the previous analysis, the effectiveness of the transverse stiffeners was less than the smeared thickness, which caused by the large width and thickness of the stiffeners. However, the width and the thickness of the transverse stiffeners of a real ship bow structure must be much more narrow and thinner than the above cases. To see the relation between the crashworthiness and the number of the side shell folds, the thickness and width of the stiffeners are ignored for this time, and the mean crushing forces of the first fold, the second fold, and the third fold are compared.

75

The expression of the minimized mean crushing forces and their values applied to the dimensions of the bow 5 as follows:

One fold:
$$P_m = \sigma_0 t^2 \{5.10\left(\frac{l}{t}\right)^{\frac{1}{3}} + \cos\varphi\tan\theta\}\cos\theta = 4078 \text{ (N)} \qquad (143)$$

Two folds:
$$P_{m1} = \sigma_0 t^2 \{4.82\left(\frac{l}{t}\right)^{\frac{1}{3}} + 1.5\cos\varphi\tan\theta)\cos\theta = 3876 \text{ (N)} \qquad (144)$$

$$P_{m2} = \sigma_0 t^2 \{6.92\left(\frac{l}{t}\right)^{\frac{1}{3}} + 2\cos\varphi\tan\theta)\cos\theta = 5559 \text{ (N)} \qquad (145)$$

Three folds:
$$P_{m1} = \sigma_0 t^2 \{4.90\left(\frac{l}{t}\right)^{\frac{1}{3}} + \cos\varphi\tan\theta)\cos\theta = 3932 \text{ (N)} \qquad (146)$$

$$P_{m2} = \sigma_0 t^2 \{6.69\left(\frac{l}{t}\right)^{\frac{1}{3}} + 1.25\cos\varphi\tan\theta)\cos\theta = 5365 \text{ (N)} \qquad (147)$$

$$P_{m3} = \sigma_0 t^2 \{8.27\left(\frac{l}{t}\right)^{\frac{1}{3}} + 1.5\cos\varphi\tan\theta)\cos\theta = 6630 \text{ (N)} \qquad (148)$$

If we take the average of the mean crushing forces of the two folds and three folds, those are 4717 and 5309. Two fold case increased bow strength 15%, and three-fold case increased 30% by the comparison with one fold case. The visual comparison is made in Figure 55 and Figure 56.
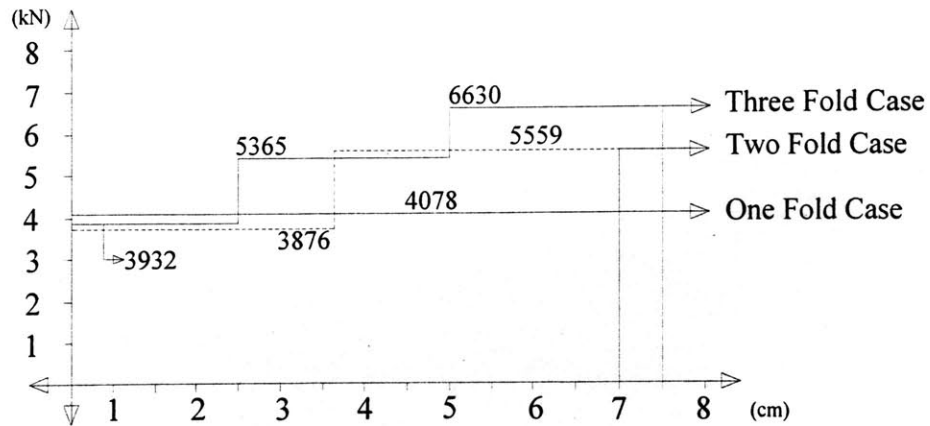

Figure 55: Strength comparison by fold numbers

As we can see from the above results, it is obvious that the forth folds and fifth folds will increase the bow strength by 45% and 60%. These are shown in the following figure.
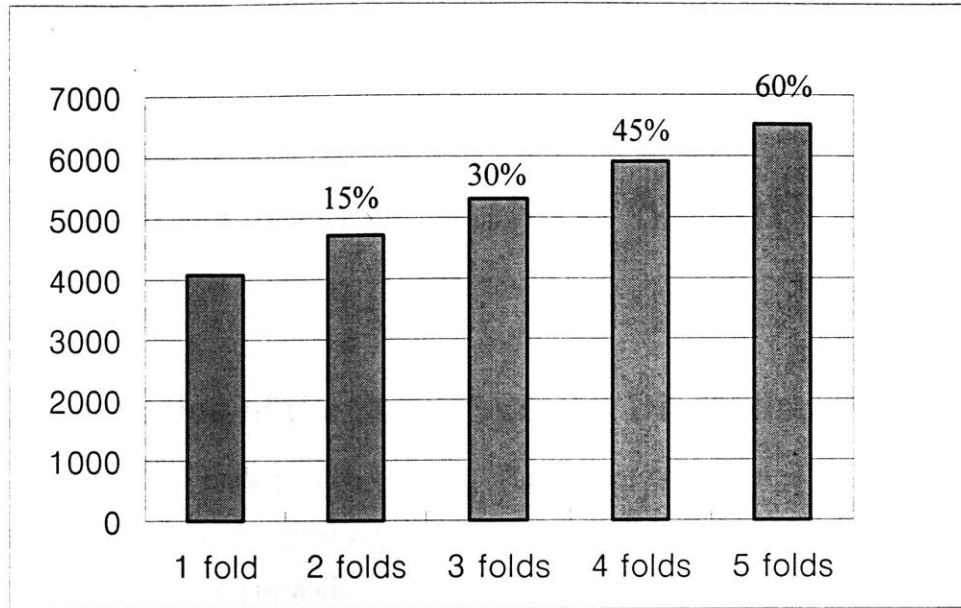

Figure 56: Prediction of the strength increased by fold numbers

Note that the one fold case is calculated only for the comparison of the contribution of the each fold because the ratio ($\frac{l}{t}$) in our concern (about 165) naturally created two folds in the model tests.

Chapter 7

DEVELOPMENT OF A BOW MODEL

7.1 Determination of the Ship Type and Dimension

In the development of scale models the bow shape must be specified in advance, because the results are based on the geometry, material properties, and plate thickness. Since the bow shapes depend on a type and a size of the ship, the determination of the scale models must be done carefully. In this report considered are oil tankers and container ships because of severe consequence of accidents and affect on ocean environment. The following table shows typical dimension of various categories of ships.

TABLE 6: Dimension by ship type

	TYPE	DISPLACEMENT (Δ)	DIMENSION(m) (L×B×D×d)
TANKER	AFRA MAX	95,000 (ton)	233×41.8×20 ×12.2
	SUEZ MAX	150,000 (ton)	264×46×23.6 ×15.85
	VLCC	310,000 (ton)	318×58×31.25 ×21.4
CONTAINER		21,000 (ton)	158×27.2×13.8 × 8.75
		35,000 (ton)	184×32.25× 21.2 ×11.3
		68,000 (ton)	262×40×24×12

(where B and d is the mid ship breadth and moulded draft. Other parameters are defined in the next section.)

78

7.2 Determination of the Bow Shell Plating Thickness

As already mentioned, the bow plate thickness is directly related to bow strength; thus, the rational procedure to determine the plate thickness is an important task for the development of the bow model. In this research the plate thickness is determined by the average thickness specified by of the International Maritime Organization rules.

According to these rules, the minimum shell plating thickness t is to be obtained from the following equation and is not to extend for more than 0.1L at the ends between the midship 0.4L and the end 0.1L the thickness of the plating may be gradually tapered.

Formulas for the determination of the bow shell thickness are as follows:

$$t = 0.0455(L+3) + 0.009s \; mm \quad for \;\; L<85 \; m$$
$$t = 0.035(L+29) + 0.009s \; mm \quad for \;\; 85 \leq L \leq 305 \; m \quad\quad (149)$$
$$t = (11.70 + 0.009 \; s)\sqrt{\frac{D}{35}} \; mm \quad for \;\; 305 \prec L \leq 427 \; m$$

$$where$$
$$s = fore \; or \; aft \; peak \; frame \; spacing \; in \; mm$$
$$2.08L + 438 \; mm \; for \;\; (L \leq 270m)$$
$$1000 \; mm \; for \;\; (270 \leq L \leq 427 \; m) \quad\quad (150)$$
$$L = Length \; of \; vessel \; in \; (m)$$
$$D = Moulded \; depth \; in \; (m)$$

7.3 Determination of the Bow Length

Having determined the ship type and the plate thickness, the bow profile of tanker and container need to be determined. In this research the most common bow profiles are shown in figure 57 and 58.
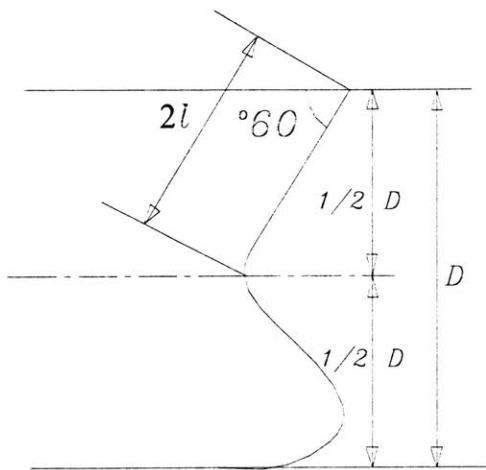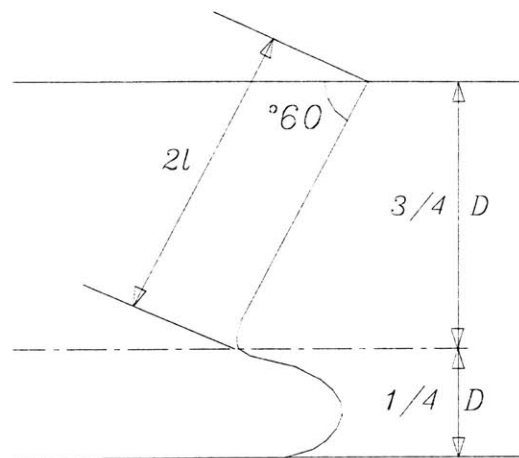

Figure 57: Bow profile of the tanker   Figure 58: Bow profile of the container

From the above typical profiles the bow length $2l$ can be determined in terms of the moulded depth. Finally, the relative bow length can be calculated by non-dimensionalization with respect to the thickness. The bow length of the model will then be determined from the known non-dimensional bow length to the plate thickness. Following table shows typical dimensions of six ships.

TABLE 7: Bow length / Plate thickness

TYPE	AFRA MAX	SUEZ MAX	VLCC	CONTAINERS		
DISPLACE-MENT	95,000 (ton)	150,000 (ton)	310,000 (ton)	21,000 (ton)	35,000 (ton)	6,800 (ton)
MOULDED DEPTH	20 (m)	23.6 (m)	31.25 (m)	13.8(m)	32.25 (m)	24(m)
FRAME SPACING	922.64 (mm)	987.12 (mm)	1000 (mm)	766.64 (mm)	820.72 (mm)	982.96 (mm)
MAXIMUM THICKESS	20.3038 (mm)	23.0841 (mm)	23.85 (mm)	15.7998 (mm)	17.586 (mm)	22.9466 (mm)
MINIMUM THICKNESS	17.4738 (mm)	19.1391 (mm)	19.5597 (mm)	13.4448 (mm)	14.818 (mm)	19.0316 (mm)
AVERAGE THICKNESS	18.9059 (mm)	21.1116 (mm)	21.7049 (mm)	14.6223 (mm)	16.219 (mm)	20.9891 (mm)
BOW LENGTH(2l)	11.5497 (m)	13.6255 (m)	18.0422 (m)	11.9511 (m)	18.359 (m)	20.784 (m)
NONDIMEN-SIONAL BOW LENGTH (l/t)	305.38	327.20	415.63	408.66	565.99	495.17

7.4 Determination of the Deck Angle θ and Bow Angle φ

The approximate side angle of the above ship type is measured between forefront and collision bulkhead. After measuring more than twenty different ships, it is proved that most tankers and commercial containers have the approximate side angle of $\theta=30°$. The approximate bow angle is assumed to be $\varphi= 60°$.

81

7.5 Model Fabrication

In order to obtain the realistic result from the model test, it is important to keep the geometric similitude law. Since the nondimensional bow length is obtained in the previous chapter, the bow length of the model is proportional to the plate thickness. Although the value of the nondimemsional bow length is approximately 325 (see the previous section, Table 6, if the inner members such as longitudinal and horizontal stiffeners are considered, it is obvious that the value of the bow length should be lower than 325. It is shown that by using the smearing technique the contribution of the inner stiffeners in the bow area is approximately the same as the twice of the original thickness. Therefore, the value of the relative bow length taken is 162 for the scenario that a bow contacts the embankment in the middle of the bowline. However, the contact point on the bowline can vary for collision situations therefore, the nondimemsional bow length 162 is not the fixed number. In this report the nondimemsional bow length l/t vary from 100 to 250 by loading conditions of each test. For the bow model fabrication two plate thickness 0.71mm(for bow 1, 2, 3, 5, 6) and 1.2mm (only for bow 4) were used. For the bow length of the bow model 1 to 4 is 130mm, and the bow model 5 and 6 is 150mm. Figure 59 show detail dimension of the bow model manufactured from a sheet. All the models are joined by rivets using lap joint join all models.
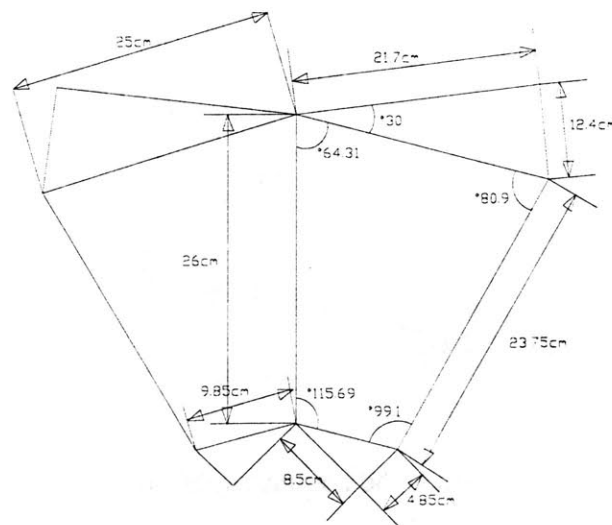

Figure 59: Model Dimensions

82

7.6 Model Test

A. Variation of the test method

The purpose of this test is to measure the force-indentation relations and observe general deformation modes. Five different types of the test were performed. For the thickness 0.71mm model three different tests were performed by changing location of the contact point, in all cases fully clamped support conditions were used (see Fig. 61).
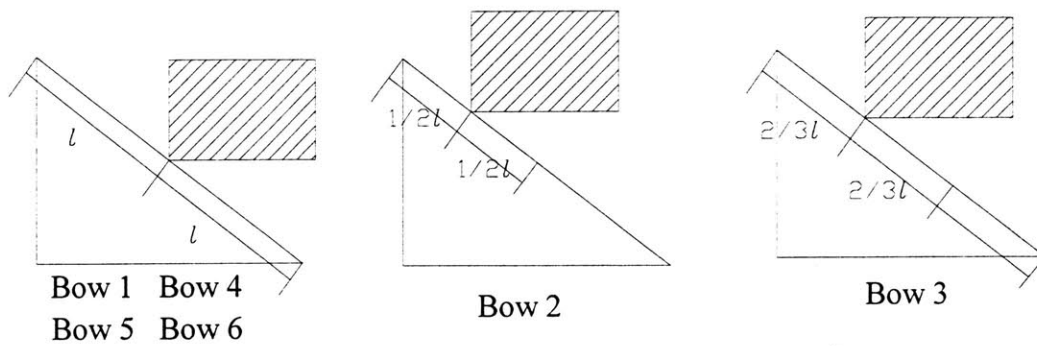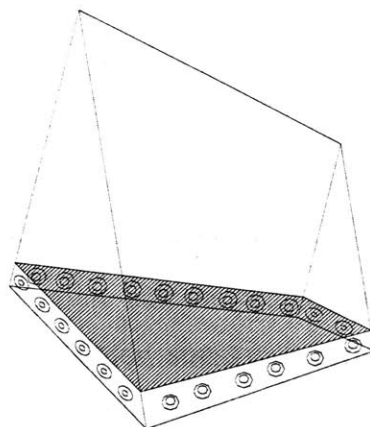

Figure 60: Loading locations

Figure 61:Fully clamped boundary conditions

B. Loading Conditions

A real ship accident is a dynamic event. However, relative ship velocities are small so that local initial effects could be neglected. Therefore, in this test quasi-static loading is applied. In this test constant crosshead velocity (0.25mm/sec) is applied from the contact point to the point Q, Figure 62. All tests were performed in the MTS testing machine with capacity of 90 KN and 150 mm stroke.
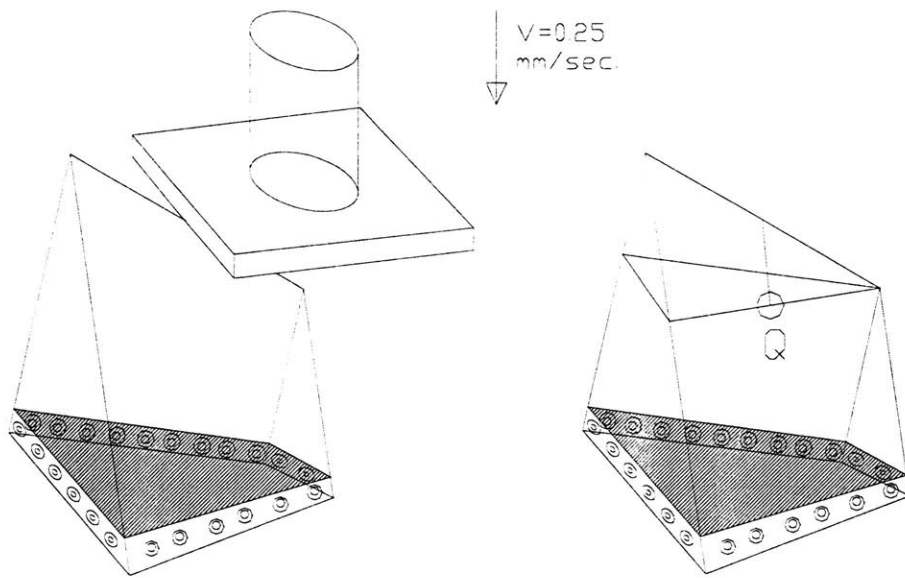

Figure 62: Loading Conditions

C. Material Characteristics

The specimens were made from cold rolled steel. Two tensile tests were performed on Instron Testing machine to obtained stress-strain characteristics. The tests were calculated at room temperature and the engineering stress strain data is shown in table 8 and figure 63, 64. The flow stress σ_0 is defined to be a geometric average of the yield stress and ultimate stress:

$$\sigma_0 = \sqrt{\sigma_y \cdot \sigma_u} \tag{151}$$

TABLE 8: Material properties

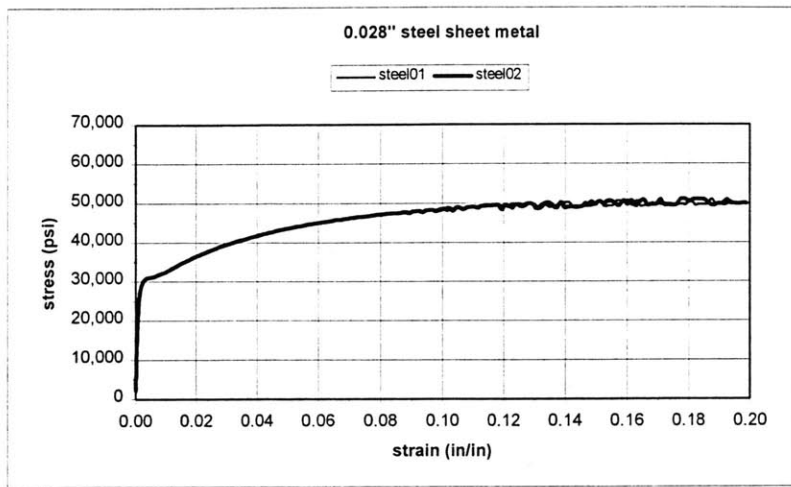| Stress / Thickness	INITIAL YIELD STRESS	ULTIMATE STRESS	CALCULATED FLOW STRESS
0.0071(m)	282.695 MPa	344.750 Mpa	312 Mpa
0.0012(m)	282.700 MPa	320.240 Mpa	301.Mpa

Figure 63:Stress-Strain Curve (t=0.71mm)

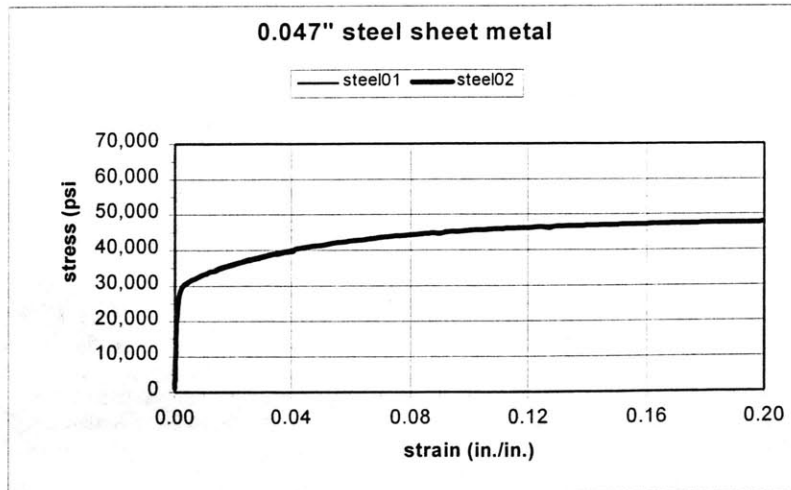Figure 64: Stress-Strain Curve (t=1.2mm)

D. Test Results

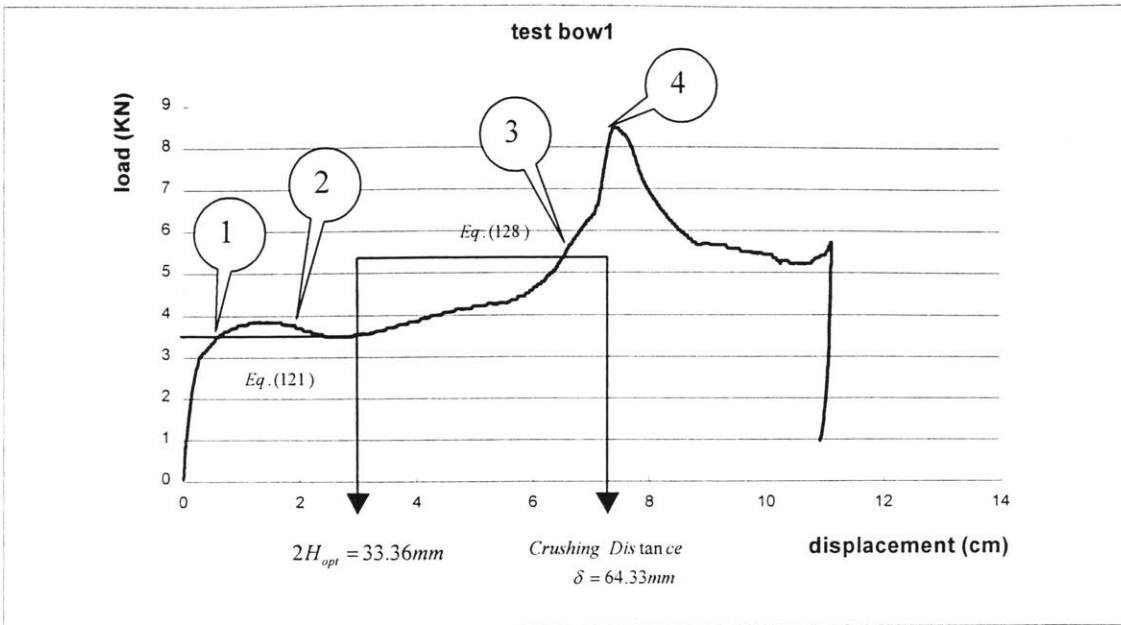
Figure 65: Force-Displacement (bow-1)
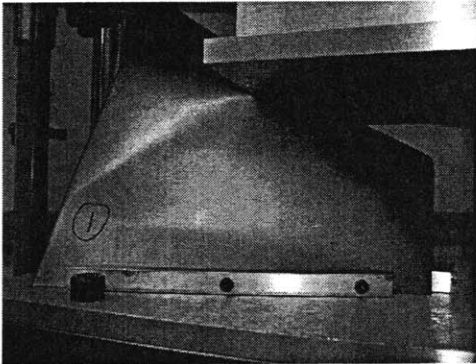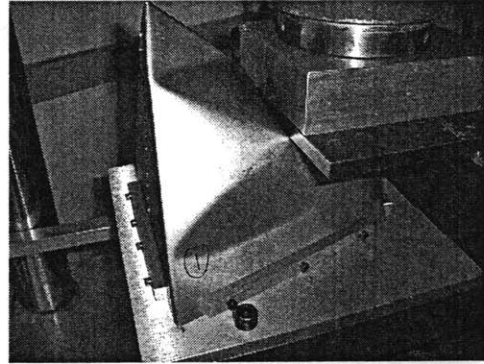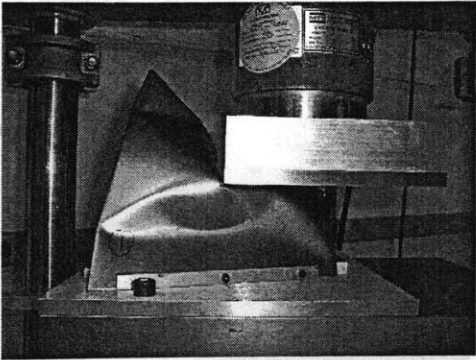

Figure 66: 1

Figure 67: 2

Figure 68: 3

Figure 69: 4

Figure 70: Force-Displacement (bow-2)

Figure 71:1

Figure 72:2

Figure 73:3

Figure 74:4

Figure 75:Force-Displacement (bow-3)

Figure 76: 1

Figure 77: 2

Figure 78: 3
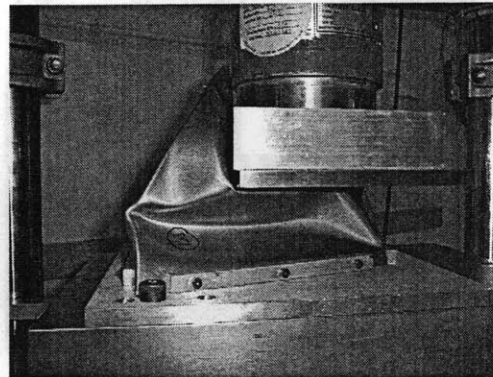
Figure 79: 4
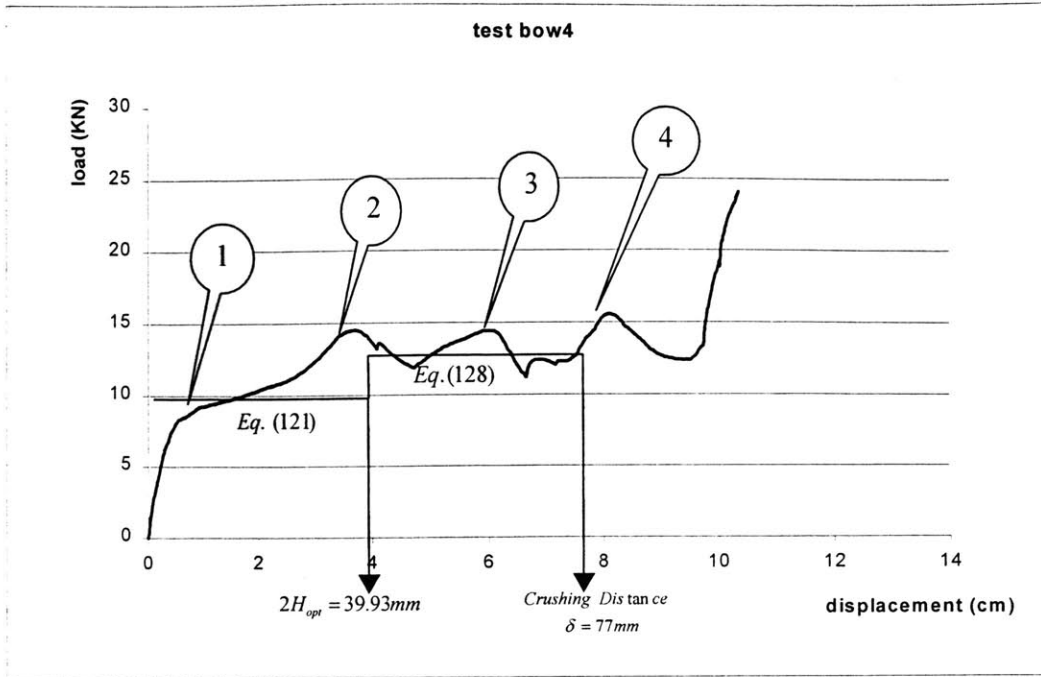
Figure 80: Force-Displacement (bow-4)
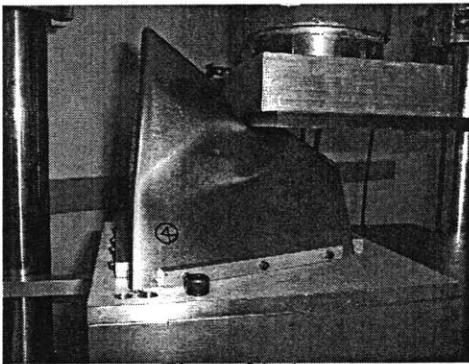
Figure 81: 1
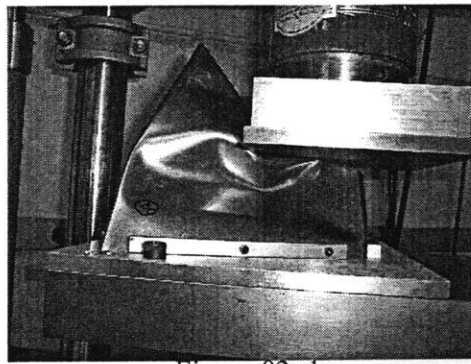
Figure 82: 1
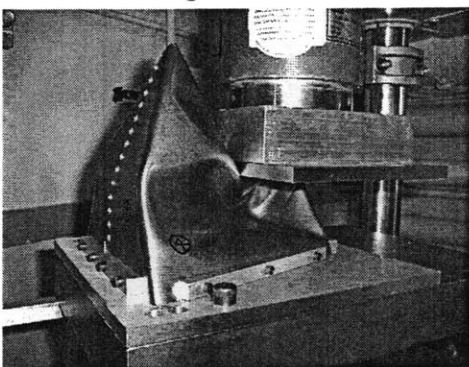
Figure 83: 3
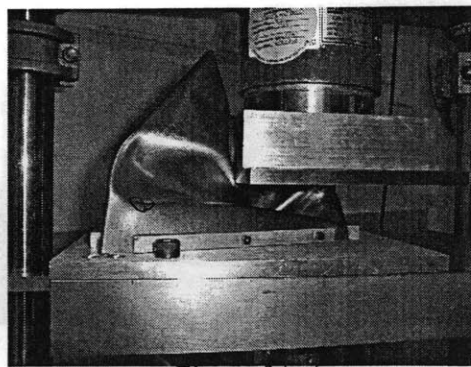
Figure 84: 4
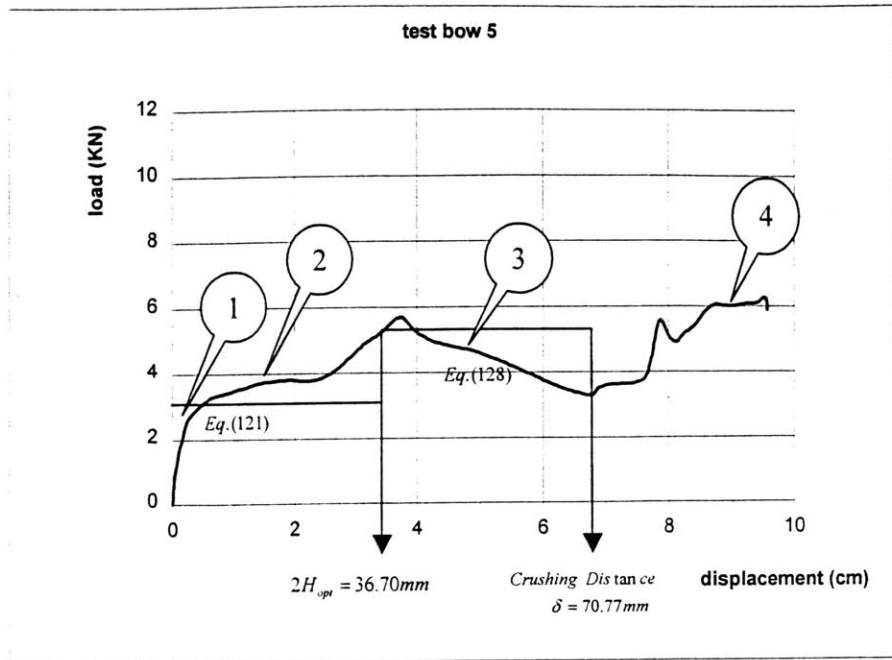
Figure 85:Force-Displacement (Bow 5)
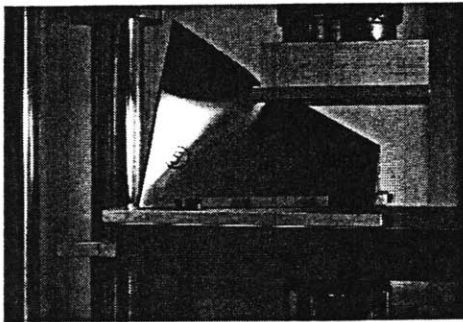
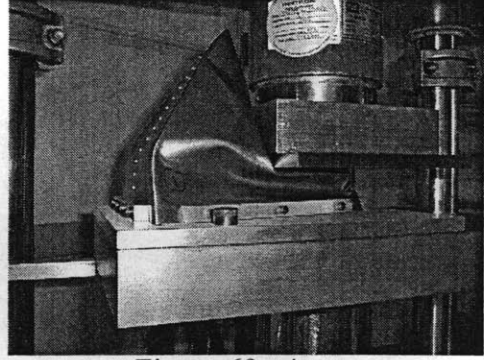Figure 86: 1
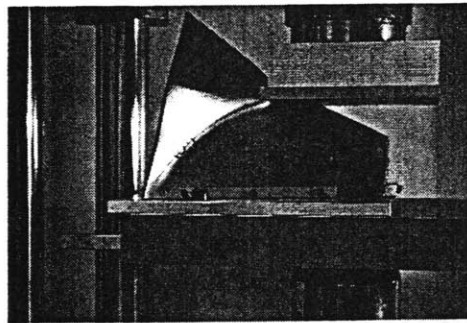
Figure 87: 2
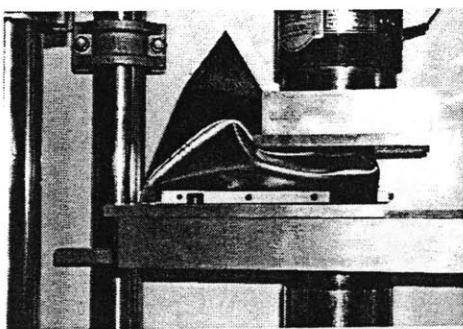
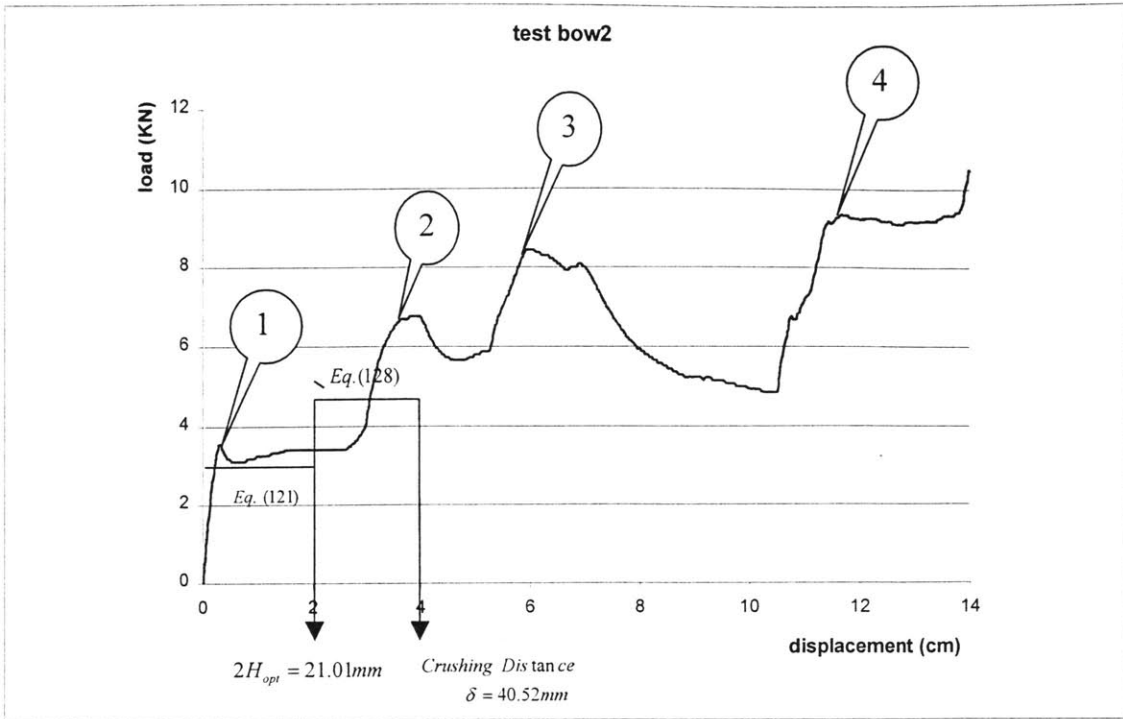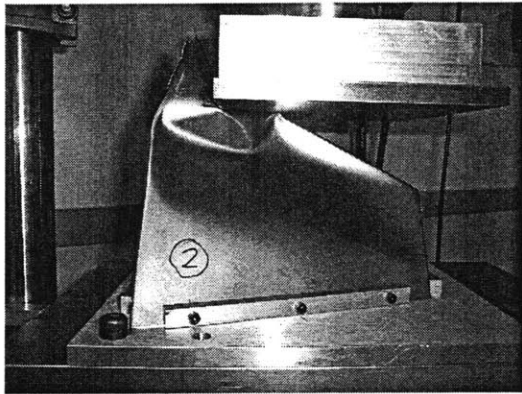Figure 88: 3
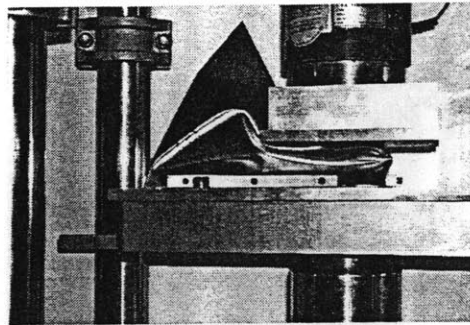
Figure 89: 4

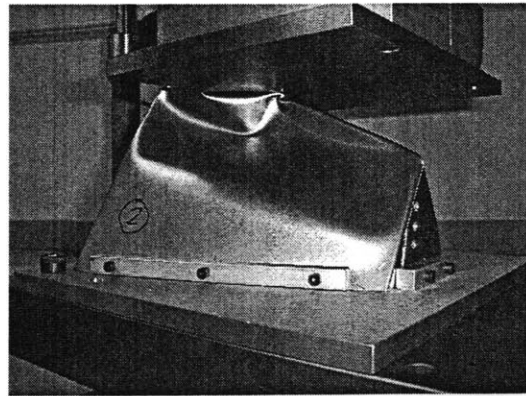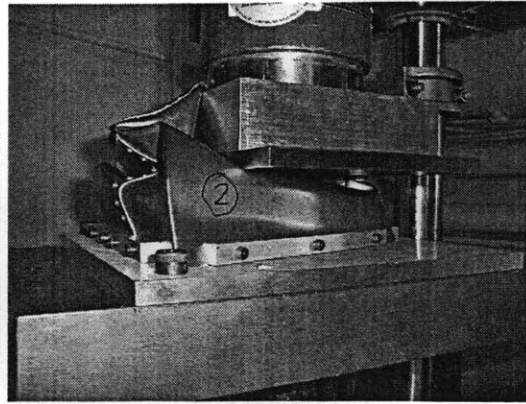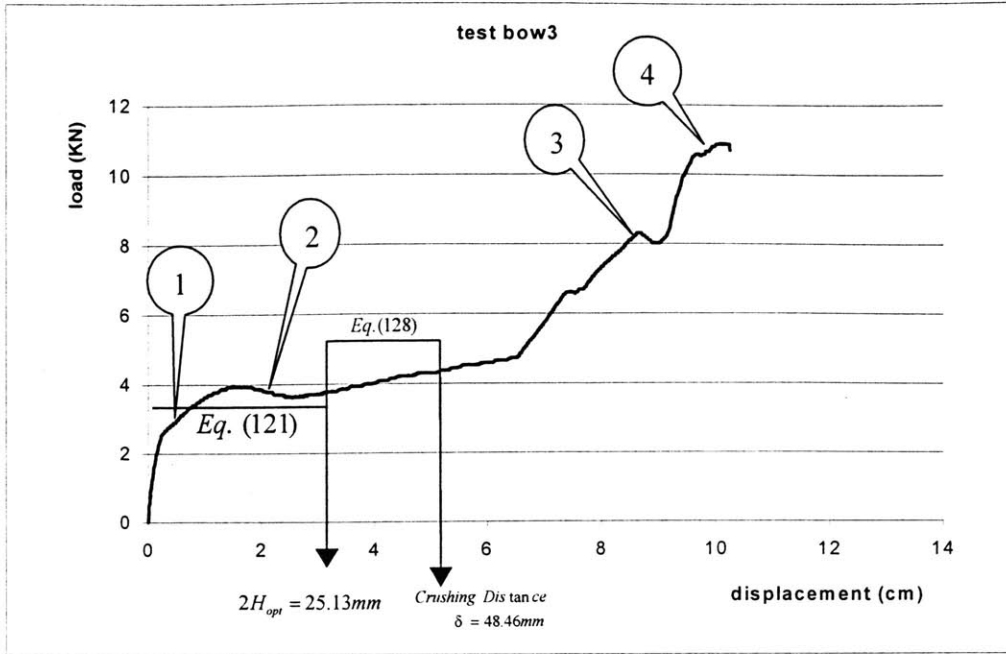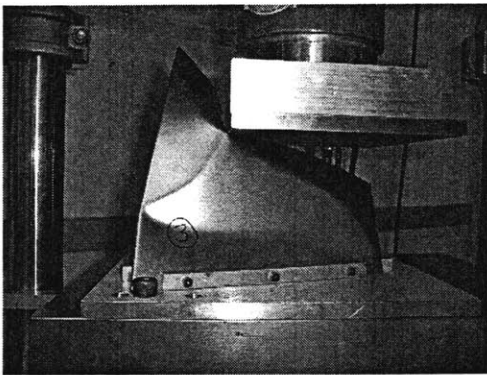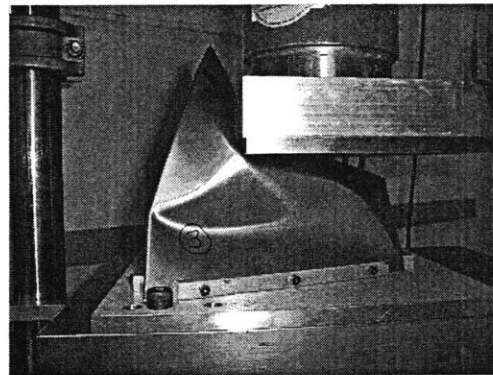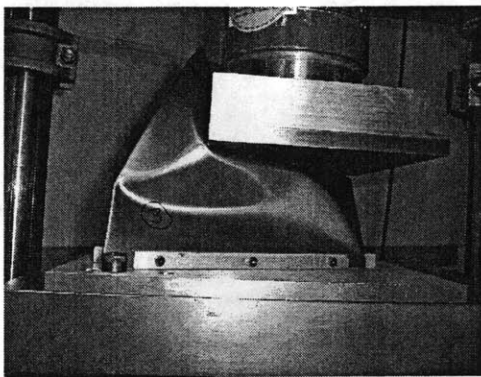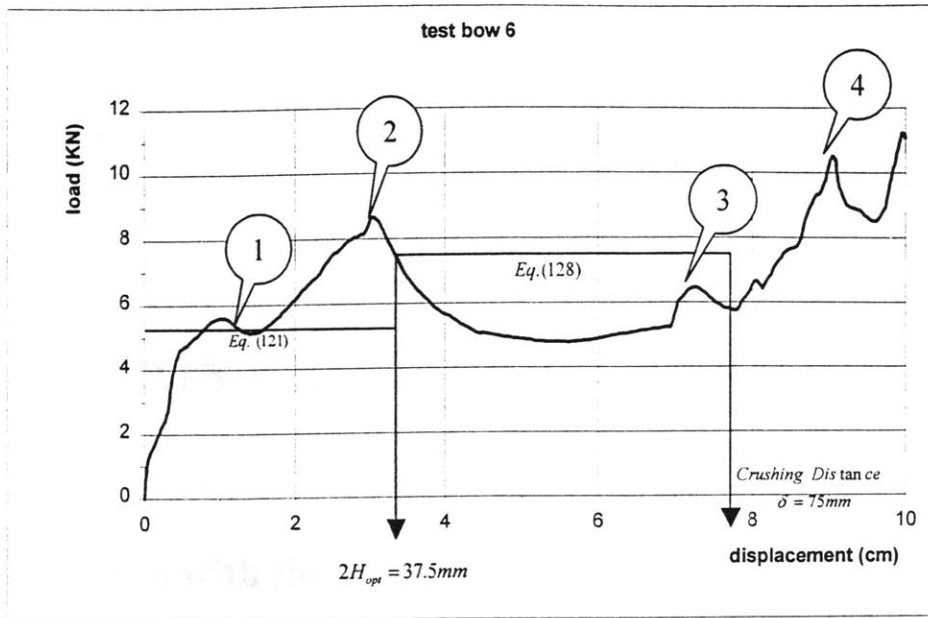Figure 90: Force-Displacement (Bow 6)
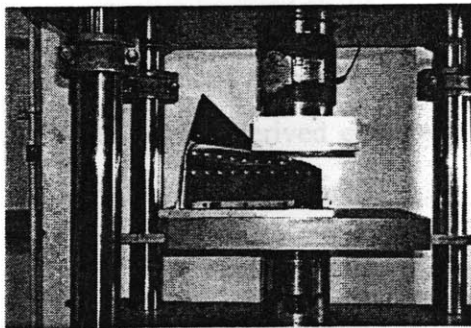
Figure 91:1
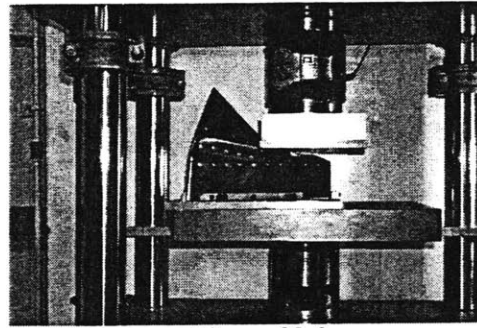
Figure 92:2
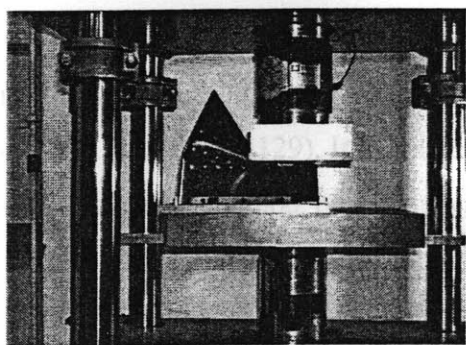
Figure 93:3
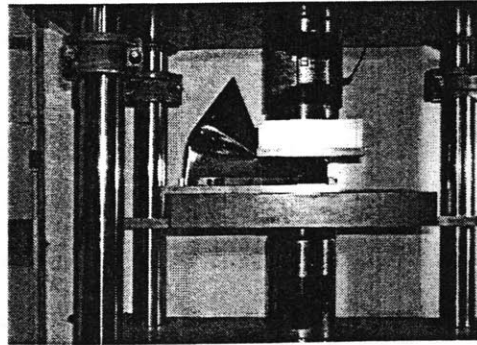
Figure 94: 4

Chapter 8

VALIDATION AND CONCLUSION

8.1 Comparison with the test results

Equation (107), (113), (121), and (129) were used to predict the theoretical value of the mean rushing force of the bow model 1~ model 5, and the equation (131) and (132) were used for stiffened bow model 6. The values of input parameters in all six tests are given in the table below together with the calculated mean crushing force P_m and the crushing distance. Note that the derived expression for the mean crushing force of the equation (113) is valid over the crush distance δ related to l by.

$$\delta = \frac{1}{2}l \qquad (152)$$

The theoretically predicted forces are compared with the experimentally determined force–displacement graphs, Fig. (65 ~ 90). The agreement is good considering simplicity of the theoretical solution and the complexity of the problem. The percentage error is within ± 10% with the worse case (Bow 1) reaching +15% for equation (107), and within 5% for equation (107), (121), and (129). It can be calculated that the Kinematic model B method 2 along with the energy method provide a good first order approximation to the crushing resistance of the ship running at a right angle into a rigid embankment, and the Kinematic model for two folding also provided good approximation to the crushing resistance of the ship running at a right angle into a rigid embankment. The strength of the stiffened bow

92

model 6 predicted by the equation (131) and (132) shows the grate accuracy. The recorded force–displacement diagrams show a considerable increase in the force level for penetration depth larger than δ. Also, there is a lack of correlation between the number of folds in the scale model test and real accident shown in Fig.19, Fig.20. In our model test there was only one or two full folds whereas in the photograph of DELEDDA a number of short wave folds was observed. This difference can be explained by the presence of transverse frames in the real ship, which limits and reduces the folding wave to a smaller value equal to the distance between the frames. However, the contribution of the multi-folds case is explained in chapter 6.3 in detail. In the model tests we used uniform thickness shell plating and the internal stiffness were induced using a smearing technique for model 1~5, and Model 6 is constructed with stiffeners.

Table 9: Predicted mean crushing strength (Model B, Method 2)

	φ	θ	σ_0(Mpa)	l (mm)	t (mm)	Crush distance δ[mm]=$2H_{opt}$(mm)	P_m(N)	Error(%)
Bow1	60°	30°	312	130	0.71	21.01	3890	-5 %
Bow2	60°	30°	312	65	0.71	13.24	3095	+5 %
Bow3	60°	30°	312	86	0.71	15.95	3394	-3 %
Bow4	60°	30°	312	130	1.2	25.15	9571	-15 %
Bow5	60°	30°	312	150	0.71	26.04	4059	-5 %

Table 10: Predicted mean crushing strength (Model B, Method 3)

	φ	θ	σ_0(Mpa)	l (mm)	t (mm)	P_m(N)	Error(%)	δ (mm)
Bow 1	60°	30°	312	130	0.71	4196	+15 %	65
Bow 2	60°	30°	312	65	0.71	2526	+8 %	32.5
Bow 3	60°	30°	312	85	0.71	3081	-12 %	43.3
Bow 4	60°	30°	312	130	1.2	8191	-15 %	65
Bow 5	60°	30°	312	150	0.71	4633	+5 %	75

Table 11: Predicted mean crushing strength ((Unstiffened two folding model-first fold)

	σ_o(Mpa)	l (mm)	t (mm)	P_{m1}(N)	Error(%)	$\delta=2H_{opt}$ (mm)
Bow 1	312	130	0.71	3698	-5 %	33.36
Bow 2	312	65	0.71	2947	+10 %	21.01
Bow 3	312	85	0.71	3217	-10 %	25.13
Bow 4	312	130	1.2	9108	-5 %	39.93
Bow 5	312	150	0.71	3248	-15 %	36.70

Table 12: Predicted mean crushing strength (Unstiffened two folding model-second fold)

	σ_o(Mpa)	l (mm)	t (mm)	P_{m1}(N)	Error(%)	$\delta=2H_{opt}$ (mm)
Bow 1	312	130	0.71	5303	+10 %	33.36~64.33
Bow 2	312	65	0.71	4225	+3 %	21.01~40.52
Bow 3	312	85	0.71	4613	+20 %	25.13~48.46
Bow 4	312	130	1.2	13059	-5 %	39.93~77
Bow 5	312	150	0.71	5558	+20 %	36.70~70.77

Table 13: Predicted mean crushing strength (Stiffened two folding model)

	σ_o(Mpa)	l (mm)	t (mm)	P_{m1}(N)	Error(%)	$\delta=2H_{opt}$ (mm)
Bow 6	312	150	0.71	4586	+10 %	37.5

	σ_o(Mpa)	l (mm)	t (mm)	P_{m2}(N)	Error(%)	$\delta=2H_{opt}$ (mm)
Bow 6	312	150	0.71	6378	-10 %	37.5~75

8.2 Comparison of Methods

To compare the each method, dimensionless mean crushing forces are obtained for equation (108), (113), (122), and (129) that gave good accuracy.

The nondimensional equation according to equation (108) is:

$$\frac{P_m}{\sigma_0 t^2} \approx 4.41\left(\frac{l}{t}\right)^{\frac{1}{3}} + 0.249 \tag{153}$$

For the equation(113) nondimensional equation can be put into the form:

$$\frac{P_m}{\sigma_0 t^2} \approx 0116\left(\frac{l}{t}\right) + 5.43 \tag{154}$$

At the same time, the equation (122) and (129) that represent mean crushing forces of the two folding case can be expressed as a liner combination of each fold, and expression is:

$$\frac{P_m}{\sigma_0 t^2} \approx 4.17\left(\frac{l}{t}\right)^{\frac{1}{3}} + 0.374 \quad \text{where } 0 < \frac{l}{t} < 107 \tag{155}$$

$$\frac{P_m}{\sigma_0 t^2} \approx 5.99\left(\frac{l}{t}\right)^{\frac{1}{3}} + 0.499 \quad \text{where } 107 < \frac{l}{t} < 250 \tag{156}$$

Figure 95

Nondimensional Comparison of Methods
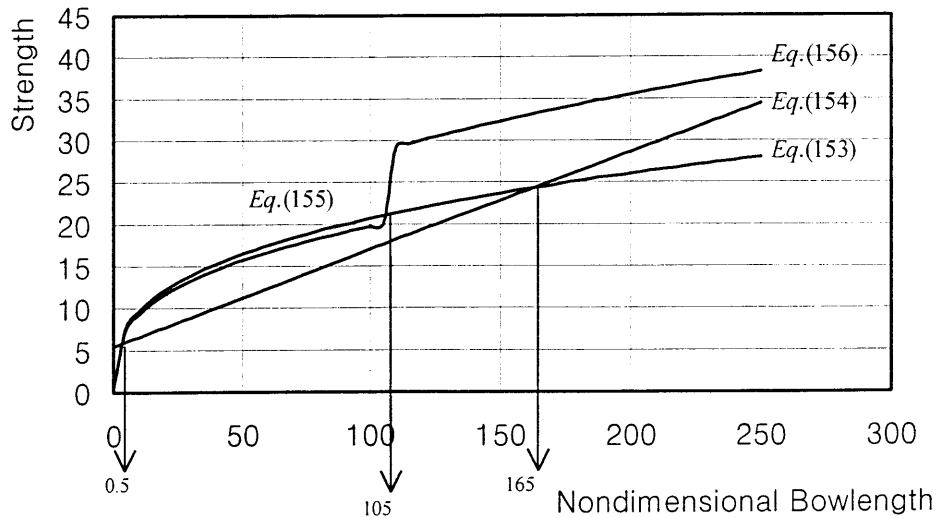
It is seen from the above figure that equation (153) and (154) gave similar results around $\frac{l}{t} = 165$, which is of practical interest.

Appendix

1. Generalization of The Triangle Supper Folding Elements.

Following types of the triangle elements were used in this thesis, and those have different ability to absorb external force as shown by the size of the stretched areas.
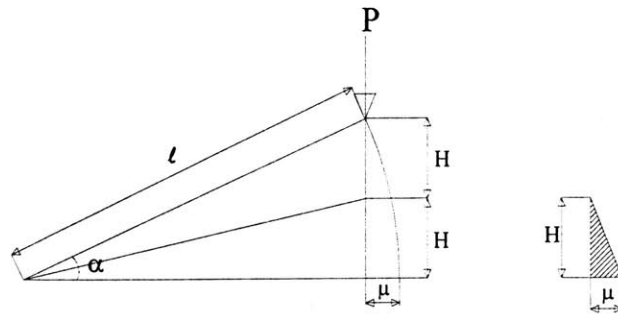
Figure 96: Super folding element 1
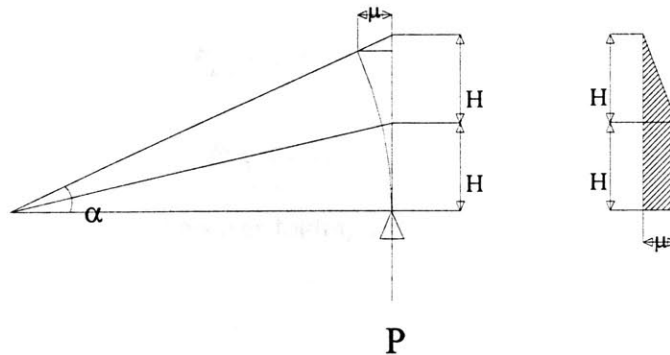
Figure 97: Super folding element 2
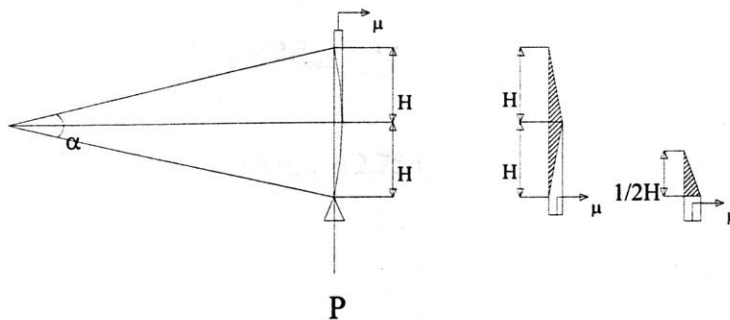
Figure 98: Super folding element 3

A. Mean Crushing Forces

Mean Crushing Force for the element 1 can be found as:

$$P_{me1} 2H = (\frac{H^3}{l} N_0 + 2M_0 l\pi)$$

$$P_{me1} = \frac{H^2}{2l} N_0 + \frac{1}{H} M_0 l\pi$$

(157)

where

$$u = l(1 - \cos\alpha) = l(1 - \sqrt{1 - \sin^2\alpha})$$

$$\approx l(1 - 1 + \frac{1}{2}\left(\frac{2H}{l}\right)^2) = \frac{2H^2}{l}$$

(158)

After minimization $\frac{\partial P_{me1}}{\partial H} = 0$, one can obtain following expression:

$$P_{me1} = 1.276\sigma_0 t^2 \left(\frac{l}{t}\right)^{\frac{1}{3}}$$

(159)

By similar process mean crushing force for element 2 and 3 are found as:

$$P_{me2} = 1.840\sigma_0 t^2 \left(\frac{l}{t}\right)^{\frac{1}{3}}$$

(160)

$$P_{me3} = 1.375\sigma_0 t^2 \left(\frac{l}{t}\right)^{\frac{1}{3}}$$

(161)

To see the linearity of the super folding elements, a pair of the folding elements is calculated:

$$P_{mep1} = 2P_{me1} = 2.55\sigma_0 t^2 \left(\frac{l}{t}\right)^{\frac{1}{3}}$$

(162)

$$P_{mep2} = 2P_{me2} = 3.68\sigma_0 t^2 \left(\frac{l}{t}\right)^{\frac{1}{3}}$$

(163)

$$P_{mep3} = 2P_{me3} = 2.75\sigma_0 t^2 \left(\frac{l}{t}\right)^{\frac{1}{3}}$$

(164)

B. Mean Crushing Force for Different Size of Element 1

Mean crushing force for $\dfrac{l}{2}$ case is:
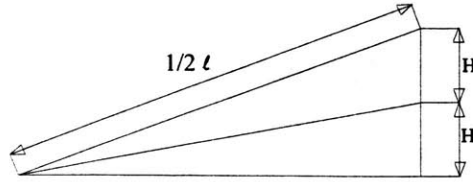
$$P_{me1} = 1.01\sigma_0 t^2\left(\frac{l}{t}\right)^{\frac{1}{3}}$$ (165)

Figure 99: Half-length super folding element 1

Mean crushing force for $\dfrac{l}{3}$ case is:
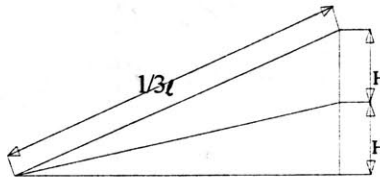
$$P_{me1} = 0.88\sigma_0 t^2\left(\frac{l}{t}\right)^{\frac{1}{3}}$$ (166)

Figure 100: One third-length super-folding element 1

Mean crushing force for $\dfrac{2l}{3}$ case is:
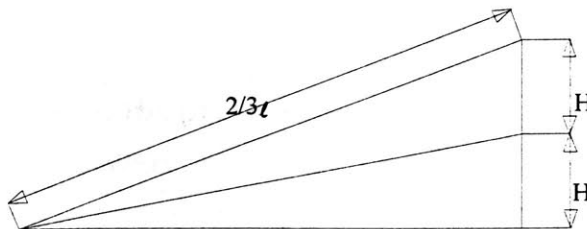
$$P_{me1} = 1.12\sigma_0 t^2\left(\frac{l}{t}\right)^{\frac{1}{3}}$$ (167)

Figure 101: Two third-length super folding element 1

2. Calculation Table for Application

The calculation of the mean crushing force can be simplified by standardization. For example the calculation standard table for the element 1 is illustrated as follows.

A. Calculation Table for the Element-1

Table 14: Simplified calculation process

	l	$l/2$	$2l/3$	$l/3$
E_m	(a)=$\dfrac{H^3}{l}N_0$	(b)=$\dfrac{2H^3}{l}N_0$	(c)=$\dfrac{3H^3}{2l}N_0$	(d)=$\dfrac{3H^3}{l}N_0$
E_b	(e)=$2M_0 l\pi$	(f)=$M_0 l\pi$	(g)=$\dfrac{4}{3}M_0 l\pi$	(f)=$\dfrac{2}{3}M_0 l\pi$
Coefficient of P_m	(1)=$\dfrac{1}{2}$ for E_m, (2)=1for E_b	(3)=1 for E_m, (4)=$\dfrac{1}{2}$ for E_b,	(5)=$\dfrac{3}{4}$ for E_m, (6)=$\dfrac{4}{6}$ for E_b,	(7)=$\dfrac{3}{2}$ for E_m, (8)=$\dfrac{1}{6}$ for E_m,
Coefficient H	(9)=$\left(\dfrac{1}{2(1)}\cdot\dfrac{1}{4}\cdot(2)l^2 t\pi\right)^{\frac{1}{3}}$ $=\left(\dfrac{1}{4}l^2 t\pi\right)^{\frac{1}{3}}=\left(\dfrac{1}{4}\right)^{\frac{1}{3}}$	Similarly as (9), (10)=$\left(\dfrac{1}{16}\right)^{\frac{1}{3}}$	(11)=$\left(\dfrac{1}{36}\right)^{\frac{1}{3}}$	(12)=$\left(\dfrac{1}{9}\right)^{\frac{1}{3}}$
Coefficient of P_m	(13) = $\{(1)\cdot(9)^2+\dfrac{1}{4}(9)^{-1}\}\pi^{\frac{2}{3}}$ $=1.276$	Similarly as (13), (14)=1.013	(15) =1.115	(16) =0.885
Final Expression	$P_m=1.276\sigma_0 t^2\left(\dfrac{l}{t}\right)^{\frac{1}{3}}$	$P_m=1.01\sigma_0 t^2\left(\dfrac{l}{t}\right)^{\frac{1}{3}}$	$P_m=1.12\sigma_0 t^2\left(\dfrac{l}{t}\right)^{\frac{1}{3}}$	$P_m=0.88\sigma_0 t^2\left(\dfrac{l}{t}\right)^{\frac{1}{3}}$

B. Application to the previous problems

To illustrate the simplicity of the calculation process, application is made to the chapter 6.3-two fold case (one fold only), and the whole process can be simply expressed as follow:

The coefficient for membrane energy for the first fold is:

$$E_m = \alpha = [2(a)+2(b)]/2 = 3 \qquad (168)$$

The coefficient for bending energy for the first fold is:

$$E_m = \beta = \{[2(e)+2(f)]/2\} = 3 \qquad (169)$$

The coefficient for H is: $\gamma = (\dfrac{1}{2\alpha} \cdot \dfrac{1}{4} \cdot \beta)^{\frac{1}{3}} = \dfrac{1}{2}$ (170)

The coefficient for P_m is: $\kappa = (\alpha\gamma^2 + \dfrac{1}{4}\beta\gamma)\pi^{\frac{2}{3}} = 4.82$ (171)

Therefore, the final expression for the mean crushing force becomes:

$$P_{m1} = 4.82\sigma_0 t^2 \left(\dfrac{l}{t}\right)^{\frac{1}{3}}$$ (172)

If we only consider the deck bending energy and deck angle θ, the expression will be exactly like equation (121)

$$P_{m1} = \sigma_0 t^2 \{4.82\left(\dfrac{l}{t}\right)^{\frac{1}{3}} + 1.5\cos\varphi\tan\theta\}\cos\theta$$ (121)

Through the above process tables for the element 2 and element 3 can be made, and the more development and standardization of super folding elements that would represent the geometries of crashed bodies will make the calculation process simple and easy.

(3) Generalization of the Theory and Application

A. Equilibrium

$$P_m \cdot 2H = (E_m + E_b)\cos\theta \tag{173}$$

where

$$\dot{E}_m = \int_S N_{\alpha\beta}\, \dot{\varepsilon}_{\alpha\beta}\, dS \tag{174}$$

$$\dot{E}_B = \int_S M_{\alpha\beta}\, \dot{k}_{\alpha\beta}\, dS \tag{175}$$

$$P_m \cdot 2H = N_0 \sum_i \Delta A_i + M_0 \sum_i \theta_i l_i \tag{176}$$

$$\Delta A_i = \int_0^{2H} \Delta\mu\, d\eta = \frac{1}{2}\mu H \tag{177}$$
$$= \frac{2H^3}{l} = \Delta_i \frac{H^3}{l}$$

$$P_m = N_0 \frac{H^2}{2l}\sum_i \Delta_i + \frac{M_0}{2H}\sum_i \theta_i l_i$$
$$N_0 \frac{H^2}{2l}\sum_i \Delta_i + \frac{M_0 l}{2H}\sum_i \alpha\theta_i \tag{178}$$
$$where\ \sum \theta_i l_i = l\sum \alpha\theta_i$$

B. Mean Crushing Force and Wave Length

$$P_m = \frac{1}{\delta_{max}}\{\int_0^{2H} P(\delta)\, d\delta\} \tag{179}$$

$$\frac{P_m}{M_0} = \frac{2H^2}{tl}\sum_i \Delta_i + \frac{1}{2H}\sum_i \theta_i l_i \tag{180}$$

$$\frac{P_m}{M_0} = \frac{2H^2}{tl}\sum_i \Delta_i + \frac{l}{2H}\sum_i \alpha\theta_i \tag{181}$$
$$where\ \sum \theta_i l_i = l\sum \alpha\theta_i$$

101

$$\frac{d \frac{P_m}{M_0}}{dH} = 0$$

$$(182)$$

$$\Rightarrow H = \frac{1}{2} \sqrt[3]{\frac{\sum_i \alpha \theta_i}{\sum_i \Delta_i} t l^2}$$

Putting (182) into (181)

$$P_m = \frac{3}{8} \sigma_0 t^2 \left(\frac{l}{t}\right)^{\frac{1}{3}} \sqrt[3]{(\sum_i \alpha \theta_i)^2 (\sum_i \Delta_i)}$$

$$(183)$$

C. About Δ
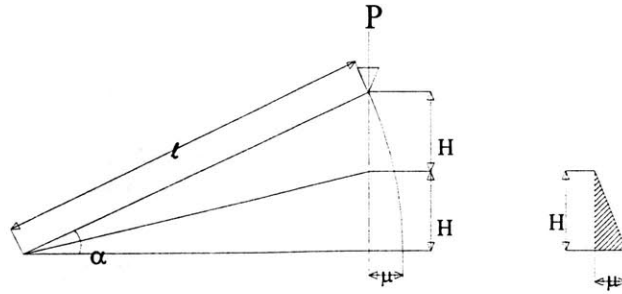
Figure 102: One folding element

$$\mu = l(1 - \cos\alpha) = l(1 - \sqrt{1 - \sin^2\alpha})$$

$$\mu \approx l(1 - 1 + \frac{1}{2}\left(\frac{2H}{l}\right)^2) = \frac{2H^2}{l}$$

$$(184)$$

$$Area = \frac{1}{2} \mu H = \frac{H^3}{l} = \Delta_i \frac{H^3}{l}$$

$$therefore \quad \Delta_i = 1 \; for \; this \; case$$

(4) Application

A. One Fold case (Bow 1, Bow2, Bow3, Bow5)

One fold case includes four triangle super folding elements. Therefore, two pairs of super folding elements on both sides of the bow
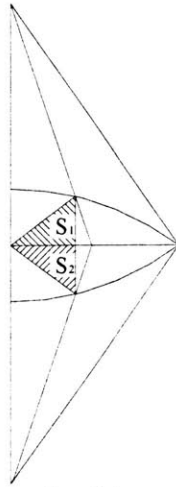
Figure 103   One pair of the super folding elements

Table 15: Calculation of coefficients

	Stretched areas	Sum	S_1	S_2	S_3	S_4
One fold case	Membrane energy Coefficient	$\sum_i \Delta_i$	Δ_1	Δ_2	Δ_3	Δ_4
	Values	4	1	1	1	1
	Bending angle	$\sum_i \theta_i$	θ_1	θ_2	....	θ_{16}
	Values	8π	$\dfrac{\pi}{2}$	$\dfrac{\pi}{2}$	.....	$\dfrac{\pi}{2}$
	Hinge Length	l_i	l_1	l_2	....	l_{16}
	Values		l	l	....	l
	Bending energy Coefficient	Total	$\theta_1 l_1$	$\theta_2 l_2$	.....	$\theta_{16} l_{16}$
	Values	$8\pi l$	$\dfrac{\pi}{2}l$	$\dfrac{\pi}{2}l$	.....	$\dfrac{\pi}{2}l$
	$\sum \alpha \theta_i$	8π				

103

$$P_m = \tfrac{3}{8}\sigma_0 t^2 \left(\tfrac{l}{t}\right)^{\frac{1}{3}} \sqrt{\left(\sum_i \alpha \theta_i\right)^2 \left(\sum_i \Delta_i\right)} \cos\theta \tag{185}$$

Therefore, the general expression of the mean crushing force for one fold case becomes

$$P_m = 5.10\sigma_0 t^2 \left(\frac{l}{t}\right)^{\frac{1}{3}} \cos\theta \tag{186}$$

Considering the Deck bending energy, above expression becomes:

$$P_m = \sigma_0 t^2 (5.10\left(\frac{l}{t}\right)^{\frac{1}{3}} + \cos\varphi \tan\theta)\cos\theta \tag{187}$$

Table 16: Application to the Bow1, 2, 3, 5

Bow1	$l=130$	$P_m = \sigma_0 t^2 (5.10\left(\dfrac{l}{t}\right)^{\frac{1}{3}} + \cos\varphi \tan\theta)\cos\theta$	3890 N
Bow2	$\dfrac{l}{2}$	$P_m = \sigma_0 t^2 (4.04\left(\dfrac{l}{t}\right)^{\frac{1}{3}} + \cos\varphi \tan\theta)\cos\theta$	3089 N
Bow3	$\dfrac{2l}{3}$	$P_m = \sigma_0 t^2 (4.45\left(\dfrac{l}{t}\right)^{\frac{1}{3}} + \cos\varphi \tan\theta)\cos\theta$	3399 N
Bow5	$l=150$	Same as Bow 1	4078 N

B. Two Fold case (Bow 4)
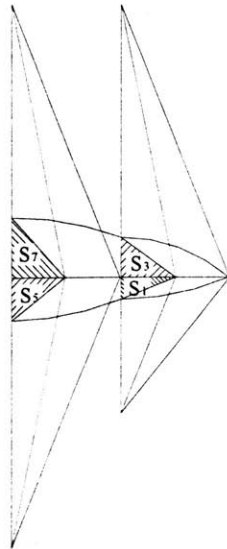
Figure 104: Super folding elements (Two fold case)

Table 17: Calculation of coefficients

		Stretched areas	Sum	S_1	S_2	S_3	S_4
Two fold case	First fold	Membrane energy Coefficient	$\sum_i \Delta_i$	Δ_1	Δ_2	Δ_3	Δ_4
		Values	6	1	1	2	2
		Bending angle	$\sum_i \theta_i$	θ_1	θ_2	....	θ_{16}
		Values	8π	$\dfrac{\pi}{2}$	$\dfrac{\pi}{2}$	.....	$\dfrac{\pi}{2}$
		Hinge Length	l_i	Lower part	$l_1 \sim l_8$	Upper part	$l_9 \sim l_{16}$
		Values			$\dfrac{l}{2}$	....	l
		Bending energy Coefficient	Total	$\sum_i \theta_i l_i$	$\theta_1 l_1 \sim \theta_8 l_8$	$\sum_i \theta_i l_i$	$\theta_9 l_9 \sim \theta_{16} l_{16}$
		Values	$6\pi l$	$2\pi l$	$\dfrac{\pi}{4} l$	$4\pi l$	$\dfrac{\pi}{2} l$
	$\sum \alpha \theta_i$		6π				

105

General expression of the mean crushing force is:

$$P_{m1} = \tfrac{3}{8}\sigma_0 t^2 \left(\tfrac{l}{t}\right)^{\tfrac{1}{3}} \sqrt[3]{\left(\sum_i \theta_i\right)^2 \left(\sum_i \Delta_i\right)} \cos\theta \qquad (188)$$

Therefore, the mean crushing force of the first fold with consideration of the deck bending becomes

$$P_{m1} = \sigma_0 t^2 \{4.82\left(\tfrac{l}{t}\right)^{\tfrac{1}{3}} + 1.5\cos\varphi\tan\theta\}\cos\theta = 9108 \qquad (189)$$

Table 18: Calculation of coefficients

		Stretched areas	Total	S_5	S_6	S_7	S_8
		Membrane energy Coefficient	$\sum_i \Delta_i$	Δ_5	Δ_6	Δ_7	Δ_8
		Values	10	2	2	3	3
Two fold case	Second fold	Bending angle	$\sum_i \theta_i$	θ_1	θ_2	....	θ_{16}
		Values	8π	$\dfrac{\pi}{2}$	$\dfrac{\pi}{2}$	.....	$\dfrac{\pi}{2}$
		Hinge Length	l_i	Lower part	$l_1 \sim l_8$	Upper part	$l_9 \sim l_{16}$
		Values			l	....	l
		Bending energy Coefficient	Total	$\sum_i \theta_i l_i$	$\theta_1 l_1 \sim \theta_8 l_8$	$\sum_i \theta_i l_i$	$\theta_9 l_9 \sim \theta_{16} l_{16}$
		Values	$8\pi l$	$4\pi l$	$\dfrac{\pi}{2}l$	$4\pi l$	$\dfrac{\pi}{2}l$
		$\sum \alpha\theta_i$	8π				

The general expression is:

$$P_{m2} = \tfrac{3}{8}\sigma_0 t^2 \left(\tfrac{l}{t}\right)^{\tfrac{1}{3}} \sqrt[3]{\left(\sum_i \theta_i\right)^2 \left(\sum_i \Delta_i\right)} \cos\theta \qquad (190)$$

Mean crushing forces for the second fold with consideration of deck bending becomes:

$$P_{m2} = \sigma_0 t^2 \{6.92\left(\tfrac{l}{t}\right)^{\tfrac{1}{3}} + 2\cos\varphi\tan\theta\}\cos\theta \qquad (191)$$

106

B. Stiffened case (Bow 6)

Considering the reduced wave length $2/3_H$ and the increased thickness $4/3_t$ for the membrane energy calculation, the equation 178 can be written as follows

$$P_m = N_0 \frac{H^2}{2l} \sum_i \Delta_i + \frac{M_0 l}{2H} \sum_i \alpha\theta_i$$

$$= \sigma_0 \left(\tfrac{3}{4}t\right) \frac{\left(\tfrac{2}{3}H\right)^2}{2l} \sum_i \Delta_i + \frac{\sigma_0 t^2 l}{8\left(\tfrac{2}{3}H\right)} \sum_i \alpha\theta_i \qquad (192)$$

$$= \sigma_0 t^2 \left(\frac{8}{27} \frac{H^2}{lt} \sum_i \Delta_i + \frac{3}{16} \frac{l}{H} \sum_i \alpha\theta_i\right)$$

Applying the coefficients of the first folding case ($\sum_i \Delta_i = 6, \sum \alpha\theta_i = 6\pi$), and considering the deck bending energy dissipation, the expression of the mean crushing force become as follows:

$$P_{m1} = \{\frac{16}{9l} H^2 \sigma_0 t + \frac{9}{8H} \sigma_0 t^2 l\pi + \frac{3}{2} \sigma_0 t^2 \cos\varphi \tan\theta\} \cos\theta \qquad (193)$$

Applying the coefficients of the second folding case ($\sum_i \Delta_i = 10, \sum \alpha\theta_i = 8\pi$), and considering the deck bending energy dissipation, the expression of the mean crushing force become as follows:

$$P_{m2} = \{\frac{80}{27l} H^2 \sigma_0 t + \frac{3}{2H} \sigma_0 t^2 l\pi + 2\sigma_0 t^2 \cos\varphi \tan\theta\} \cos\theta \qquad (194)$$

We can notice that the above equations are exactly same as the equation 131 and 132. By the application of the $H=18.75$mm, $l=150$mm $\theta=30°$, $\varphi=60°$, $t=0.71$mm, above, crushing force become:

$$\begin{aligned} P_{m1} &\approx 4586N \\ P_{m2} &\approx 6378N \end{aligned} \qquad (195)$$

107

References

[1] Cowper, G. R and Symonds, P. S., "Strain-hardening and strain-rate effect in the impact loading in cantilever beams", Technical Report, No. 28, Brown University, 1957.

[2] V. U. Minorsky, An analysis of ship collisions with reference to protection of nuclear power plants, Journal of Ship Research, 1959.

[3] Pugsley, A. G., "The crumpling of tubular structures under impact conditions", In Proceeding of a Symposium on the use of aluminum in railway rolling stock, Institution of Locomotive Engineers, London, paper 4, 1960, pp 33-41.

[4] Macaulay, M, A. and Redwood, R. G. "Small scale model railway coaches under impact", The Engineer, Vol. 25, December 1964, pp. 1041-1046.

[5] Akita, Y., Ando, N.,Fujita, Y. and Kitamura, K., "Studies on collision protective structures in nuclear powered ships", Nuclear Engineering and Design, 19, 1972, pp.365-401.

[6] Lowe, W. T., Al-Hassani, S. T. S. and Johnson, W., "Impact behavior of small scale model moter coaches", Proc Instn Mech. Engrs, Auto Division, Vol. 186, 1972, pp.409-419.

[7] Nagasawa, H., Arita, K., Tani, M. and Oka, S., "A study on the collapse of ship structure in collision with bridge piers", Journal of the Society of Naval Architect of Japan, Vol. 142, 1977, pp. 323-332.

[8] Magee, C. L. and Thornton, P. H., "Design considerations in energy absorption by structural collapse", S.A.E. paper, No. 780434, 1987.

[9] Von Mater, P.R. and Giannotti, J.G., "Critical evaluation of low energy ship collision damage theories and design methodologies", Ship Structure Committee, Report No. SSC-285, 1979.

[10] Jones, N., "A literature survey on the collision and grounding protection of ships", Ship Structure Committee, Report No. SSC-283, 1979.

[11] Nagasawa, H., Arita, K., Tani, M. and Oka, S., "A study on the collapse of ship structure in collision with bridge piers (2nd Report)", Journal of the Society of Naval Architects of Japan, Vol. 146 pp. 329-337, 1979.

[12] Nagasawa, H., Arita, K., Tani, M. and Oka, S., "A study on the collapse of ship structure in collision with bridge piers (3rd Report)", Joirnal of the Society of Naval Architects of Japan, Vol. 151, 1982, pp. 174-186.

[13] Mahmood, H. F. and Paluszny, A., "Design of thin walled column for crash energy management-their strength and mode of collapse", S.A.E. paper, No.811302, 1981.

[14] Wierzbicki, T., "Crushing behaviour of plate intersections", Chap. 3 in Structural Crashworthiness, eds. N. Jones and T. Wierzbicki, Butterworths, 1982.

[15] Ohnishi, T., Kearkami, H., Yasukawa, W. and Nagasawa, H., "On the ultimate strength of bow construction", Journal of the Society of Naval Architects of Japan, Vol. 151, 1982, pp. 174-186.

[16] Amdahl, J., "Energy absorption in ship-platform impacts", Division of Marine Structures, University of Trondheim, Report No. UR-83-34, Trondheim, Norway, September 1983.

[17] Meng, Q., Al-Hassani, S. T. S., and Soden, P. D., "Axial crushing of square tubes", Int. J. Mech. Sci., Vol. 25, No. 9-10 983, pp. 747-773.

[18] Lee, J.W., "On the optimization design of soft bow structure, Proc. PRADS, 1983, pp. 429-435.

[19] Kierkegaard, H., "Ship bow response in high energy collision", Marne Structures, Vol. 6, 1993, pp. 359-376.

[20] Abramowicz, W. and Jones, N., "Dynamic axial crushing of square tubes", Int. J. of Impact Engng., Vol. 2, No. 4, 1984, pp.179-208.

[21] Samuelides, E. and Frieze, P., "Literature review on ship-ship collision", Report NAOE-84-01, Department of Naval Architecture and Ocean Engineering, University of Glasgow, 1984.

[22] Kawai, T., Toi, Y. and Suzuki, N., "Numerical simulations on the crushing behavior of structural member", Naval Architecture and Ocean Engineering, Society of Naval Architects of Japan, Vol. 158, 1985, pp. 435-443.

[23] Abramowicz, W. and Jones, N., " Dynamic progressive buckling of circular and square tubes", Int. J. of Impact Engineering Vol. 4, No. 4, 1986, pp. 243-270.

[24] Yang , P. D. C. and Caldwell, J. B., "Collision energy absorption of ship's bow structures", International Journal of Impact Engineering, Vol. 7, No.2, 1988.

[25] Toi, Y., Yuge, K., Nagayama, T. and Obata, K., "Numerical and experimental studies on the crashworthiness of structural members", Naval Architecture and Ocean Engineering, Society of Naval Architects of Japan, Vol. 26, 1988 pp. 91-101.

[26] Jones, N., " Structural Impact", Cambridge University Press, pp.403-405, 1989.

[27] Jones, N. and Birch. R. S., " Dynamic and static axial crushing of axially stiffened square tubes", Proc. Inst. Mech, Engrs., Vol. 204, 1990, pp. 293-310.

[28] Perdersen, P. T., Valsgard, S., Olsen, D. and Spangenberg, S., "Ship Impacts: Bow Collisions". Int. J. Impact Engng., Vol. 13, No. 2, 1993 pp 163-187.

[29] Kierkegaard, H., "Ship bow response in high energy collision", Marine Structures, Vol. 6, 1993, pp 359-376.

[30] Ohtsube, H. and Suzuki, K., "The crushing mechanics of bow structure in head on collision (1st Report)", Journal of the Society of Naval Architects of Japan, Vol. 176, 1994, pp. 301-308.

[31] Abramowicz, W., "Crush resistance of "T", "Y" and "X" section", Joint MIT-Industry Program on Tanker Safety, Report No. 24, Department of Ocean Engineering. Massachusetts Institute of Technology, Cambridge, January 1994.

[32] Wang, G. and Suzuki, K., "The crushing mechanics of bow structure in head on collision (2nd Report")", Journal of Society of Naval Architects of Japan, Vol. 177, 1995, pp. 357-363.

[33] Paik, J. K. and Pederden, P. T., Modeling of the internal mechanics in ship collisions", Ocean Engineering , An International Journal of Research and Development, Vol. 23, No. 2, 1996, pp 107-142.

[34] Paik, J. K. and Wierzbicki, T., "A benchmark study on collision and grounding of plated structures", J. of Ship Research, Oct. 1996.

[35] Chung, J. Y. Ph.D. Thesis on "Bow Collision Strength of Ships", Department of Naval Architecture & Ocean Engineering, Pusan National University. 1997.

[36] M Maestro, A Marino "Search for a Predictive Mode of Structural Damage in Ship Collisions: from a Case Study to Some Proposals a New Approach.